Role and Relevance of PHT1 in Brain Disposition and Pharmacokinetics of L-Histidine

by

Xiaoxing Wang

A dissertation submitted in partial fulfillment
of the requirements for the degree of
Doctor of Philosophy
(Pharmaceutical Sciences)
in the University of Michigan
2017

Doctoral Committee:

Professor David E. Smith, Chair
Professor Gordon L. Amidon
Professor Richard F. Keep
Professor Kerby A. Shedden
Professor Duxin Sun

Xiaoxing Wang

Xiaoxing@umich.edu

ORCID iD: 0000-0001-6961-8667

ACKNOWLEDGEMENTS

Yuqing Wang, Daniel Epling, Feifeng Song, and Brain Thompson for their collaboration, support, and friendship. Also thank all my friends in the College of Pharmacy for their help and companionship.

I would like to acknowledge the PhD program in Pharmaceutical Sciences and the University of Michigan. This is my first stop in the US, as well as a great starting point of my career. I will always feel privileged being a Wolverine. I received financial support from the College of Pharmacy and Rackham Barbour Scholarship for my PhD study. Many thanks for their support and encouragement.

Last but not least, I would like to express my love to my dearest mother Jiping Guo and father Aiguo Wang, for their great parenting and education; to my husband Yangbing Li and my daughter Avery. Their unconditional love and endless support make me brave.

PREFACE

The following papers have been or will be published as related to my doctoral studies:

1. Wang XX, Hu Y, Keep RF, Toyama-Sorimachi N, Smith DE. A novel role for PHT1 in the disposition of L-histidine in brain: in vitro slice and in vivo pharmacokinetic studies in wildtype and Pht1 null mice. Biochem Pharmacol 124: 94-102, 2017.

2. Wang XX, Liu W, Zheng T, Park JM, Smith DE, Feng MR. Population pharmacokinetics of mycophenolic acid and its glucuronide metabolite in lung transplant recipients with and without cystic fibrosis. Xenobiotica. [Epub ahead of print].

3. Wang XX, Feng MR, Nguyen H, Smith DE, Cibrik DM, Park JM. Population pharmacokinetics of mycophenolic acid in lung transplant recipients with and without cystic fibrosis. Eur J Clin Pharmacol. 71(6): 673-9, 2015.

4. Wang XX, Li YB, Feng MR, Smith DE. Semi-Mechanistic Population Pharmacokinetic Modeling of L-Histidine Disposition and Brain Uptake in Wildtype and Pht1 Null Mice. (In preparation)

TABLE OF CONTENTS

LIST OF TABLES

LIST OF FIGURES

LIST OF APPENDICES

ABSTRACT

PHT1 (SLC15A4) is responsible for translocating L-histidine (L-His), di/tripeptides and peptide-like drugs across biological membranes. Previous studies have indicated that PHT1 is located in brain parenchyma, however, its role and significance in brain, along with its impact on the biodistribution of substrates is unknown. In the present study, adult gender-matched *Pht1*-competent (wildtype) and *Pht1*-deficient (null) mice were used to investigate the effect of PHT1 on L-His brain disposition via *in vitro* slice and *in vivo* pharmacokinetic approaches. Initial phenotyping of the two genotypes and expression measurements of select transporters/enzymes were also performed. No significant differences were observed between genotypes in serum chemistry, body weight, viability and fertility. Polymerase chain reaction (PCR) analyses indicated that Pept2 had a compensatory up-regulation in *Pht1* null mice (about 2-fold) as compared to wildtype animals, which was consistent in different brain regions and confirmed by immunoblots. The uptake of L-His was reduced in brain slices by 50% during PHT1 ablation. The L-amino acid transporters accounted for 30% of the uptake, and passive (other) pathways for 20% of the uptake. During the *in vivo* pharmacokinetic (PK) studies, plasma concentration-time profiles of L-His were comparable between the two genotypes after intravenous administration. Still, biodistribution studies

revealed that, when sampled 5 min after dosing, L-His values were 28–48% lower in *Pht1* null mice as compared to wildtype animals, in brain parenchyma but not cerebrospinal fluid.

Concentration-time profiles of the *in vivo* samples were then analyzed using nonlinear mixed effects modeling with NONMEM v7.3. In addition to active PHT1-mediated uptake into brain parenchyma, influx and efflux rate constants of L-His between plasma, brain parenchyma and CSF were modeled as first-order processes. Diffusion between brain parenchyma and CSF, CSF bulk flow and tissue volumes were obtained from the literature. The disposition kinetics of L-His in plasma, CSF and brain parenchyma was best described by a four-compartment model. We observed that the plasma and CSF PK profiles of L-His were comparable in WT and KO mice. However, a more rapid uptake of L-His occurred in the brain parenchyma of WT mice due to active transport by PHT1, which was modeled with a Michaelis-Menten term (K_m = 39.9 µM and V_{max} = 0.140 nmol/min).

Our model quantitatively described the transport kinetics of PHT1-mediated uptake of L-His in brain, for the first time, under *in vivo* conditions. The results suggest that PHT1 may play an important role in histidine transport in brain, and resultant effects on histidine/histamine homeostasis and neuropeptide regulation. The findings also provide a valuable tool in predicting the disposition of L-His in brain and the potential of PHT1 as a drug target to treat serious CNS diseases.

CHAPTER 1

RESEARCH OBJECTIVES

Peptide/histidine transporter 1 (PHT1), a member of the proton-coupled oligopeptide transporter (POT) superfamily, is an integral membrane protein that translocates various di-/tri-peptides, peptidomimetics and L-histidine across the biological membrane. Currently four members of the POT family have been identified in mammals, including PEPT1 (SLC15A1), PEPT2 (SLC15A2), PHT1 (SLC15A4) and PHT2 (SLC15A3) [1]. Among them, the localization, expression, function and pharmacological relevance of peptide transporters PEPT1 and PEPT2 were most extensively studied. However, little is known about the peptide/histidine transporters, PHT1 and PHT2 [2]. Each of the four POT family proteins displays a distinct pattern of tissue expression with specific physiological and pathological roles [3]. PEPT1 is primarily expressed in the small intestine, where it is responsible for the absorption of di-/tri-peptides from dietary proteins and gastrointestinal secretions [4, 5]. In the kidney, PEPT1 is located in S1 segments whereas PEPT2 is preferentially expressed in brush border membranes of the latter parts of the proximal tubule (S3 segments) in kidney [6]. Together, PEPT1 and PEPT2 govern the efficient reabsorption of peptides/mimetics from the tubular fluid [7]. PEPT2 protein also has strong expression in choroid plexus and brain parenchyma, the level of which shows an age-dependent declining expression [8]. PEPT2 in brain

appears to regulate neuropeptides homeostasis and protect against neurotoxicity [9]. PHT1 proteins are found in brain and eye [10, 11]. In contrast to PEPT2, PHT1 has an age-dependent increasing expression in brain. The expression of PHT1 increases in a similar manner with the function and localization progression of the histaminergic system [12-16]. Moreover, PHT1 function dominates in adult rodents, suggesting a significant role in regulating both endogenous and exogenous L-histidine and peptides/mimetics in brain [17]. PHT1 transcripts are also detected in rat thyroid gland [18], and skeletal muscle [19]. A recent study showed that PHT1 and PHT2 are involved in the immune response. PHTs are preferentially expressed by dendritic cells, located at endosomes and lysosomes, mediating the release of bacterially-derived components into the cytosol [20].

L-Histidine is a basic and hydrophilic α-amino acid, and is a specific substrate of PHT1. It is one of the proteinogenic amino acids, which is obtained from dietary, metabolic and protein turnover [21]. L-histidine possesses several crucial biological functions, including the formation of myelin sheath, the detoxification of heavy metals, the manufacture of white and red blood cells, and others. It is a precursor of histamine, carnosine, ergothioneine, and vitamin C [22]. Studies on the PHT1-mediated transport of L-histidine in brain would extend our understanding of neuropeptide regulation, histamine homeostasis, and PHT1 as a potential target for drug delivery to neuronal and non-neuronal cells. In the central nervous system (CNS), the major transporters for L-histidine include the Na^+-coupled neutral amino acid transporters (e.g. SNATs, belong to SLC38 family) [23, 24], some members of the Na^+-and Cl^--dependent neurotransmitter transporter family (e.g. B^0AT2 and

NTT4, belong to SLC6 family) [25-27], as well as the peptide/histidine transporters (e.g. PHT1, belongs to SLC15 family) [17, 28].

Histamine is one of the most important metabolites of L-histidine, formed during catalysis by L-histidine decarboxylase (HDC). Significant changes in brain histamine levels have been observed in several neurological diseases, such as multiple sclerosis, Alzheimer's disease, Down's syndrome and Wernicke's encephalopathy [29]. Histamine, however, cannot pass through the barrier systems of the brain [30] and depends upon L-histidine uptake first. The dysfunction of HDC and L-histidine transporters in brain may be related to these neurological disorders.

Pht1-deficient mice provide a powerful tool to investigate the role and relevance of PHT1 in L-histidine disposition in brain, as well as histamine levels with or without exogenous L-histidine being supplied. We hypothesize that PHT1 ablation will reduce the uptake of L-histidine in brain slices of adult mice and substantially lower histamine production. The following specific aims are proposed in this study:

1) To determine the influence of PHT1 depletion on the uptake of L-histidine in different tissue sections of brain slices in wildtype and *Pht1* null mice

2) To investigate the importance of PHT1 in affecting the *in vivo* pharmacokinetics and tissue distribution of L-histidine in wildtype and *Pht1* null mice

3) To develop a pharmacokinetic model that accurately characterizes the disposition of L-histidine in wildtype and *Pht1* null mouse plasma, cerebrospinal fluid and brain parenchyma

REFERENCE

1.   Daniel, H. and G. Kottra, *The proton oligopeptide cotransporter family SLC15 in physiology and pharmacology.* Pflugers Arch, 2004. **447**(5): p. 610-8.

2.   Smith, D.E., B. Clemencon, and M.A. Hediger, *Proton-coupled oligopeptide transporter family SLC15: physiological, pharmacological and pathological implications.* Mol Aspects Med, 2013. **34**(2-3): p. 323-36.

3.   Botka, C.W., et al., *Human proton/oligopeptide transporter (POT) genes: identification of putative human genes using bioinformatics.* AAPS PharmSci, 2000. **2**(2): p. E16.

4.   Jappar, D., et al., *Significance and regional dependency of peptide transporter (PEPT) 1 in the intestinal permeability of glycylsarcosine: in situ single-pass perfusion studies in wild-type and Pept1 knockout mice.* Drug Metab Dispos, 2010. **38**(10): p. 1740-6.

5.   Ogihara, H., et al., *Immuno-localization of H+/peptide cotransporter in rat digestive tract.* Biochem Biophys Res Commun, 1996. **220**(3): p. 848-52.

6.   Smith, D.E., et al., *Tubular localization and tissue distribution of peptide transporters in rat kidney.* Pharm Res, 1998. **15**(8): p. 1244-9.

7.   Shen, H., et al., *Localization of PEPT1 and PEPT2 proton-coupled oligopeptide transporter mRNA and protein in rat kidney.* Am J Physiol, 1999. **276**(5 Pt 2): p. F658-65.

8.   Shen, H., et al., *Immunolocalization of the proton-coupled oligopeptide transporter PEPT2 in developing rat brain.* Mol Pharm, 2004. **1**(4): p. 248-56.

9.   Hu, Y., et al., *Peptide transporter 2 (PEPT2) expression in brain protects against 5-aminolevulinic acid neurotoxicity.* J Neurochem, 2007. **103**(5): p. 2058-65.

10.   Yamashita, T., et al., *Cloning and functional expression of a brain peptide/histidine transporter.* J Biol Chem, 1997. **272**(15): p. 10205-11.

11.   Sakata, K., et al., *Cloning of a lymphatic peptide/histidine transporter.* Biochem J, 2001. **356**(Pt 1): p. 53-60.

12.   Martres, M.P., M. Baudry, and J.C. Schwartz, *Histamine synthesis in the developing rat brain: evidence for a multiple compartmentation.* Brain Res, 1975. **83**(2): p. 261-75.

13.	Reiner, P.B., et al., *Ontogeny of histidine-decarboxylase-immunoreactive neurons in the tuberomammillary nucleus of the rat hypothalamus: time of origin and development of transmitter phenotype.* J Comp Neurol, 1988. **276**(2): p. 304-11.

14.	Subramanian, N., et al., *Ontogeny of histaminergic neurotransmission in the rat brain: concomitant development of neuronal histamine, H-1 receptors, and H-1 receptor-mediated stimulation of phospholipid turnover.* J Neurochem, 1981. **36**(3): p. 1137-41.

15.	Tran, V.T., et al., *Ontogenetic development of histamine H1-receptor binding in rat brain.* J Neurochem, 1980. **34**(6): p. 1609-13.

16.	Toledo, A., et al., *Properties and ontogenic development of membrane-bound histidine decarboxylase from rat brain.* J Neurochem, 1988. **51**(5): p. 1400-6.

17.	Hu, Y., et al., *Divergent Developmental Expression and Function of the Proton-Coupled Oligopeptide Transporters PepT2 and PhT1 in Regional Brain Slices of Mouse and Rat.* J Neurochem, 2014. **129**(6): p. 955-965.

18.	Romano, A., et al., *Functional expression of SLC15 peptide transporters in rat thyroid follicular cells.* Mol Cell Endocrinol, 2010. **315**(1-2): p. 174-81.

19.	Everaert, I., et al., *Gene expression of carnosine-related enzymes and transporters in skeletal muscle.* Eur J Appl Physiol, 2013. **113**(5): p. 1169-79.

20.	Nakamura, N., et al., *Endosomes are specialized platforms for bacterial sensing and NOD2 signalling.* Nature, 2014. **509**(7499): p. 240-4.

21.	Kopple, J.D. and M.E. Swendseid, *Evidence that histidine is an essential amino acid in normal and chronically uremic man.* J Clin Invest, 1975. **55**(5): p. 881-91.

22.	Stifel, F.B. and R.H. Herman, *Histidine metabolism.* Am J Clin Nutr, 1971. **24**(2): p. 207-17.

23.	Schioth, H.B., et al., *Evolutionary origin of amino acid transporter families SLC32, SLC36 and SLC38 and physiological, pathological and therapeutic aspects.* Mol Aspects Med, 2013. **34**(2-3): p. 571-85.

24.	Hagglund, M.G., et al., *Identification of SLC38A7 (SNAT7) protein as a glutamine transporter expressed in neurons.* J Biol Chem, 2011. **286**(23): p. 20500-11.

25.	Fredriksson, R., et al., *The solute carrier (SLC) complement of the human genome: phylogenetic classification reveals four major families.* FEBS Lett, 2008. **582**(27): p. 3811-6.

26.	Hagglund, M.G., et al., *Characterization of the transporterB0AT3 (Slc6a17) in the rodent central nervous system.* BMC Neurosci, 2013. **14**: p. 54.

27.	Hagglund, M.G., et al., *B(0)AT2 (SLC6A15) is localized to neurons and astrocytes, and is involved in mediating the effect of leucine in the brain.* PLoS One, 2013. **8**(3): p. e58651.

28.   Bhardwaj, R.K., et al., *The functional evaluation of human peptide/histidine transporter 1 (hPHT1) in transiently transfected COS-7 cells.* Eur J Pharm Sci, 2006. **27**(5): p. 533-42.

29.   Haas, H.L., O.A. Sergeeva, and O. Selbach, *Histamine in the nervous system.* Physiol Rev, 2008. **88**(3): p. 1183-241.

30.   Schwartz, J.C., et al., *Histaminergic transmission in the mammalian brain.* Physiol Rev, 1991. **71**(1): p. 1-51.

CHAPTER 2

BACKGROUND AND LITERATURE REVIEW

2.1 Proton-coupled oligopeptide transporters

Proton-coupled oligopeptide transporters (POTs), which also belong to the solute carrier protein (SLC15) family, are integral membrane proteins that translocate various di-/tri-peptides and peptidomimetics across the biological membrane. Currently four members in the POT family have been identified in mammals, including PEPT1 (SLC15A1), PEPT2 (SLC15A2), PHT1 (SLC15A4) and PHT2 (SLC15A3) [1]. The first identified H^+-coupled transporter of oligopeptides and peptide-derived antibiotics, PEPT1, was cloned from rabbit small intestine [2, 3]. Following that, PEPT2 was isolated from kidney by screening a human cDNA library [4]. Then, with further investigation into transporters of the nervous system, the peptide/histidine transporters (PHT1/ PHT2) were isolated from rat brain [5, 6]. Localization and functional characterization of PHT1 and PHT2 were done in Xenopus laevis oocytes, showing that they can also recognize L-histidine, unlike PEPT1 and PEPT2 [5, 6]. PEPT1 and PEPT2 share similar hydrophobic domains, with about 51% sequence homology [7, 8]. However, the protein sequences of PHT1 and PHT2 show weak similarity to PEPT1 and PEPT2 (less than 26%) [8]. Among the POTs, the localization, expression, function, and the pharmaceutical relevance of

PEPT1 and PEPT2 were most extensively studied, while little is known about the peptide/histidine transporters PHT1 and PHT2 [9].

2.1.1 Structural characteristics

POT proteins are all integral membrane proteins. Since the crystal structures of human POTs have not been characterized yet, they are predicted to be composed of 12 transmembrane helices (TMH or H), with the N- and C-termini facing the cytoplasm (Figure 2-1) [10, 11].

PEPT1 and PEPT2 proteins have around 707-740 amino acid residues depending on species. The human PEPT1 and PEPT2 share 51% amino acid identity. The structure of PEPTs has a large extracellular loop connecting the segments 9 and 10 (H9 and H10). With much lower identity to the PEPT proteins (less than 26%), human PHT1 has 577 amino acid residuals and PHT2 has 581, sharing 48% amino acid identity [8]. Mouse PHT1 has 85% amino acid identity to its human ortholog, while rat PHT1 has 89% amino acid identity to human [8]. There is no large extracellular loop between H9 and H10 in PHT1.

The relationship between protein regions and their functional characteristics showed different organizations on PEPT1 and PEPT2. Much of the transport mechanism of these proteins, as well as their 3-D structure, is inferred from chimeras combining, model predictions and molecular modeling [11-13]. Basically, peptide/mimetic substrates are transported through a central pore, where several key residues face this transmembrane channel for peptide binding [14, 15], and proton binding [16]. The role of the extracellular loop connecting H9 and H10 is still

unknown. The H1-H4 and H7-H9 of PEPT1 and PEPT2 might contribute to pH-dependency and substrate affinity [1, 9].

Although there are significant differences in sequence homology among the POTs, several highly conserved motifs were discovered in H1, H2, H3 and H5. Point mutations by these motifs could alter the substrate affinity, pH-dependent transport, or even complete loss of function[2, 15, 17].

POTs have typical features of major facilitator superfamily (MFS) members, which include the E.coli proton-coupled lactose permease (LacY), the glycerol-3-phosphate/inorganic phosphate antiporter (GlpT) and the multidrug transporter EmrD [2, 10, 18]. As a result the crystal structures for them could be a good reference for the 3-D structure of 12-TM transporters. The 3-D structure of a prokaryotic homologue of mammalian PEPT, $PEPT_{so}$, was recently confirmed (Figure 2-2) [18, 19]. $PEPT_{so}$ consists of the central and extracellular cavities. Similar with the structures of LacY, the two hydrophilic cavities are potentially separated by an extracellular gate, formed by H7 and H2. And the intracellular side is restricted by side chain interactions among H4, 5, 10, and 11 [18]. However, the exact protein structure and function residues still need to be elucidated.

2.1.2 Transport function and mechanisms

PEPT1 and PEPT2 proteins may mediate the transport of all 400 different dipeptides and 8000 different tripeptides from the 20 L-α-amino-acids in a sequence independent manner [1]. However, the peptide bond is not a prerequisite for transport since some omega-amino fatty acids (e.g. delta-aminolevulinic acid) are also substrates of PEPT1 and PEPT2 [9, 20]. With respect to pharmacological

relevance, PEPT1 and PEPT2 can also transport a variety of peptide-like drugs (e.g. cefadroxil, enalapril, valacyclovir), aminocephalosporins, angiotensin-converting enzyme inhibitors (ACE inhibitors) and others [11, 21]. Specifically, PEPT1 is a "high-capacity, low-affinity" transporter, while PEPT2 is a "low-capacity, high-affinity" transporter. Substrate affinity is also determined by membrane potential and external pH, where lower external pH values are favored for transport of negatively charged dipeptides, higher pH values increase the uptake rate of positively charged dipeptides, and neutral ones are not significantly affected [22]. PHT1 and PHT2 can recognize L-histidine as a substrate, unlike the PEPT proteins. The rat PHT1 isoform exhibited a high affinity transport activity, as judged by the K_m = 17μM for L-histidine [5]. Also, the function of PHT proteins is pH-dependent with an optimal pH at pH 5.5 [5], or pH 5.0 [23]. More detailed information about the substrate specificity of PHT proteins is not yet available.

The driving force of substrate uptake for POTs is an inwardly directed H^+ gradient (Figure 2-3). It was confirmed that there is an acid microclimate at the intervillous space of jejunum (pH value is 6.1-6.6) related to H^+ secretion, while the intracellular pH of enterocytes is 7.3 [24]. Na^+/H^+ antiporter activity could drive and maintain the pH transmembrane gradient by Na^+ exchanging [25, 26]. The basolateral Na^+/K^+-ATPase can generate the energy, as well as the transmembrane and transepithelial concentration gradient of Na^+ needed for this process [27].

2.1.3 Tissue distribution and expression regulation

Each of the four POT family members displays a distinct pattern of tissue expression, as discussed below [8].

2.1.3.1 PEPT1

Many studies have demonstrated that PEPT1 is primarily expressed in the small intestine, including duodenum, jejunum and ileum [28, 29]. Immunolocalization studies demonstrated that PEPT1 was abundantly expressed at the apical membrane of enterocytes in human and mouse, and is responsible for the absorption of di-/tri-peptides from dietary proteins and gastrointestinal secretions [30-32]. The expression levels of PEPT1 protein in rat small intestine were maximal 3-5 days after birth, decreased slowly, and then rose to 59-88% of maximal expression at day 24 [33, 34]. In adult animals, small intestine PEPT1 level is up regulated on high-protein diet, fast state, as well as some pathological conditions (e.g. inflammation) [35-37].

In colon, the expression of PEPT1 is controversial. It was once considered that PEPT1 was neither expressed nor functioning in normal proximal and distal colon [28, 29]. However, the Daniel group recently reported that PEPT1 was expressed in the distal colon of normal mouse, rat and human. According to their studies, colonic expression of PEPT1 contributed to water absorption. Moreover, PEPT1 was down regulated under conditions of acute and chronic intestinal inflammation [38, 39].

In the kidney, PEPT1 is found in brush border membranes of the early parts (S1 segment) of proximal tubule [40]. PEPT1 is also expressed in the bile duct, pancreas, liver, immune cells and several cancer cell lines [21, 41-43]. However, the detailed functions and expression levels in these latter tissues are largely unknown.

2.1.3.2 PEPT2

PEPT2 is preferentially expressed in brush border membrane of the latter parts of the proximal tubule (S3 segments) in kidney [40]. Together with PEPT1, they are responsible for the reabsorption of peptides/mimetics from the tubular fluid [44]. In brain, PEPT2 protein is strongly expressed in cerebral cortex, olfactory bulb, basal ganglia, cerebellum, hindbrain and the apical surface of choroid plexus epithelia. In neonate rat, PEPT2 was detected in both astrocytes and neurons, while in adult rat PEPT2 was only detected in neurons. The expression levels declined in an age-dependent manner [45]. PEPT2 functions in brain by regulating neuropeptides homeostasis and by protecting the brain against neurotoxicity. It is also responsible for the removal of substrates from cerebrospinal fluid (CSF) to blood at the brain-CSF barrier (BCSFB) [46, 47]. Finally, PEPT2 is found in the lung, mammary gland and spleen, however, its function in these tissues is unclear [11, 21].

2.1.3.3 PHT1 and PHT2

Compared with PEPT1 and PEPT2, the tissue expression of PHT1 and PHT2 is much less clear. PHT1 and PHT2 mRNA were found in several regions of the human and rat gastrointestinal tract (GIT), as well as the Caco-2 cell model [48]. As determined by immunohistochemical analyses, PHT1 was expressed in the villous epithelium along human small intestine [23], however, its relevance in substrate absorption was unclear. PHT1 proteins are also found in the brain and eye [5, 6]. A recent study showed that PHT1 has an age-dependent increasing expression in brain, in contrast to that of PEPT2 [49]. The ascending level of PHT1 occurs in a similar manner with the function and localization of the histaminergic system [50-54]. Specifically, the function of PHT1 dominates in adult rodents, suggesting a

significant role in regulating both endogenous and exogenous L-histidine and peptides/mimetics in brain [49]. In the immune system, PHT1 transcripts are found in plasmacytoid dendritic cells [55]. Its protein expression is significantly up-regulated in colonic biopsies from inflammatory bowel disease (IBD) patients, which may contribute to the transport of Nod1 ligands to the cytosol [56]. PHT1 transcripts are also detected in rat thyroid gland [57], and skeletal muscle [58]. PHT2 mRNA is found in the lung, spleen and thymus [6].

Unlike PEPT proteins, which are mainly expressed on the plasma membrane, PHT proteins are expressed in the intracellular compartment. Subcellular localization studies show that PHT1 co-localizes with endosome and lysosome markers, which may transport free histidine and oligopeptides from inside the endosome to the cytosol [56, 59]. Rat PHT2 protein has also been localized to the lysosomal membrane [6]. A recent study showed that PHT1 and PHT2 are highly involved in the immune response. PHT1 expressed in dendritic cells is intimately involved in the immunologic diseases related to TLR9 stimulation, such as lupus, colitis and persistent viral infection [59-61]. Recent genome-wide association studies on systemic lupus erythematosus identified PHT1 variants as an Asian-specific locus for this disease [62-64].

2.2 L-Histidine transporters in brain

Histidine is a basic and hydrophilic α-amino acid. The active isomer is L-histidine (Figure 2-4). It is one of the 21 proteinogenic amino acids essential for human health. It is obtained from dietary, metabolism and protein turnover [65]. The imidazole functional group in histidine has a pKa of approximately 6.0. The

imidazole aromatic ring is protonated and carries a positive charge when the pH value is below 6.0, which can serve as a general acid. The unprotonated imidazole is nucleophilic and can serve as a general base (Figure 2-4). As a result, L-histidine is a common participant in enzyme-catalyzed reactions. L-histidine is involved in several biological functions, including formation of the myelin sheath, detoxification of heavy metals, manufacturing white and red blood cells, and others. It is also a precursor for the synthesis of histamine, carnosine, ergothioneine, and vitamin C [66]. Studies on the transport of L-histidine in brain would extend our understanding of neuropeptide regulation, histamine homeostasis, and the potential for drug delivery to neuronal and non-neuronal cell types.

2.2.1 Transport of L-histidine across brain barrier systems

Access of amino acids to the living brain is restricted by the cerebral barrier systems [67]. The blood-brain barrier (BBB) plays the major role in restriction and regulation of amino acid transport between the blood and brain compartments. The BBB consists of a single layer of capillary endothelial cells and an underlying thick basement membrane [68]. The tight junctions among the adjacent cells form the barrier, sealing off the paracellular diffusion space. Thus, to cross the BBB, solutes have to partition into and diffuse through the cell membrane, or be transported by carriers. Despite the highly reduced flux rate across the BBB, brain capillaries are still the primary site of exchange for most solutes between the brain compartment and blood because of its large surface area [69]. Intensive research has focused on the transport of amino acids across the BBB. Many transporter systems were identified at the luminal (blood-facing) or abluminal (brain-facing) membranes of

14

the endothelial cells. Regarding the mechanisms of L-histidine transport into brain, several amino acid transporters are discussed below.

The system L transporters (LAT1 and LAT2, encoded as SLC7A5 and SLC7A8, respectively) mediate the uptake of amino acids with large neutral side chains, including L-histidine, across the BBB into brain [70, 71]. They are located on both the luminal and abluminal surfaces of endothelial cells, facilitating the transport of amino acids in a high affinity, Na^+-independent, bidirectional manner [72]. System L transporter function can be inhibited by 2-aminobicyclo[2,2,1]heptane-2-carboxylic acid (BCH) [73].

Low affinity transport systems for L-histidine include the system y^+ cationic amino acid transporters (CATs, belong to SLC7 family), which are expressed in both luminal and abluminal membranes of the BBB, with preferential expression at the abluminal side. Although considered Na^+-independent transporters, they can also transport neutral amino acid substrates in a Na^+ dependent manner but with low efficiency [74].

Unlike the Na^+-independent transporters described previously, the Na^+-dependent transporters are expressed only in abluminal membranes [75]. Na^+-dependent transporters possess the ability to transfer amino acids from brain extracellular fluid into endothelial cells with high affinity [76]. Moreover, these carriers are able to efflux substrates from the extracellular fluid (ECF) to endothelial cells and, hence to the systemic circulation, utilizing the Na^+-electrochemical potential gradient. This vectorial transport may explain the significantly lower concentrations of amino acids in brain ECF than in plasma [72]. Na^+-dependent

transporters can be inhibited by BCH and a wide range of amino acids. [75] According to current research, the Na^+-dependent transporter of L-histidine at the BBB includes the following: system A transporters SNAT1 and SNAT2 [77] and system N transporters SNAT3 and SNAT5 [78, 79], of which all belong to the SLC38 family; and the system $B^{0,+}$ transporter B^0AT3 (SLC6A17) [80]. SLC38 family proteins will be discussed in more detail in subsequent sections.

Cerebrospinal fluid (CSF) is a bodily fluid existing in the cerebral ventricle and the subarachnoid space around brain and spine, providing a basic mechanical and immunological protection to the brain. CSF is mainly (more than 75%) formed in the choroid plexuses (CPs). The barrier between CSF and CPs is called the blood-CSF barrier (BCSFB). The structural basis of the BCSFB consists of CP cuboidal epithelium cells, which are also linked by tight junctions [81]. However, the tight junctions of BCSFB are much weaker than that of the BBB, making CPs belong to the class of leaky epithelia [82]. Several L-histidine transporter systems expressed on both the CPs and BBB include LAT1 [83], LAT2, SNAT3 [84], and Asc-1 (SLC7A10) [85].

The mRNA of PHT1 was also identified in CPs [5]. However, PHT1 may not contribute to the transport of L-histidine at this site, as the uptake of L-histidine into brain is not inhibited by dipeptides [86, 87], nor is the transport of dipeptides inhibited by L-histidine [88, 89].

2.2.2 Transport of L-histidine in brain parenchyma

Although the brain barrier systems determine the concentration of amino acids in CSF and ECF, transporters expressed on the membranes of parenchyma

cells also participate in the regulation of intracellular fluid homeostasis [75]. More importantly, transporters in brain paranchyma are responsible for translocation of metabolic substrates, neurotransmitters and neurotransmitter precursors, regulating the signaling pathway [90]. The major amino acid transporters of L-histidine in brain parenchyma include the Na^+-coupled neutral amino acid transporters (e.g., SNATs, which belong to the SLC38 family) [91, 92], Na^+-independent amino acid transporters (e.g., LATs and CATs, which belong to the SLC7 family) [70, 71], some members of the Na^+-and Cl^--dependent neurotransmitter transporter family (e.g., B^0AT2 and NTT4, which belong to the SLC6 family) [93-95], as well as the peptide/histidine transporters (e.g., PHT1 and PHT2, which belong to the SLC15 family) [23, 49].

SNATs have a very broad tissue distribution and are responsible for the net flux of amino acids in CNS [91, 96]. As mentioned above, system A and system N transporters are the two major divisions of this protein family. System A transporters (SNAT1, 2, 4 and 8) are Na^+ dependent, having a classical inhibitor amino acid analogue 2-methylamino-isobutyric acid (MeAIB). System N transporters (SNAT3, 5 and 7) are Na^+ and H^+ dependent, having no MeAIB selectivity. However, the classification of SNATs is still controversial. Some transporters are more likely to be treated as the "orphan members", such as SNAT7/8/10 [97]. The major physiological function of SNATs in the CNS is to transport glutamine in the glutamate/glutamine cycle [98]. Affinity of SNATs to L-histidine is relatively low, with Michaelis-Menten (Km) values in the millimolar range [78, 79, 99].

SLC6 family transporters are also known as neurotransmitter transporters. Several SLC6 members expressed in synapses are important in neurotransmission termination and clearance [94]. In this family, SLC6A15-encoded B^0AT2 is mainly expressed in neurons and astrocytes [95], where the major substrates are proline, methionine, isoleucine and leucine. Its affinity to L-histidine is low (millimolar values of Km) [100]. NTT4 (SLC6A17) is identified only in the nervous system, especially in synaptic vesicles, with a Km of 1-2 mM for proline and glycine and interestingly no affinity for L-His [43]. L-histidine can self-inhibit its transport, while the uptake kinetics for L-histidine is unknown. According to the affinity of other amino acid substrates, the apparent affinity of NTT4 for L-histidine is relatively low [101].

PHT1 may also contribute to the uptake of L-histidine in neuronal cells. PHT1 proteins are detected in brain and eye [5, 6, 102]. A recent study showed that PHT1 had an age-dependent increase in brain expression, in contrast to PEPT2 which decreased over time. The increasing expression of PHT1 from neonate to adult age was similar to the function and localization progression of the histaminergic system [50-54]. Moreover, the function of PHT1 dominated in adult rodents, suggesting a significant role in regulating both endogenous and exogenous L-histidine and Peptides/mimetics in brain [49].

2.3 Histamine in the central nervous system (CNS)

Histamine is an organic nitrogenous compound, formed from the decarboxylation of histidine by the enzyme L-histidine decarboxylase (HDC). It is a hydrophilic vasoactive amine. Histamine is generated by various cells throughout

18

the body, including CNS neurons, gastric mucosa parietal cells, mast cells, basophils and lymphocytes [103]. After formation, histamine is preferentially inactivated by histamine-N-methyltransferase in brain, but it can also be inactivated by diamine oxidase. (Figure 2-5) Tele-methylhistamine is the major metabolite of histamine. The fluctuations of both histamine and tele-methylhistamine provide the activity of the histaminergic system [104].

Under normal physiological conditions, availability of amino acids in the CNS is not a rate-limiting step for the synthesis of brain proteins and neurotransmitters [82]. However, this may not be the case for some diseases. Significant changes in brain histamine levels have been observed in several neurological diseases, such as multiple sclerosis, Alzheimer's disease, Down's syndrome and Wernicke's encephalopathy [105]. The activity of HDC and L-histidine transporters may both contribute to the pathological processes.

2.3.1 Histamine in nonneuronal tissues

Histamine plays a central role in local immune responses, including allergy and inflammation, immunomodulation and autoimmunity [105]. It can cause dilation and permeability enhancement of substances across the blood vessels, and regulate the functions of monocytes, dendritic cells, T cells and B cells [103]. In peripheral tissues, mast cells along the blood vessels and the enteric mucosa can store and release histamine. Together with other signaling molecules, histamine is crucial to the immune response [106].

Histamine is a regulator in the gastrointestinal tract, controlling gastric acid secretion as a local stimulator [107]. The discovery of histamine receptors revolutionized the treatment of stomach ulcers [108].

2.3.2 Mast cells

Histamine hardly passes through the barrier systems of the brain [109]. In the CNS, histamine is synthesized by mast cells and histaminergic neurons, under the availability of L-histidine [110-112].

Mast cells reside mainly on the brain side of the blood-brain barrier (BBB) [113], concentrated along the blood vessels in thalamus [114], hippocampus and entorhinal cortex [115]. The study by Goldschmidt [116] showed that mast cells contributed up to 90% of the histamine in thalamus, and up to 50% of whole brain histamine levels in mice. Mast cell-deficient rat also showed reduced histamine content compared with wildtype rat [117]. Under LPS-induced sepsis, histamine production in mast cell-deficient mice could reach the same level as wildtype mice [118].

However, the detailed regulation and contribution of mast cells in histamine production in adult animals is not clear. It was suggested by the Panula group that mast cells were the origin of histamine production only during the first postnatal days (until postnatal day 4), responsible for the transient peak of histamine level in the developing rat brain [119, 120]. Later in adulthood, the histamine-storing mature mast cells no longer expressed clearly detectable HDC, which might only act as a reservoir for brain histamine [119]. The number of mast cells in adult rodents fluctuates greatly in response to altered physiological conditions [121], varies

greatly between species, regions, time and behavioral state [105]. They can penetrate brain blood vessels and migrate rapidly between blood and brain [121].

2.3.3 Histaminergic system

The histaminergic somata only exist in tuberomamillary nucleus (TMN) and the adjacent areas of posterior hypothalamus. Starting from there, the histaminergic fibers have projections to the whole CNS, similar to other amine systems (Figure 2-6). The TMN is a subnucleus of the posterior third of the hypothalamus, located at the tuber cinereum between the mammillary bodies and the optic chiasm (Figure 2-7). The histaminergic system was first characterized in rat brain. TMN is divided into different subdivisions according to the accumulation of histaminergic neurons. TMN includes the ventral part (TMV) at the rostral and caudal sides of mammillary bodies, a medial part (TMM) around the mammillary recess, and the diffuse part [122]. The subdivisions respond differently to environmental stimuli, connected by scattered neurons [122, 123]. The location and structure of histaminergic neurons in mouse is similar to that of rat, only with smaller soma size and density [124].

Using retrograde and anterograde tracing techniques, histaminergic neurons were found to form a relatively loose network of fine varicose axons [111, 122], reaching the whole CNS through two ascending and one descending bundles. (Figure 6) One of the ascending bundles reaches the hypothalamus, the diagonal band, the olfactory bulb, hippocampus and cortex along the ventral surface; the other ascending bundle goes to the thalamus, basal ganglia, hippocampus, amygdala and cortex. The descending bundle reaches the brain stem and spinal cord [105]. A variety of neuronal, humoral and paracrine signals can provide afferent input for the

histaminergic neurons. Their target is the dendrites radiating out from the nucleus, overlapping with the TMN projections [125].

The histaminergic system in brain changes during development. In embryonic mouse and rat, a transient neuronal system first appears to synthesize histamine and serotonin, with peak expression at E16 followed by gradual decline until E20 [51]. Later in the postnatal period, the TMN system takes part in histamine production, which develops to steady state levels around 2-3 weeks postnatal [50, 51, 54]. The transient neuronal system undergoes some transformation, and then stops synthesizing histamine. The expression of histamine receptors is also age-dependent; they start to be detected in the rat CNS since embryonic period (E14-E15), and then the number of receptor sites gradually increases with age [53, 119].

2.3.4 Histamine receptors

Four histamine receptor types (H1R-H4R) have been identified as far, all of them being G protein coupled receptors (GPCRs). H1R-H3R are abundantly expressed in the brain. H4R mainly exists in peripheral tissues (blood, spleen, lung, liver, and gut) [119, 126]. Using isotope binding, H1R was densely located in hypothalamus, aminergic and cholinergic brainstem nuclei, thalamus, hippocampus and cortex, where they relate to neuroendocrine, behavioral and nutritional state control [105]. The highest density of H2R was found in hippocampus, basal ganglia and cortex [127]. H2R contributed to the regulation of nociception, cognition, gastric acid secretion and immune function [108]. H3R was expressed in the globus pallidus, anterior parts of the cerebral cortex, hippocampus, olfactory tubercles, cerebellum and brain stem in the human brain [105, 127]. Unlike H1R and H2R, H3R has

constitutive activity *in vivo*. H3R can feedback inhibit the release of histamine, as well as control some other neurotransmitters (biogenic amines, acetylcholine, glutamate, GABA and peptidergic systems) [105, 128].

2.3.5 Function of histamine

Histamine plays a very important role in the CNS, regulating many physiological activities, such as the sleep-wake cycle, biological rhythms, neuroendocrine regulation, body weight, energy metabolism, as well as some higher brain functions (e.g. cognition, mood, learning and memory) [105, 129]. Histamine also participates in many pathological and pathophysiological processes in the CNS, although the mechanism is not clearly understood. Changes in histamine blood concentrations may cause disorders in many physiological activities such as sleep, eating, or mood disorders. In Alzheimer's disease (AD) patients, blood histamine levels can be indicator of disease severity, which may be caused by up-regulation of the histaminergic system as the global deterioration scale (GDS) stage gets higher. For patients with vascular dementia (VD), blood histamine level decrease as the disease gets more severe [129]. As these diseases progress, the level of H1R binding was lower. A similar phenomenon was also found during aging, schizophrenia and depression[105].
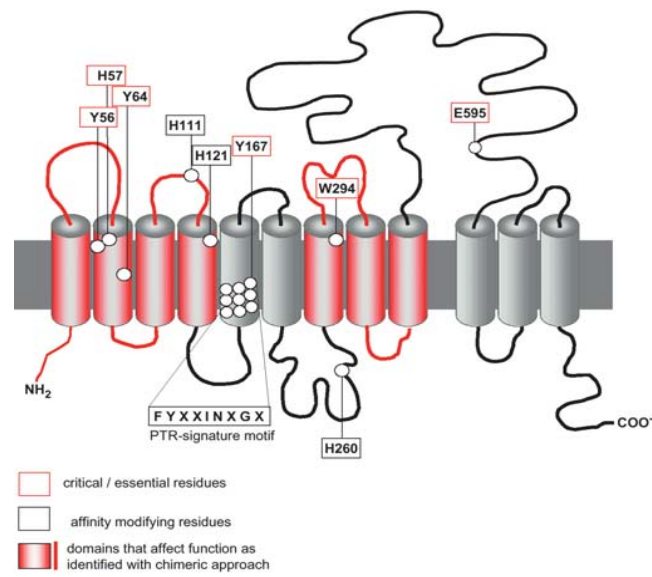
Figure 2-1. Membrane topology model of PEPT1. [1]
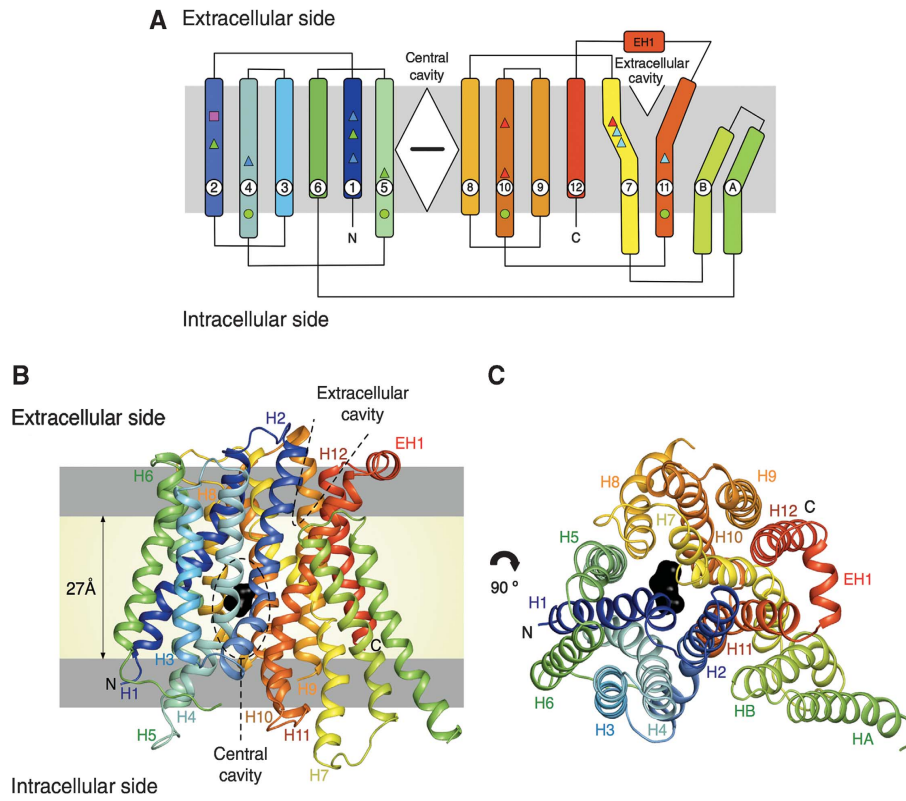
Figure 2-2. Structure of PEPT$_{so}$ and putative substrate binding site [19].
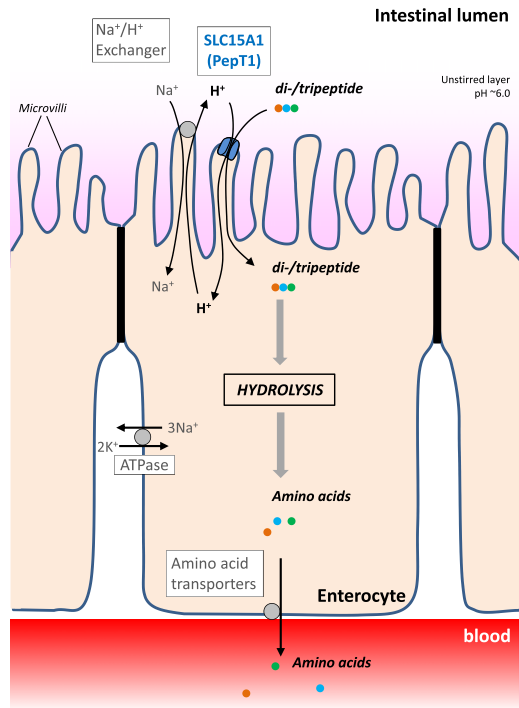
Figure 2-3. Peptide transporters driven by H⁺ gradient [9].
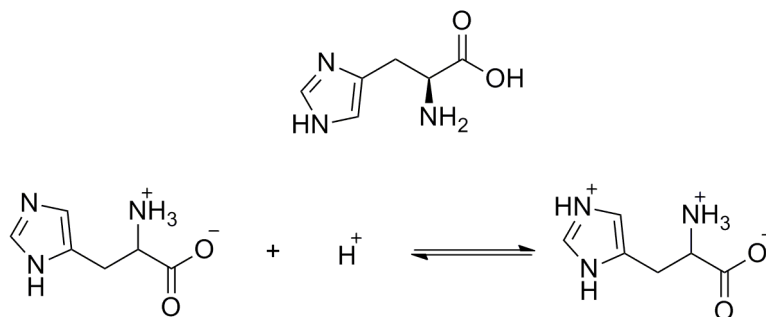
Figure 2-4. Molecular structure of L-histidine (upper panel) and histidine protonation equilibrium (lower panel)
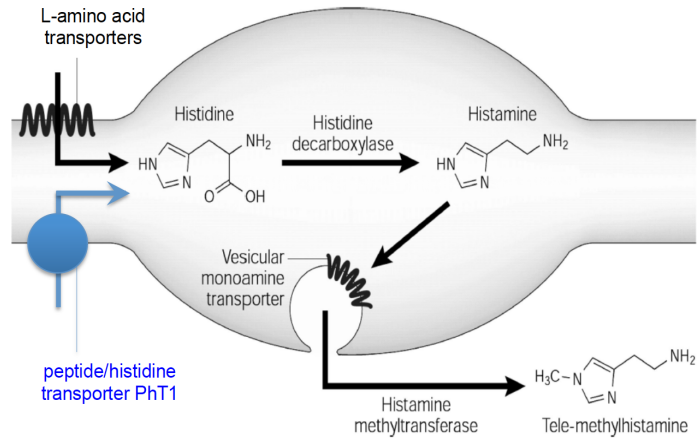
Figure 2-5. Schematic of histamine homeostasis. [105]
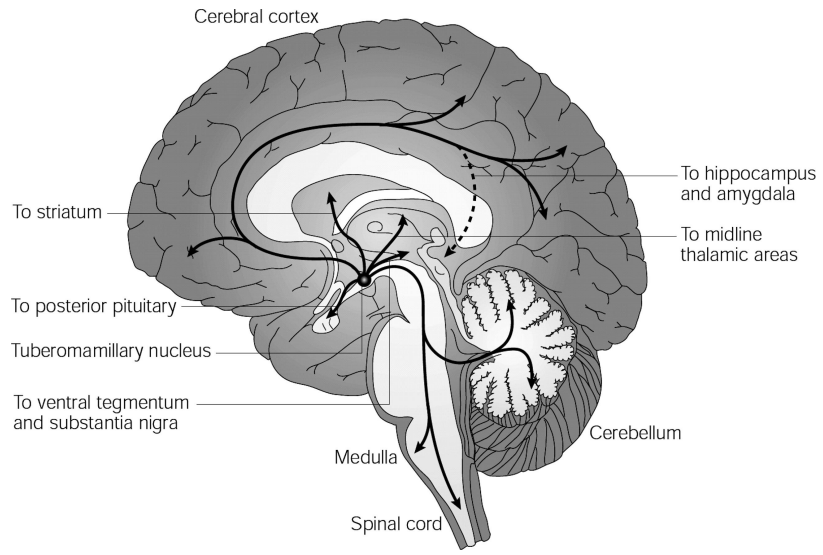
Figure 2-6. The histaminergic system in the human brain. [105]
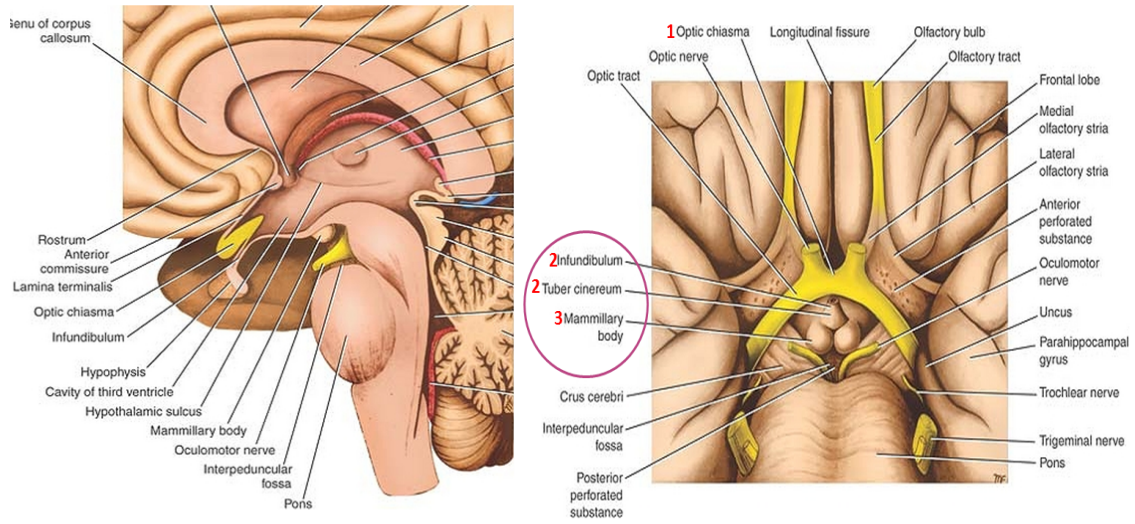
Figure 2-7. Structures of hypothalamus and tuber cinereum in the human brain.

(http://teachinganatomy.blogspot.com/2013/01/Hypothalamus-anatomy-

subdivisions-nuclei-and-connections.html)

REFERENCE

1. Daniel, H. and G. Kottra, *The proton oligopeptide cotransporter family SLC15 in physiology and pharmacology.* Pflugers Arch, 2004. **447**(5): p. 610-8.

2. Fei, Y.J., et al., *Expression cloning of a mammalian proton-coupled oligopeptide transporter.* Nature, 1994. **368**(6471): p. 563-6.

3. Boll, M., et al., *Expression cloning of a cDNA from rabbit small intestine related to proton-coupled transport of peptides, beta-lactam antibiotics and ACE-inhibitors.* Pflugers Arch, 1994. **429**(1): p. 146-9.

4. Liu, W., et al., *Molecular cloning of PEPT 2, a new member of the H+/peptide cotransporter family, from human kidney.* Biochim Biophys Acta, 1995. **1235**(2): p. 461-6.

5. Yamashita, T., et al., *Cloning and functional expression of a brain peptide/histidine transporter.* J Biol Chem, 1997. **272**(15): p. 10205-11.

6. Sakata, K., et al., *Cloning of a lymphatic peptide/histidine transporter.* Biochem J, 2001. **356**(Pt 1): p. 53-60.

7. Wang, M., et al., *Comparative analysis of vertebrate PEPT1 and PEPT2 genes.* Genetica, 2010. **138**(6): p. 587-99.

8. Botka, C.W., et al., *Human proton/oligopeptide transporter (POT) genes: identification of putative human genes using bioinformatics.* AAPS PharmSci, 2000. **2**(2): p. E16.

9. Smith, D.E., B. Clemencon, and M.A. Hediger, *Proton-coupled oligopeptide transporter family SLC15: physiological, pharmacological and pathological implications.* Mol Aspects Med, 2013. **34**(2-3): p. 323-36.

10. Covitz, K.M., G.L. Amidon, and W. Sadee, *Membrane topology of the human dipeptide transporter, hPEPT1, determined by epitope insertions.* Biochemistry, 1998. **37**(43): p. 15214-21.

11. Rubio-Aliaga, I. and H. Daniel, *Mammalian peptide transporters as targets for drug delivery.* Trends Pharmacol Sci, 2002. **23**(9): p. 434-40.

12. Terada, T., et al., *N-terminal halves of rat H+/peptide transporters are responsible for their substrate recognition.* Pharm Res, 2000. **17**(1): p. 15-20.

13. Meredith, D. and R.A. Price, *Molecular modeling of PepT1--towards a structure.* J Membr Biol, 2006. **213**(2): p. 79-88.

14. Bolger, M.B., et al., *Structure, function, and molecular modeling approaches to the study of the intestinal dipeptide transporter PepT1.* J Pharm Sci, 1998. **87**(11): p. 1286-91.

15. Yeung, A.K., et al., *Molecular identification of a role for tyrosine 167 in the function of the human intestinal proton- coupled dipeptide transporter (hPepT1).* Biochem Biophys Res Commun, 1998. **250**(1): p. 103-7.

16. Chen, X.Z., A. Steel, and M.A. Hediger, *Functional roles of histidine and tyrosine residues in the H(+)-peptide transporter PepT1.* Biochem Biophys Res Commun, 2000. **272**(3): p. 726-30.

17. Hauser, M., et al., *Substrate preference is altered by mutations in the fifth transmembrane domain of Ptr2p, the di/tri-peptide transporter of Saccharomyces cerevisiae.* Mol Membr Biol, 2005. **22**(3): p. 215-27.

18. Newstead, S., et al., *Crystal structure of a prokaryotic homologue of the mammalian oligopeptide-proton symporters, PepT1 and PepT2.* EMBO J, 2011. **30**(2): p. 417-26.

19. Newstead, S., *Towards a structural understanding of drug and peptide transport within the proton-dependent oligopeptide transporter (POT) family.* Biochem Soc Trans, 2011. **39**(5): p. 1353-8.

20. Doring, F., et al., *Minimal molecular determinants of substrates for recognition by the intestinal peptide transporter.* J Biol Chem, 1998. **273**(36): p. 23211-8.

21. Brandsch, M., I. Knutter, and E. Bosse-Doenecke, *Pharmaceutical and pharmacological importance of peptide transporters.* J Pharm Pharmacol, 2008. **60**(5): p. 543-85.

22. Amasheh, S., et al., *Transport of charged dipeptides by the intestinal H+/peptide symporter PepT1 expressed in Xenopus laevis oocytes.* J Membr Biol, 1997. **155**(3): p. 247-56.

23. Bhardwaj, R.K., et al., *The functional evaluation of human peptide/histidine transporter 1 (hPHT1) in transiently transfected COS-7 cells.* Eur J Pharm Sci, 2006. **27**(5): p. 533-42.

24. Daniel, H., C. Fett, and A. Kratz, *Demonstration and modification of intervillous pH profiles in rat small intestine in vitro.* Am J Physiol, 1989. **257**(4 Pt 1): p. G489-95.

25. Daniel, H., *Function and molecular structure of brush border membrane peptide/H+ symporters.* J Membr Biol, 1996. **154**(3): p. 197-203.

26. Nussberger, S., et al., *Symmetry of H+ binding to the intra- and extracellular side of the H+-coupled oligopeptide cotransporter PepT1.* J Biol Chem, 1997. **272**(12): p. 7777-85.

27. Thwaites, D.T. and C.M. Anderson, *H+-coupled nutrient, micronutrient and drug transporters in the mammalian small intestine.* Exp Physiol, 2007. **92**(4): p. 603-19.

28. Jappar, D., et al., *Significance and regional dependency of peptide transporter (PEPT) 1 in the intestinal permeability of glycylsarcosine: in situ single-pass perfusion studies in wild-type and Pept1 knockout mice.* Drug Metab Dispos, 2010. **38**(10): p. 1740-6.

29. Ogihara, H., et al., *Immuno-localization of H+/peptide cotransporter in rat digestive tract.* Biochem Biophys Res Commun, 1996. **220**(3): p. 848-52.

30. Liang, R., et al., *Human intestinal H+/peptide cotransporter. Cloning, functional expression, and chromosomal localization.* J Biol Chem, 1995. **270**(12): p. 6456-63.

31. Fei, Y.J., et al., *cDNA structure, genomic organization, and promoter analysis of the mouse intestinal peptide transporter PEPT1.* Biochim Biophys Acta, 2000. **1492**(1): p. 145-54.

32. Groneberg, D.A., et al., *Intestinal peptide transport: ex vivo uptake studies and localization of peptide carrier PEPT1.* Am J Physiol Gastrointest Liver Physiol, 2001. **281**(3): p. G697-704.

33. Miyamoto, K., et al., *Sequence, tissue distribution and developmental changes in rat intestinal oligopeptide transporter.* Biochim Biophys Acta, 1996. **1305**(1-2): p. 34-8.

34. Shen, H., D.E. Smith, and F.C. Brosius, 3rd, *Developmental expression of PEPT1 and PEPT2 in rat small intestine, colon, and kidney.* Pediatr Res, 2001. **49**(6): p. 789-95.

35. Ogihara, H., et al., *Peptide transporter in the rat small intestine: ultrastructural localization and the effect of starvation and administration of amino acids.* Histochem J, 1999. **31**(3): p. 169-74.

36. Shiraga, T., et al., *Cellular and molecular mechanisms of dietary regulation on rat intestinal H+/Peptide transporter PepT1.* Gastroenterology, 1999. **116**(2): p. 354-62.

37. Merlin, D., et al., *Colonic epithelial hPepT1 expression occurs in inflammatory bowel disease: transport of bacterial peptides influences expression of MHC class 1 molecules.* Gastroenterology, 2001. **120**(7): p. 1666-79.

38. Wuensch, T., et al., *The peptide transporter PEPT1 is expressed in distal colon in rodents and humans and contributes to water absorption.* Am J Physiol Gastrointest Liver Physiol, 2013. **305**(1): p. G66-73.

39. Wuensch, T., et al., *Colonic Expression of the Peptide Transporter PEPT1 Is Downregulated During Intestinal Inflammation and Is Not Required for NOD2-dependent Immune Activation.* Inflamm Bowel Dis, 2014. **20**(4): p. 671-84.

40. Smith, D.E., et al., *Tubular localization and tissue distribution of peptide transporters in rat kidney.* Pharm Res, 1998. **15**(8): p. 1244-9.

41. Lu, H. and C. Klaassen, *Tissue distribution and thyroid hormone regulation of Pept1 and Pept2 mRNA in rodents.* Peptides, 2006. **27**(4): p. 850-7.

42. Smith, P.D., et al., *Intestinal macrophages lack CD14 and CD89 and consequently are down-regulated for LPS- and IgA-mediated activities.* J Immunol, 2001. **167**(5): p. 2651-6.

43. Gonzalez, D.E., et al., *An oligopeptide transporter is expressed at high levels in the pancreatic carcinoma cell lines AsPc-1 and Capan-2.* Cancer Res, 1998. **58**(3): p. 519-25.

44. Shen, H., et al., *Localization of PEPT1 and PEPT2 proton-coupled oligopeptide transporter mRNA and protein in rat kidney.* Am J Physiol, 1999. **276**(5 Pt 2): p. F658-65.

45. Shen, H., et al., *Immunolocalization of the proton-coupled oligopeptide transporter PEPT2 in developing rat brain.* Mol Pharm, 2004. **1**(4): p. 248-56.

46. Hu, Y., et al., *Peptide transporter 2 (PEPT2) expression in brain protects against 5-aminolevulinic acid neurotoxicity.* J Neurochem, 2007. **103**(5): p. 2058-65.

47. Kamal, M.A., R.F. Keep, and D.E. Smith, *Role and relevance of PEPT2 in drug disposition, dynamics, and toxicity.* Drug Metab Pharmacokinet, 2008. **23**(4): p. 236-42.

48. Herrera-Ruiz, D., et al., *Spatial expression patterns of peptide transporters in the human and rat gastrointestinal tracts, Caco-2 in vitro cell culture model, and multiple human tissues.* AAPS PharmSci, 2001. **3**(1): p. E9.

49. Hu, Y., et al., *Divergent Developmental Expression and Function of the Proton-Coupled Oligopeptide Transporters PepT2 and PhT1 in Regional Brain Slices of Mouse and Rat.* J Neurochem, 2014. **129**(6): p. 955-965.

50. Martres, M.P., M. Baudry, and J.C. Schwartz, *Histamine synthesis in the developing rat brain: evidence for a multiple compartmentation.* Brain Res, 1975. **83**(2): p. 261-75.

51. Reiner, P.B., et al., *Ontogeny of histidine-decarboxylase-immunoreactive neurons in the tuberomammillary nucleus of the rat hypothalamus: time of origin and development of transmitter phenotype.* J Comp Neurol, 1988. **276**(2): p. 304-11.

52. Subramanian, N., et al., *Ontogeny of histaminergic neurotransmission in the rat brain: concomitant development of neuronal histamine, H-1 receptors, and H-1 receptor-mediated stimulation of phospholipid turnover.* J Neurochem, 1981. **36**(3): p. 1137-41.

53. Tran, V.T., et al., *Ontogenetic development of histamine H1-receptor binding in rat brain.* J Neurochem, 1980. **34**(6): p. 1609-13.

54. Toledo, A., et al., *Properties and ontogenic development of membrane-bound histidine decarboxylase from rat brain.* J Neurochem, 1988. **51**(5): p. 1400-6.

55. Blasius, A.L., et al., *Slc15a4, AP-3, and Hermansky-Pudlak syndrome proteins are required for Toll-like receptor signaling in plasmacytoid dendritic cells.* Proc Natl Acad Sci U S A, 2010. **107**(46): p. 19973-8.

56. Lee, J., et al., *pH-dependent internalization of muramyl peptides from early endosomes enables Nod1 and Nod2 signaling.* J Biol Chem, 2009. **284**(35): p. 23818-29.

57. Romano, A., et al., *Functional expression of SLC15 peptide transporters in rat thyroid follicular cells.* Mol Cell Endocrinol, 2010. **315**(1-2): p. 174-81.

58. Everaert, I., et al., *Gene expression of carnosine-related enzymes and transporters in skeletal muscle.* Eur J Appl Physiol, 2013. **113**(5): p. 1169-79.

59. Sasawatari, S., et al., *The solute carrier family 15A4 regulates TLR9 and NOD1 functions in the innate immune system and promotes colitis in mice.* Gastroenterology, 2011. **140**(5): p. 1513-25.

60. Baccala, R., et al., *Essential requirement for IRF8 and SLC15A4 implicates plasmacytoid dendritic cells in the pathogenesis of lupus.* Proc Natl Acad Sci U S A, 2013. **110**(8): p. 2940-5.

61. Dosenovic, P., et al., *Slc15a4 function is required for intact class switch recombination to IgG2c in response to TLR9 stimulation.* Immunol Cell Biol, 2014.

62. Han, J.W., et al., *Genome-wide association study in a Chinese Han population identifies nine new susceptibility loci for systemic lupus erythematosus.* Nat Genet, 2009. **41**(11): p. 1234-7.

63. Lee, H.S., et al., *Ethnic specificity of lupus-associated loci identified in a genome-wide association study in Korean women.* Ann Rheum Dis, 2014. **73**(6): p. 1240-5.

64. Wang, C., et al., *Genes identified in Asian SLE GWASs are also associated with SLE in Caucasian populations.* Eur J Hum Genet, 2013. **21**(9): p. 994-9.

65. Kopple, J.D. and M.E. Swendseid, *Evidence that histidine is an essential amino acid in normal and chronically uremic man.* J Clin Invest, 1975. **55**(5): p. 881-91.

66. Stifel, F.B. and R.H. Herman, *Histidine metabolism.* Am J Clin Nutr, 1971. **24**(2): p. 207-17.

67. Lajtha, A., *Amino acid transport in the brain in vivo and in vitro*, G.E.W. Wolstenholme and D.W. Fitzsimons, Editors. 1974, John Wiley & Sons, Ltd.: Chichester, UK.

68. Engelhardt, B. and L. Sorokin, *The blood-brain and the blood-cerebrospinal fluid barriers: function and dysfunction.* Semin Immunopathol, 2009. **31**(4): p. 497-511.

69. Smith, Q.R., *Transport of glutamate and other amino acids at the blood-brain barrier.* J Nutr, 2000. **130**(4S Suppl): p. 1016S-22S.

70.   Usui, T., et al., *Beta-alanine and l-histidine transport across the inner blood-retinal barrier: potential involvement in L-carnosine supply.* Exp Eye Res, 2013. **113**: p. 135-42.

71.   Broer, A., et al., *The heterodimeric amino acid transporter 4F2hc/y+LAT2 mediates arginine efflux in exchange with glutamine.* Biochem J, 2000. **349 Pt 3**: p. 787-95.

72.   Hawkins, R.A., et al., *Structure of the blood-brain barrier and its role in the transport of amino acids.* J Nutr, 2006. **136**(1 Suppl): p. 218S-26S.

73.   Smith, Q.R., et al., *Kinetics of neutral amino acid transport across the blood-brain barrier.* J Neurochem, 1987. **49**(5): p. 1651-8.

74.   White, M.F., *The transport of cationic amino acids across the plasma membrane of mammalian cells.* Biochim Biophys Acta, 1985. **822**(3-4): p. 355-74.

75.   O'Kane, R.L. and R.A. Hawkins, *Na+-dependent transport of large neutral amino acids occurs at the abluminal membrane of the blood-brain barrier.* Am J Physiol Endocrinol Metab, 2003. **285**(6): p. E1167-73.

76.   Christensen, H.N., *Role of amino acid transport and countertransport in nutrition and metabolism.* Physiol Rev, 1990. **70**(1): p. 43-77.

77.   Albers, A., et al., *Na+ transport by the neural glutamine transporter ATA1.* Pflugers Arch, 2001. **443**(1): p. 92-101.

78.   Fei, Y.J., et al., *Primary structure, genomic organization, and functional and electrogenic characteristics of human system N 1, a Na+- and H+-coupled glutamine transporter.* J Biol Chem, 2000. **275**(31): p. 23707-17.

79.   Nakanishi, T., et al., *Structure, function, and tissue expression pattern of human SN2, a subtype of the amino acid transport system N.* Biochem Biophys Res Commun, 2001. **281**(5): p. 1343-8.

80.   Vanslambrouck, J.M., et al., *Renal imino acid and glycine transport system ontogeny and involvement in developmental iminoglycinuria.* Biochem J, 2010. **428**(3): p. 397-407.

81.   Smith, D.E., C.E. Johanson, and R.F. Keep, *Peptide and peptide analog transport systems at the blood-CSF barrier.* Adv Drug Deliv Rev, 2004. **56**(12): p. 1765-91.

82.   Redzic, Z., *Molecular biology of the blood-brain and the blood-cerebrospinal fluid barriers: similarities and differences.* Fluids Barriers CNS, 2011. **8**(1): p. 3.

83.   Duelli, R., et al., *Expression of large amino acid transporter LAT1 in rat brain endothelium.* J Cereb Blood Flow Metab, 2000. **20**(11): p. 1557-62.

84.   Ho, H.T., A. Dahlin, and J. Wang, *Expression Profiling of Solute Carrier Gene Families at the Blood-CSF Barrier.* Front Pharmacol, 2012. **3**: p. 154.

85.   Kasai, Y., et al., *Transport systems of serine at the brain barriers and in brain parenchymal cells.* J Neurochem, 2011. **118**(2): p. 304-13.

86.   Novotny, A., et al., *Mechanisms of 5-aminolevulinic acid uptake at the choroid plexus.* J Neurochem, 2000. **75**(1): p. 321-8.

87.   Fujita, T., et al., *Interaction of kyotorphin and brain peptide transporter in synaptosomes prepared from rat cerebellum: implication of high affinity type H+/peptide transporter PEPT2 mediated transport system.* Neurosci Lett, 1999. **271**(2): p. 117-20.

88.   Teuscher, N.S., R.F. Keep, and D.E. Smith, *PEPT2-mediated uptake of neuropeptides in rat choroid plexus.* Pharm Res, 2001. **18**(6): p. 807-13.

89.   Teuscher, N.S., et al., *Functional evidence for presence of PEPT2 in rat choroid plexus: studies with glycylsarcosine.* J Pharmacol Exp Ther, 2000. **294**(2): p. 494-9.

90.   He, L., K. Vasiliou, and D.W. Nebert, *Analysis and update of the human solute carrier (SLC) gene superfamily.* Hum Genomics, 2009. **3**(2): p. 195-206.

91.   Schioth, H.B., et al., *Evolutionary origin of amino acid transporter families SLC32, SLC36 and SLC38 and physiological, pathological and therapeutic aspects.* Mol Aspects Med, 2013. **34**(2-3): p. 571-85.

92.   Hagglund, M.G., et al., *Identification of SLC38A7 (SNAT7) protein as a glutamine transporter expressed in neurons.* J Biol Chem, 2011. **286**(23): p. 20500-11.

93.   Fredriksson, R., et al., *The solute carrier (SLC) complement of the human genome: phylogenetic classification reveals four major families.* FEBS Lett, 2008. **582**(27): p. 3811-6.

94.   Hagglund, M.G., et al., *Characterization of the transporterB0AT3 (Slc6a17) in the rodent central nervous system.* BMC Neurosci, 2013. **14**: p. 54.

95.   Hagglund, M.G., et al., *B(0)AT2 (SLC6A15) is localized to neurons and astrocytes, and is involved in mediating the effect of leucine in the brain.* PLoS One, 2013. **8**(3): p. e58651.

96.   Reimer, R.J., et al., *Amino acid transport system A resembles system N in sequence but differs in mechanism.* Proc Natl Acad Sci U S A, 2000. **97**(14): p. 7715-20.

97.   Sundberg, B.E., et al., *The evolutionary history and tissue mapping of amino acid transporters belonging to solute carrier families SLC32, SLC36, and SLC38.* J Mol Neurosci, 2008. **35**(2): p. 179-93.

98.   Conti, F. and M. Melone, *The glutamine commute: lost in the tube?* Neurochem Int, 2006. **48**(6-7): p. 459-64.

99.   Hatanaka, T., et al., *Evidence for the transport of neutral as well as cationic amino acids by ATA3, a novel and liver-specific subtype of amino acid transport system A.* Biochim Biophys Acta, 2001. **1510**(1-2): p. 10-7.

100. Broer, A., et al., *The orphan transporter v7-3 (slc6a15) is a Na+-dependent neutral amino acid transporter (B0AT2).* Biochem J, 2006. **393**(Pt 1): p. 421-30.

101. Zaia, K.A. and R.J. Reimer, *Synaptic Vesicle Protein NTT4/XT1 (SLC6A17) Catalyzes Na+-coupled Neutral Amino Acid Transport.* J Biol Chem, 2009. **284**(13): p. 8439-48.

102. Ocheltree, S.M., et al., *Preliminary investigation into the expression of proton-coupled oligopeptide transporters in neural retina and retinal pigment epithelium (RPE): lack of functional activity in RPE plasma membranes.* Pharm Res, 2003. **20**(9): p. 1364-72.

103. Jutel, M., K. Blaser, and C.A. Akdis, *The role of histamine in regulation of immune responses.* Chem Immunol Allergy, 2006. **91**: p. 174-87.

104. Miyamoto, Y., et al., *Simultaneous fluorometric measurement of histamine and tele-methylhistamine levels in rodent brain by high-performance liquid chromatography.* Anal Biochem, 2004. **334**(1): p. 89-96.

105. Haas, H.L., O.A. Sergeeva, and O. Selbach, *Histamine in the nervous system.* Physiol Rev, 2008. **88**(3): p. 1183-241.

106. Ennis, M., et al., *Inhibition of histamine secretion from mast cells.* Nature, 1981. **289**(5794): p. 186-7.

107. Barocelli, E. and V. Ballabeni, *Histamine in the control of gastric acid secretion: a topic review.* Pharmacol Res, 2003. **47**(4): p. 299-304.

108. Black, J.W., et al., *Definition and antagonism of histamine H 2 -receptors.* Nature, 1972. **236**(5347): p. 385-90.

109. Schwartz, J.C., et al., *Histaminergic transmission in the mammalian brain.* Physiol Rev, 1991. **71**(1): p. 1-51.

110. Watanabe, T., et al., *Evidence for the presence of a histaminergic neuron system in the rat brain: an immunohistochemical analysis.* Neurosci Lett, 1983. **39**(3): p. 249-54.

111. Watanabe, T., et al., *Distribution of the histaminergic neuron system in the central nervous system of rats; a fluorescent immunohistochemical analysis with histidine decarboxylase as a marker.* Brain Res, 1984. **295**(1): p. 13-25.

112. Panula, P., H.Y. Yang, and E. Costa, *Histamine-containing neurons in the rat hypothalamus.* Proc Natl Acad Sci U S A, 1984. **81**(8): p. 2572-6.

113. Silver, R. and J.P. Curley, *Mast cells on the mind: new insights and opportunities.* Trends Neurosci, 2013. **36**(9): p. 513-21.

114. Hough, L.B., et al., *Normal levels of histamine and tele-methylhistamine in mast cell-deficient mouse brain.* Brain Res, 1984. **292**(1): p. 133-8.

115. Chikahisa, S., et al., *Histamine from brain resident MAST cells promotes wakefulness and modulates behavioral states.* PLoS One, 2013. **8**(10): p. e78434.

116. Goldschmidt, R.C., L.B. Hough, and S.D. Glick, *Rat brain mast cells: contribution to brain histamine levels.* J Neurochem, 1985. **44**(6): p. 1943-7.

117. Sugimoto, K., et al., *Brain histaminergic system in mast cell-deficient (Ws/Ws) rats: histamine content, histidine decarboxylase activity, and effects of (S) alpha-fluoromethylhistidine.* J Neurochem, 1995. **65**(2): p. 791-7.

118. Nautiyal, K.M., et al., *Mast cells are necessary for the hypothermic response to LPS-induced sepsis.* Am J Physiol Regul Integr Comp Physiol, 2009. **296**(3): p. R595-602.

119. Panula, P., M. Sundvik, and K. Karlstedt, *Developmental roles of brain histamine.* Trends Neurosci, 2014. **37**(3): p. 159-68.

120. Panula, P. and S. Nuutinen, *The histaminergic network in the brain: basic organization and role in disease.* Nat Rev Neurosci, 2013. **14**(7): p. 472-87.

121. Silverman, A.J., et al., *Mast cells migrate from blood to brain.* J Neurosci, 2000. **20**(1): p. 401-8.

122. Ericson, H., T. Watanabe, and C. Kohler, *Morphological analysis of the tuberomammillary nucleus in the rat brain: delineation of subgroups with antibody against L-histidine decarboxylase as a marker.* J Comp Neurol, 1987. **263**(1): p. 1-24.

123. Inagaki, N., et al., *An analysis of histaminergic efferents of the tuberomammillary nucleus to the medial preoptic area and inferior colliculus of the rat.* Exp Brain Res, 1990. **80**(2): p. 374-80.

124. Parmentier, R., et al., *Anatomical, physiological, and pharmacological characteristics of histidine decarboxylase knock-out mice: evidence for the role of brain histamine in behavioral and sleep-wake control.* J Neurosci, 2002. **22**(17): p. 7695-711.

125. Ericson, H., A. Blomqvist, and C. Kohler, *Origin of neuronal inputs to the region of the tuberomammillary nucleus of the rat brain.* J Comp Neurol, 1991. **311**(1): p. 45-64.

126. de Esch, I.J., et al., *The histamine H4 receptor as a new therapeutic target for inflammation.* Trends Pharmacol Sci, 2005. **26**(9): p. 462-9.

127. Martinez-Mir, M.I., et al., *Three histamine receptors (H1, H2 and H3) visualized in the brain of human and non-human primates.* Brain Res, 1990. **526**(2): p. 322-7.

128. Morisset, S., et al., *High constitutive activity of native H3 receptors regulates histamine neurons in brain.* Nature, 2000. **408**(6814): p. 860-4.

129. Fernandez-Novoa, L. and R. Cacabelos, *Histamine function in brain disorders.* Behav Brain Res, 2001. **124**(2): p. 213-33.

CHAPTER 3

A NOVEL ROLE FOR PHT1 IN THE DISPOSITION OF L-HISTIDINE IN BRAIN: *IN VITRO* SLICE AND *IN VIVO* PHARMACOKINETIC STUDIES IN WILDTYPE AND *PHT1* NULL MICE

3.1 Abstract

PHT1 (SLC15A4) is responsible for translocating L-histidine (L-His), di/tripeptides and peptide-like drugs across biological membranes. Previous studies have indicated that PHT1 is located in brain parenchyma, however, its role and significance in brain along with effect on the biodistribution of substrates is unknown. In this study, adult gender-matched *Pht1*-competent (wildtype) and *Pht1*-deficient (null) mice were used to investigate the effect of PHT1 on L-His brain disposition via *in vitro* slice and *in vivo* pharmacokinetic approaches. We also evaluated the serum clinical chemistry and expression levels of select transporters and enzymes in the two genotypes. No significant differences were observed between genotypes in serum chemistry, body weight, viability and fertility. PCR analyses indicated that *Pept2* had a compensatory up-regulation in *Pht1* null mice (about 2-fold) as compared to wildtype animals, which was consistent in different brain regions and confirmed by immunoblots. The uptake of L-His was reduced in brain slices by 50% during PHT1 ablation. The L-amino acid transporters

accounted for 30% of the uptake, and passive (other) pathways for 20% of the uptake. During the *in vivo* pharmacokinetic studies, plasma concentration-time profiles of L-His were comparable between the two genotypes after intravenous administration. Still, biodistribution studies revealed that, when sampled 5 min after dosing, L-His values were 28-48% lower in *Pht1* null mice, as compared to wildtype animals, in brain parenchyma but not cerebrospinal fluid. These findings suggest that PHT1 may play an important role in histidine transport in brain, and resultant effects on histidine/histamine homeostasis and neuropeptide regulation.

3.2 Introduction

PHT1 (SLC15A4), a member of the proton-coupled oligopeptide transporter (POT) superfamily, is responsible for translocating various di/tripeptides and peptide-like drugs across biological membranes, as well as the amino acid L-histidine [1]. Unlike two other peptide transporters, PEPT1 (SLC15A1) and PEPT2 (SLC15A2), which have been well studied, there is little known about PHT1 expression, localization, function and pharmacological relevance. PHT1 is abundantly found in the brain and eye [2, 3]. PHT1 has an age-dependent increase in brain expression [4], similar to the changes found in the histaminergic system [4-8]. In contrast, PEPT2 shows an age-dependent decrease in brain expression and PHT1 function dominated in the uptake of a dipeptide in brain slices from adult rodents, suggesting a significant role in regulating both endogenous and exogenous L-histidine (L-His) and peptides/mimetics in brain [9]. PHT1 transcripts are also detected in rat thyroid gland [10] and skeletal muscle [11]. A recent study showed that PHT1 and PHT2 are involved in the immune response [12]. These authors

reported that PHTs were preferentially expressed in dendritic cells, located at endosomes and lysosomes, mediating the release of bacterially derived components into the cytosol.

L-Histidine (L-His) is one of the proteinogenic amino acids, which is obtained from dietary metabolism and protein turnover [12]. L-His possesses several crucial biological functions, including formation of the myelin sheath, detoxification of heavy metals, and the manufacturing of white and red blood cells. It is also a precursor of histamine, carnosine, ergothioneine, and vitamin C [13]. Studies on the transport of L-His in brain would extend our understanding of neuropeptide regulation, histamine homeostasis, and potential targets for drug delivery to neuronal and non-neuronal cells. In the central nervous system (CNS), major transporters for L-His include the Na^+-coupled neutral amino acid transporters (e.g., SNATs, which belong to the SLC38 family) [14, 15], Na^+-independent amino acid transporters (e.g., LATs and CATs, which belong to the SLC7 family) [16, 17], some members of the Na^+-and Cl^--dependent neurotransmitter transporter family (e.g., B^0AT2 and NTT4, which belong to the SLC6 family) [18-20], as well as the peptide/histidine transporters (e.g., PHT1 and PHT2, which belong to the SLC15 family) [9, 21].

Histamine, one of the most important metabolites of L-His, is formed in the brain during catalysis by histidine decarboxylase (HDC). While much of the research effort has focused on the enzymatic production of histamine via HDC, little attention has been paid to the mechanism by which L-His gains entry into neurons. Due to its polarity and lack of a transport system, histamine cannot pass through the

barrier systems of the brain [22]. Moreover, the availability of its precursor, L-His, is positively correlated with brain histamine production and, consequently the regulatory functions of histamine [23, 24]. Significant changes in brain histamine levels have been observed in several neurological diseases, such as multiple sclerosis, Alzheimer's disease, Down's syndrome and Wernicke's encephalopathy [25]. Dysfunction of HDC and the L-His transporters in brain may be related to these neurological disorders.

In the present study, we hypothesized that PHT1 ablation would substantially reduce the uptake of L-His in the brain of adult mice. Initial phenotypic analyses were performed in *Pht1*-competent (wildtype) and *Pht1*-deficient (null) mice, along with gene expression levels of POTs and select transporter/enzyme proteins. Subsequent studies evaluated the functional activity of PHT1 by studying the *in vitro* uptake of L-His in regional brain slices, and the *in vivo* pharmacokinetics and biodistribution of L-His after intravenous administration.

3.3 Materials and methods

3.3.1 Chemicals

L-[^{3}H]histidine (500 mCi/mmol), L-[^{14}C]histidine (322 mCi/mmol), [^{14}C]mannitol (53 mCi/mmol) and [^{3}H]dextran-70,000 (110 mCi/mg) were purchased from American Radiolabeled Chemicals (St. Louis, MO). Unlabeled L-histidine, mannitol and dextran-70,000 were purchased from Sigma-Aldrich (St. Louis, MO). Protease inhibitor cocktail was purchased from Roche (Seattle, WA). Power SYBR Green PCR Master Mix was purchased from Applied Biosystems (Foster City, CA). All other chemicals were obtained from standard sources.

3.3.2 Animals

Gender- and age-matched *Pht1*-competent (wildtype or *Pht1$^{+/+}$*) and *Pht1*-deficient (null or *Pht1$^{-/-}$*) mice, 7-10 weeks old, were used in this study [26]. PCR analysis, using genomic DNA isolated from tail biopsies, was performed to confirm the subsequent production of *Pht1* null mice. The *Pht1* gene had a forward primer 5´-GATCGAGGTCCAGAAGCCACTCG-3´ and a reverse primer 5´-GAGTTGTGTCACTCACCCACTTCT-3´. The Neo gene, inserted during homologous recombination in *Pht1* null mice, had a forward primer 5´-GGAGAGGCTATTCGGCTATG-3´ and a reverse primer 5´-GCTCTTCAGCAATATCACGG-3´. All animals were bred on a C57BL/6 background ($\geq$ 99%). The mice were housed in a temperature-controlled environment with 12 h light and dark cycles, and received a standard diet and water ad libitum (Unit of Laboratory Animal Medicine, University of Michigan, Ann Arbor, MI). All mouse studies were performed in accordance with the Guide for the Care and Use of Laboratory Animals as adopted and promulgated by the U.S. National Institutes of Health.

3.3.3 Initial phenotypic analyses

Pht1 null mice were evaluated for body weight and serum clinical chemistry in comparison to those of wildtype mice (by Animal Diagnostic Core, ULAM, University of Michigan, Ann Arbor, MI), as described previously for *Pept1* null mice [27]. Viability and fertility were also monitored.

3.3.4 Gene and protein expression

Quantitation of POTs (*Pept1*, *Pept2*, *Pht1* and *Pht2*), select amino acid transporters (*Lat1*, *Snat1*, *Snat3* and *Ntt4*) and histidine decarboxylase (*Hdc*) was performed in several tissues of adult wildtype and *Pht1* null mice using a 7300 Real-Time PCR system (Applied Biosystems, Foster City, CA) [28]. Tissues of interest included cerebral cortex, cerebellum, hippocampus, hypothalamus and choroid plexus. In brief, 2.0 μg of total RNA, isolated using the RNeasy Plus Mini Kit (Qiagen, Valencia, CA), was reverse-transcribed into cDNA using the Omniscript RT Kit (Qiagen, Valencia, CA) with 16-mer random primers. The mouse *Gapdh* gene was used as an internal control of cDNA quality and quantity. The primers were designed using Primer 3.0 (Applied Biosystems, Foster City, CA) and synthesized by Integrated DNA Technologies (Coraville, IA) (Table 3-1). The real-time PCR thermal conditions were 1 cycle at 50 °C for 2 min, 1 cycle at 95 °C for 10 min, 40 cycles at 95 °C for 15 s and then 60 °C for 1 min. The ΔCT method was used to calculate the relative levels of target gene transcripts in mice, where the ratio of target gene to *Gapdh* was equal to $2^{-\Delta CT}$, $\Delta CT = CT(gene) - CT(Gapdh)$.

Immunoblot analysis was performed for PEPT2 protein, as described previously with minor changes [29]. Tissue lysis buffer consisted of neuronal protein extraction reagent (Thermo Scientific, Rockford, IL) with the addition of proteinase inhibitor cocktail. Kidney protein served as positive control for PEPT2 [30].

3.3.5 *In vitro* uptake of L-His in regional brain slices

Adult wildtype and *Pht1* null mice were used to evaluate the contribution of PHT1 in L-His uptake. Brain slices, prepared using a method described previously

[9], were incubated in buffer containing 2 μM [^{3}H]L-His (0.1 μCi) and [^{14}C]mannitol (0.05 μCi). The incubation was performed in a chamber filled with artificial cerebrospinal fluid (aCSF) buffer at 37°C, which was continuously bubbled with 5% CO_2 and 95% O_2. The aCSF buffer consisted of (mM): 127 NaCl, 20 $NaHCO_3$, 2.4 KCl, 0.5 KH_2PO_4, 1.1 $CaCl_2$, 0.85 $MgCl_2$, 0.5 Na_2SO_4 and 5.0 glucose (pH 7.4). Incubation times were 1, 3, 5 and 10 min, after which time 1.5 mL ice-cold aCSF buffer was added to the chamber to terminate the reaction. The samples were immediately filtered through 100 μm nylon mesh and then washed five times with 1.5 mL ice-cold aCSF buffer. The filter (and tissue slices) were transferred to a scintillation vial containing 0.33 mL hyamine hydroxide and left overnight at 37°C to dissolve the tissue. The samples were then mixed with a 7.0-mL aliquot of Cytoscint cocktail (MP Biomedicals, Solon, OH). Radioactivity was measured using a Beckman LS 6000 SC dual-channel liquid scintillation counter (Beckman Coulter Inc., Fullerton, CA).

The uptake of L-His in brain slices was determined using the following equation [31]:

$Histidine\ Uptake$

$$= \frac{\left(Histidine_t - Histidine_f\right) - \left(Mannitol_t - Mannitol_f\right) \times \frac{Histidine_{media}}{Mannitol_{media}}}{Tissue\ Weight \times Histidine_{media}}$$

where *uptake* was calculated as μL/mg wet tissue weight. The subscript *t* represents the total radioactivity, *f* the filter-binding and *media* the amount of drug in the incubation media.

To further investigate the contribution of amino acid transporters on L-His uptake, as well as the substrate specificity of PHT1, excess amounts (5 mM) of L-His, L-glutamine, L-leucine, L-asparagine or BCH (2-amino-2-norbornanecarboxylic acid) were added as inhibitors of the amino acid transporters. Similarly, dipeptides (glycylsarcosine and carnosine) were used as inhibitors of the peptide transporters. These studies were performed on hypothalamus slices following a 3-min incubation period.

3.3.6 *In vivo* pharmacokinetics and biodistribution of L-His

L-His solutions were prepared by mixing appropriate amounts of [^{14}C]labeled and unlabeled L-His in normal saline to reach the desired dose of 1 nmol/g (0.4 μCi/mouse). A 100-μL volume of solution was administrated by tail vein injection. Serial blood samples (15-20 μL), obtained via tail nicks, were then collected at 0.5, 1, 2, 5, 10, 15, 20 and 30 min after the intravenous dose. Blood samples were collected in 0.2-mL microcentrifuge tubes containing heparin. Heparinized blood samples were centrifuged immediately at 3000 g for 3 min at ambient temperature. A 5- to 10-μl aliquot of plasma was then mixed with 6.0 mL of Cytoscint cocktail. Radioactivity was measured using a dual-channel liquid scintillation counter.

A single CSF sample (5 μL) was obtained from the cisterna magna of each mouse at 2, 5, 10, 20 and 30 min after dosing. The mouse was euthanized and decapitated, and select tissues of brain (e.g. cerebral cortex, cerebellum, hypothalamus and hippocampus) were then isolated, blotted dry and weighed. The samples were dissolved in 330 μL of 1 M hyamine hydroxide and incubated overnight at 37°C. An intravenous bolus injection of [^{3}H]dextran-70,000 (0.25

μCi/mouse) was administered just prior to harvesting the tissue samples to correct for the vascular space.

A noncompartmental pharmacokinetic analysis of L-His was performed on the plasma concentrations of L-His after intravenous bolus dosing using Phoenix/WinNonlin version 6.4 (Pharsight Inc. Mountain View, CA). Total area under the plasma concentration-time curve (AUC) was calculated using the trapezoidal rule. Clearance (CL), volume of distribution (V_{ss}), half-life ($t_{1/2}$), terminal disposition rate constant (λ_z) and mean residence time (MRT) were calculated using standard methods.

3.3.7 Statistics

All the experimental results were reported as mean ± SE. A two-tailed unpaired Student's t-test was applied when comparing statistical differences between two treatment groups. For multiple comparisons, one-way analysis of variance (ANOVA) was used followed by Tukey's test for pairwise comparisons between all the treatment groups. A p value ≤ 0.05 was considered significant. All linear and nonlinear regressions were performed by Prism v5.0 (GraphPad Software, Inc., La Jolla, CA).

3.4 Results

3.4.1 Identification and initial phenotypic analyses of *Pht1* null mice

These studies were performed to test for obvious differences in fundamental characteristics between the two mouse genotypes. In this regard, PCR analyses of genomic DNA extracted from tail biopsies demonstrated that *Pht1* genomic DNA was present in wildtype but not *Pht1* null mice (Fig. 1). Since *Pht1* null primers

were designed specifically to target the *Neo* gene, a band was observed in *Pht1* null mice but not in wildtype animals. No obvious behavioral abnormality was observed in *Pht1* null mice when compared with wildtype animals. *Pht1* null mice were fertile and appeared healthy. There were no significant differences between genotypes in body weight or in any of the serum clinical chemistry values (Table 3-2).

3.4.2 Gene and protein expression

The purpose of these studies was to determine if *Pht1* mice were different, as compared to wildtype animals, in their gene expression of POT family members and other relevant transporters and enzymes. Protein expression for a particular transporter was also performed in select cases. PCR analyses in wildtype mice indicated that *Pht1* was expressed, along with *Pept2*, in the cerebral cortex, cerebellum, hypothalamus, hippocampus and choroid plexus (Fig. 2). Interestingly, *Pept2* showed a compensatory up-regulation in *Pht1* null mice (about 2-fold), which was consistently observed in the different brain regions. Expression of other peptide transporters (*Pept1* and *Pht2*) and *Hdc* were comparable between the two genotypes. Some of the amino acid transporters had different transcription levels between genotypes, however, there was no consistent pattern in the different brain regions. The upregulation of *Pept2* in *Pht1* null mouse brain was confirmed by immunoblot analysis (Fig. 3). PEPT2 protein could be detected in different brain regions, in which expression was increased about 2-fold in the cerebral cortex, hippocampus and hypothalamus of *Pht1* null mice as compared to wildtype animals.

3.4.3 *In vitro* uptake of L-His in regional brain slices

These studies were performed to examine if regional functional activity, along with substrate specificity, differed between wildtype and *Pht1* null mice in the brain uptake of a model substrate, L-His, using an *in vitro* model. L-[^{3}H]His uptake was linearly correlated with time over the first 3-10 min, with no consistent trend for either genotype or regional brain slice (Fig. 4A). As a result, 3-min uptakes were used to estimate the initial rates of L-His, which were reduced by 37-60% during PHT1 ablation depending upon the regional brain slice studied (Fig. 4B). To assess the substrate specificity of PHT1, the 3-min uptake of L-[^{3}H]His was evaluated in hypothalamus by inhibition studies (Fig. 5). In wildtype mice, the uptake of L-His was reduced to 20% of normal by the amino acids L-histidine, L-glutamine, L-lysine and L-asparagine, and to 45-72% of normal by the dipeptides glycylsarcosine and carnosine (5 mM each). In contrast, residual uptake values of L-His in *Pht1* null mice were similar between control animals (L-His alone) and in the presence of dipeptides. In the presence of amino acids, values for L-His uptake were significantly reduced in *Pht1* null mice, and similar between the two genotypes. Finally, in comparing control values, the uptake of L-His in *Pht1* null mice was 50% of that observed in wildtype animals.

3.4.4 *In vivo* pharmacokinetics and biodistribution of L-His

These studies were designed to evaluate whether or not the *in vivo* distribution of a model Pht1 substrate, L-His, was different between genotypes with respect to its systemic plasma exposure, accumulation in regional brain sections and CSF concentrations. In this regard, we found that the plasma concentration-time profiles of L-[^{14}C]His after intravenous injection were comparable in wildtype and *Pht1* null

mice (Fig. 6). As a result, the pharmacokinetic properties of L-His were not different between the two genotypes, as judged by noncompartmental analyses (Table 3-3). Still, biodistribution studies in brain revealed that L-His values were 28-48% lower in *Pht1* null mice, as compared to wildtype animals, in the cerebral cortex, cerebellum, hippocampus and hypothalamus, but not CSF, when sampled 5 min after dosing (Fig. 7).

3.5 Discussion

Compared with PEPT1 and PEPT2, little is known about the expression, localization, function and pharmacological relevance of PHT1, another member of the SLC15 family. Based on limited previous reports [2, 9], PHT1 protein was expressed in the brain and retina of rat, and showed high affinity for L-His in *Pht1*-transfected Xenopus laevis oocytes [2]. PHT1 protein was also expressed in the brain of adult but not neonatal rats and mice, showing a dominant role in glycylsarcosine brain uptake in adult rodents [9]. However, the significance of PHT1 in uptake of its amino acid substrate, L-His, in brain was not evaluated in these studies [4]. Thus, the *in vitro* brain slice and *in vivo* pharmacokinetic/biodistribution studies proposed here for L-His in brain are a good starting point from which to understand the role and significance of PHT1 in neuropeptide regulation, histamine homeostasis, and the potential for targeted drug delivery to neuronal and non-neuronal cell types.

Several novel findings were revealed through phenotypic analyses, *in vitro* brain slice uptake incubation and *in vivo* pharmacokinetic studies in wildtype and *Pht1* null mice. Specifically: 1) *Pht1* null mice displayed no obvious phenotype and

51

had serum clinical chemistry values that were comparable to wildtype mice; 2) PHT1 was expressed, along with PEPT2, in the brain parenchyma (cortex, cerebellum, hippocampus and hypothalamus) of wildtype mice; 3) the mRNA and protein levels of PEPT2 were significantly up-regulated in *Pht1* null mouse brain, suggesting a compensatory role of PEPT2 in these mice; 4) the uptake of L-[^{3}H]His was about 50% lower in *Pht1* null mouse brain slices as compared to those from wildtype mice, indicating that PHT1 makes a significant contribution towards L-His uptake into brain parenchyma; 5) the uptake of L-[^{3}H]His could be inhibited by dipeptides and, in addition to L-His, by several other amino acids; and 6) PHT1 deficiency did not affect the *in vivo* systemic exposure of L-[^{14}C]His in plasma or CSF, but reduced its distribution into brain parenchyma during the first 5 min of intravenous dosing. These findings suggest that PHT1 may play an important role in L-His transport and, perhaps, in histidine-histamine homeostasis in the brain.

The results in Fig. 5 indicated there were key differences (and similarities) in the inhibition profiles of wildtype and *Pht1* null mice. For example, in comparing the inhibition studies in wildtype mice alone, the amino acids (except for leucine) reduced the uptake of L-His to about 20% of control, whereas the dipeptides reduced L-His uptake to 40-65% of control (all changes were significant). These profiles reflected the collective contributions of PHT1, amino acid transporters and nonsaturable/passive pathways for the uptake of L-His in wildtype mice. In comparing the inhibition studies in *Pht1* null mice alone, the same amino acids resulted in significant changes from control, however, L-His uptake in the presence of dipeptides was not significantly different. Most importantly, the control value in

Pht1 null mice was only 50% of the control value in wildtype mice, indicating a major influence of PHT1 in the uptake of L-His. Thus, these profiles reflected the collective contributions of amino acid transporters and nonsaturable/passive pathways for the uptake of L-His in the absence of PHT1. Overall, the combined mechanisms for L-His uptake in brain (hypothalamus) were PHT1 (50%), amino acid transporters (30%) and nonsaturable/passive processes (20%).

Of the POTs, PEPT2 is expressed in the brain of adult rats, especially in epithelial cells of the choroid plexus [29]. The brain expression of PEPT2 is maximal in the fetus, declining with age to 14% of those levels in the adult brain. In contrast, the expression and function of PHT1 protein gradually increases with age, agreeing with its function as indicated by the uptake of glycylsarcosine in adult rodent brain slices [4]. Another POT, PHT2 can also recognize L-His as a substrate, but this transporter is barely detected in brain [3, 9], as is PEPT1 [30]. The effect of *Pht1* depletion on the transcription of those other POTs, amino acid transporters and related enzymes, as well as on the total brain entry of L-His was unknown and the present study was able to address this with the availability of *Pht1* null mice [32]. PEPT2 protein was up-regulated in different brain regions of *Pht1* null mice, which may suggest a compensatory role of PEPT2 as a transporter for di/tripeptides in brain (Fig. 3). This was not observed in other tissues, such as kidney, testis, lung, intestine, spleen or colon (data not shown). As expected, there was no gene expression of *Pept1* or *Pht2* in the brain of both genotypes, which was consistent with previous studies in wildtype rodents [9]. Interestingly, in rat synaptosomes prepared from cerebral cortex [34], the uptake of L-His (2 μM) was not inhibited by

GlySar (2.5 mM) nor was the uptake of GlySar (20 µM) inhibited by L-His (2.5 mM). Thus, the functional data of Fujita et al. [34] in synaptosomes suggest that, although PHT1 expression will not be synaptic, its expression may reflect a cell body or axonal distribution in neurons.

Although brain barrier systems determine the concentration of amino acids in CSF and extracellular fluid (ECF), transporters expressed on the membranes of brain parenchyma cells also participate in the regulation of intracellular fluid homeostasis [33]. More importantly, transporters in brain parenchyma are responsible for the translocation of metabolic substrates, neurotransmitters and neurotransmitter precursors, which can regulate signaling pathways [34]. Amino acid transporters of L-His in brain parenchyma include the Na^+-dependent neutral amino acid transporters (SNATs, SLC38 family) [14, 15], some members of the sodium- and chloride-dependent neurotransmitter transporter family (SLC6 family) (e.g. B^0AT2, and NTT4) [18-20], Na^+-independent amino acid transporters (e.g. LATs and CATs, belong to SLC7 family) [16, 17], and the peptide/histidine transporter PHT1 [9, 21]. Among the amino acid transporters tested in the present study, NTT4, SNAT1 and SNAT3 showed extensive transcription. SNATs have a very broad tissue distribution and are responsible for the net flux of amino acids in CNS [14, 35]. The major physiological function of SNATs in the central nervous system is to transport glutamine in the glutamate/glutamine cycle [36]. Affinity of SNATs to L-His is relatively low, with Michaelis-Menten (K_m) values in the millimolar range [37-39]. NTT4 (SLC6A17) is identified only in the nervous system, especially in synaptic vesicles [40, 41], with a Km of 1-2 mM for proline and glycine and interestingly no

affinity for L-His [43].

Another important consideration was that of differences in the gene expression of amino acid transporters in wildtype and *Pht1* null mice. In this regard, there appeared to be no consistent pattern of change in either a specific amino acid transporter or brain region with respect to the up-/down-regulation between genotypes. Using hypothalamus as an example, since the *in vitr*o inhibition studies were performed in this brain region along with *in vivo* studies, the only amino acid transporter that showed a statistically significant difference was Ntt4, with gene expression being reduced by only 12% (Fig. 2). However, in *Pht1* null mice, the *in vivo* uptake of L-His was reduced 2-fold relative to the values observed in wildtype animals (Fig. 6). Moreover, similar reductions in the *in vivo* L-His uptake were observed in other brain regions even though Ntt4 gene expression increased 2-fold in cortex, had no change in cerebellum, and was reduced only 20% in hippocampus. These findings make it unlikely that changes in the gene expression of amino acid transporters can explain the differences in transport acitivity of L-His during *Pht1* ablation. Still, it would be important to measure, in future studies, if protein expression had also changed.

PHT1 made a significant contribution towards L-His disposition in brain slices. With PHT1 ablation, L-His uptake was reduced by 50% *in vitro* during 3-min brain slice incubations, and by 28-48% *in vivo* in brain regions after intravenous dosing. The rat PHT1 isoform is a high affinity transporter, as judged by a K_m = 17 μM for L-His uptake in oocytes expressing PHT1 protein [2]. As shown in Fig. 5, the transport of L-His by PHT1 could be inhibited, as expected, by dipeptides (e.g., carnosine and

glycylsarcosine) and excess L-His. However, an interesting finding was that some amino acids (not including L-leucine) and a system L-amino acid transport inhibitor, BCH, substantially reduced the uptake of L-His via PHT1. This phenomenon has not been reported previously. Therefore, the interaction between amino acids with positive (L-His, L-lysine) or uncharged polar (L-asparagine, L-glutamine) side chains and PHT1 needs further investigation to test whether other amino acids, in addition to L-His, are substrates for PHT1.

An effect of PHT1 ablation on the brain disposition of L-His was also found *in vivo* with a 28-48% reduction into uptake into brain regions after intravenous dosing (Fig. 7). These results suggest a role of PHT1 at the blood-brain barrier. Carl et al. [44] reported the protein expression of PHT1 in hCMEC/D3 cells, an immortalized human brain endothelial cell line commonly used for *in vitro* blood-brain barrier studies. Those cells showed some evidence of polarized L-His and carnosine (a dipeptide) transport. The role of PHT1 in di/tripeptide, peptidomimetic and amino acid transport at the blood-brain barrier merits further investigation.

In this study, no obvious phenotype was observed when comparing the body weight, fertility, serum clinical chemistry and routine behavior of wildtype and *Pht1* null mice. Indeed, this observation is not unusual during transporter ablation and, often times, requires that the animals be challenged by a certain stress (e.g., drug, chemical or disease state). This scenario was clearly demonstrated by the death of *Mdr1(-/-)* knockout mice during ivermectin exposure [45] and by the phototoxic ear lesions observed in *Bcrp1(-/-)* knockout mice when fed a diet containing alfalfa [46].

Increased neurotoxicity was also observed in *Pept2(-/-)* knockout mice given chronic administration of the heme precursor 5-aminolevulinic acid [47] as well as increased analgesia in *Pept2(-/-)* knockout mice given the endogenous neuropeptide L-kyotorphin [48]. While this study represents an analysis of L-His disposition in the brain of wildtype and *Pht1* null mice, as evaluated by *in vitro* brain slices and *in vivo* biodistribution studies, these results allow us to explore subsequently if these kinetic differences will translate into pharmacological and/or pathological differences. Still, in their initial study using wildtype and *Pht1* null mice, Sasawatari et al. [27] reported that PHT1 promoted a dextran sodium sulfate-induced colitis through its interaction with Toll-like receptor 9 and NOD1-dependent innate immune responses.

Taken as a whole, it appears that PHT1 accounted for 50% of the total uptake of L-His in brain slices and L-amino acid transporters for 30% of the uptake. In addition, PHT1 ablation significantly affected the *in vivo* blood to brain distribution of L-His. These findings are the first of their kind and suggest that PHT1 plays an important role in histidine transport and perhaps drug delivery to neuronal and non-neuronal cell types.

TABLES AND FIGURES

Table 3-1 Quantitative real-time PCR primers in mouse

Gene	Forward Primer (5'-3')	Reverse Primer (5'-3')
Pht1 (Slc15a4)	AGCTTTTTCACAGGCTACCTGATT	AGGCTTGGTGATGAAGACACTCT
Pht2 (Slc15a3)	GCTGAAGCTTGCGTTCCAA	AACAGGTGGGCACTTTCAGAGT
Pept1 (Slc15a1)	CCACGGCCATTTACCATACG	TGCGATCAGAGCTCCAAGAA
Pept2 (Slc15a2)	TGCAGAGGCACGGACTAGATAC	GGGTGTGATGAACGTAGAAATCAA
Lat1 (Slc7a5)	GGATGCCCATCTGTAGGTTTTTAT	AAAATAGAAAGCACTGGGCAAAAT
Snat1 (Slc38a1)	GCAGAACTCGACAGTCAGTGCTA	GCGATGGTTGGTAAAGCATACA
Snat3 (Slc38a3)	GCTGCCCATATATACAGAGCTCAA	CAGCAATGGACAGGTTGGAGAT
Ntt4 (Slc6a17)	ACGATGAGACGCGCTTCAT	AGCGTCCGTTGGGATTGTT
Hdc	AACCCCATCTACCTCCGACAT	GGGATCTGCCAATGCATGA

Hdc, histidine decarboxylase.

Table 3-2 Body weight and serum clinical chemistry of wildtype and *Pht1* null mice[a]

Parameter	Wildtype mice	*Pht1* null mice
Body weight		
7-8 weeks (g)		
Male	24.1 ± 0.5 (9)	23.2 ± 1.0 (9)
Female	18.6 ± 0.4 (12)	18.5 ± 0.3 (10)
Serum		
Sodium (mmol/L)	138 ± 3 (5)	140 ± 4 (6)
Potassium (mmol/L)	9.4 ± 3.0 (5)	9.2 ± 3.7 (6)
Chloride (mmol/L)	111 ± 1 (5)	112 ± 2 (4)
Albumin (g/dL)	3.9 ± 0.5 (6)	4.5 ± 0.9 (6)
Protein (g/dL)	8.2 ± 1.9 (6)	6.7 ± 1.5 (5)
Creatinine (mg/dL)	0.33 ± 0.05 (5)	0.56 ± 0.34 (6)
Bilirubin (mg/dL)	0.10 ± 0 (5)	0.10 ± 0 (5)
Glucose (mg/dL)	178 ± 21 (6)	153 ± 31 (6)
Calcium (mg/dL)	9.2 ± 0.3 (5)	9.2 ± 0.3 (5)
BUN (mg/dL)	38 ± 2 (5)	35 ± 4 (6)
ALT (U/L)	53 ± 4 (5)	50 ± 3 (4)
ALP (U/L)	128 ± 13 (5)	124 ± 9 (5)
AST (U/L)	185 ± 53 (5)	181 ± 20 (6)

[a]Data are expressed as mean ± SE (number of mice). BUN, urea nitrogen; ALT, alanine aminotransferase; ALP, alkaline phosphates; and AST, aspartate aminotransferase. No statistical differences were observed between the two genotypes, as determined by a Student's t-test.

Table 3-3 Noncompartmental pharmacokinetic analysis of [^{14}C]L-histidine in wildtype (WT) and *Pht1* null (Null) mice after 1 nmol/g intravenous bolus dose

Parameter	Unit	WT	Null
AUC$_{0-30}$	µM*min	21.7 (4.8)	24.6 (4.7)
AUC$_{0-\infty}$	µM*min	42.0 (8.0)	43.4 (6.3)
CL	mL/min	0.71 (0.15)	0.59 (0.10)
V$_{ss}$	mL	8.4 (0.7)	7.5 (0.7)
t$_{1/2}$	min	13.3 (3.8)	11.1 (1.6)
λ_z	min^{-1}	0.084 (0.015)	0.083 (0.014)
MRT	min	17.9 (4.6)	15.7 (2.3)

Data are expressed as mean (± SE) (n=11 for WT and 12 for *Pht1* null mice). No significant differences were observed between the two genotypes, as determined by a Student's t-test.
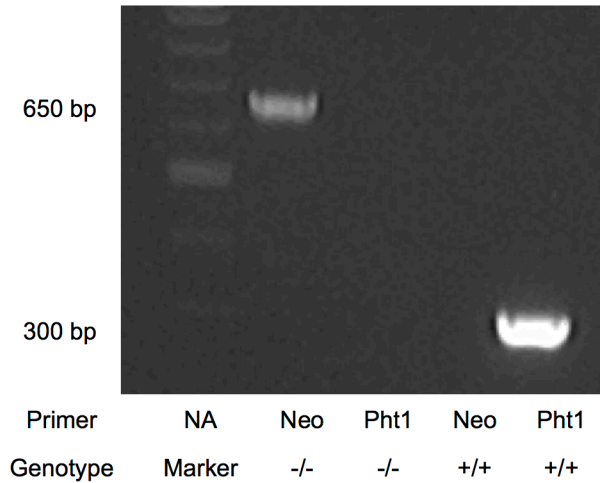
Figure 3-1 Genotyping results for the identification of *Pht1* null mice. NA (Marker), gene-specific primer not applicable in DNA ladder consisting of 100 bp repeats; Neo (-/-), neomycin-specific primer in *Pht1* null mice; *Pht1* (-/-), *Pht1* gene-specific primer in *Pht1* null mice; Neo (+/+), neomycin-specific primer in wildtype mice; *Pht1* (+/+), *Pht1*-specific primer in wildtype mice.

62
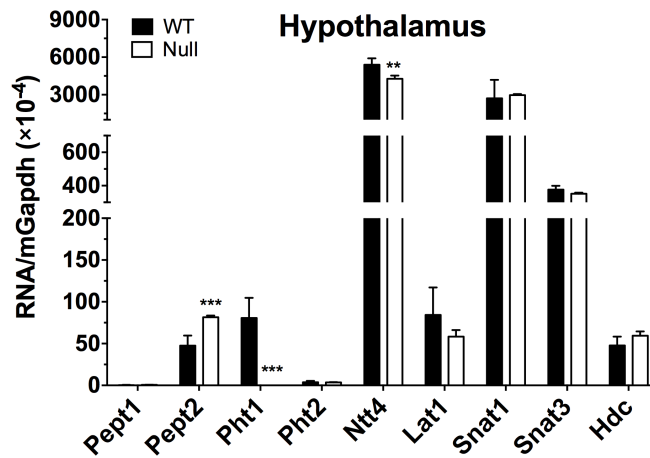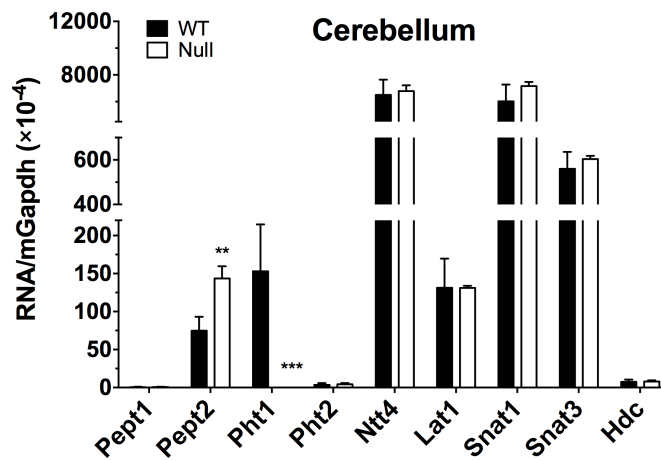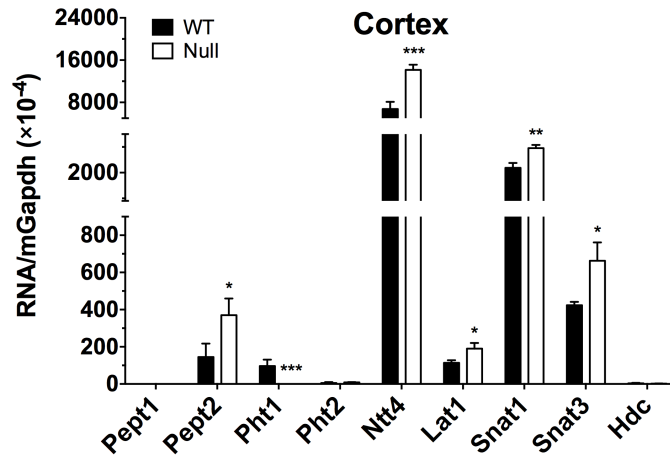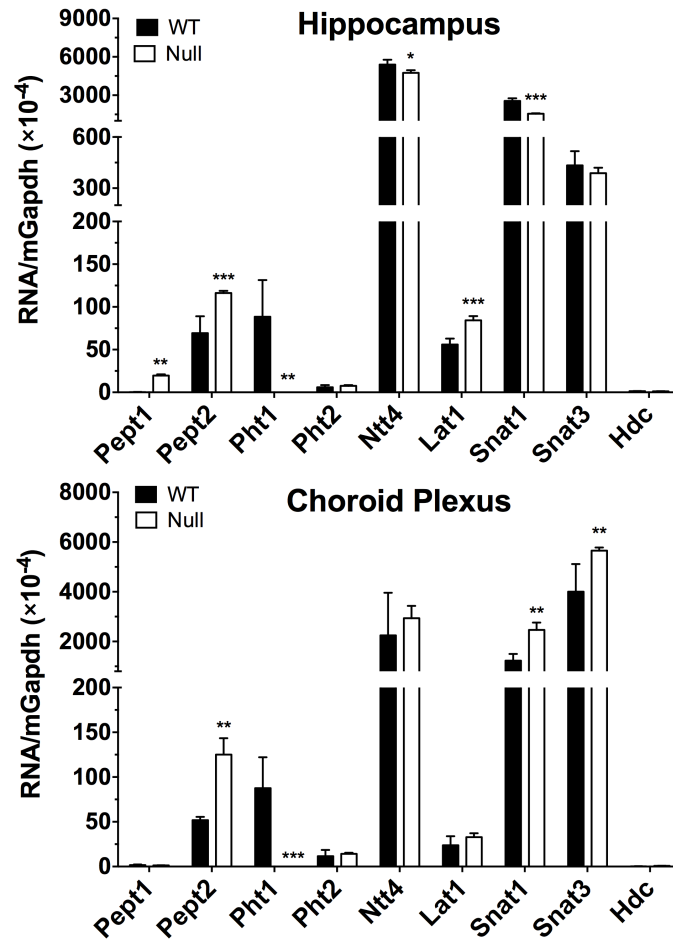
Figure 3-2 mRNA expression of POTs (*Pept1, Pept2, Pht1, Pht2*), select amino acid

transporters (*Ntt4, lat1, Snat1, Snat3*) and histidine decarboxylase (*Hdc*)

in brain regions of adult wildtype (WT) and *Pht1* null mice (Null).

Values are mean ± SE (n=4-6). *p ≤ 0.05, **p ≤ 0.01 and ***p ≤ 0.001, as

compared to WT mice, using a Student's t-test.

Genotype	-/-	+/+	-/-	+/+	-/-	+/+	-/-	+/+	-/-	+/+	+/+
Tissue	Cortex		Cereb		Hippo		Hypo		CP		Kid
Fold Change	1.71 (0.35)		1.58 (0.39)		2.76 (0.93)		4.78 (2.85)		1.61 (0.44)		NA
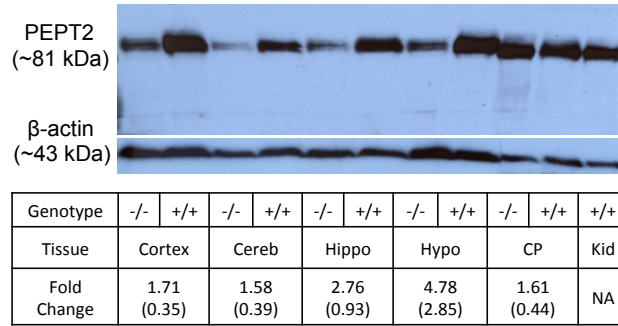
Figure 3-3 Immunoblots of PEPT2 protein in cerebral cortex, cerebellum, hippocampus and hypothalamus of wildtype (+/+) and *Pht1* null (-/-) mice. β-Actin served as a loading control. Kidney from wildtype mice was a positive control for PEPT2 protein. Fold change represents the expression ratio of β-actin-corrected PEPT2 protein in *Pht1* null mice, as compared to WT animals (n=4). NA, not applicable.
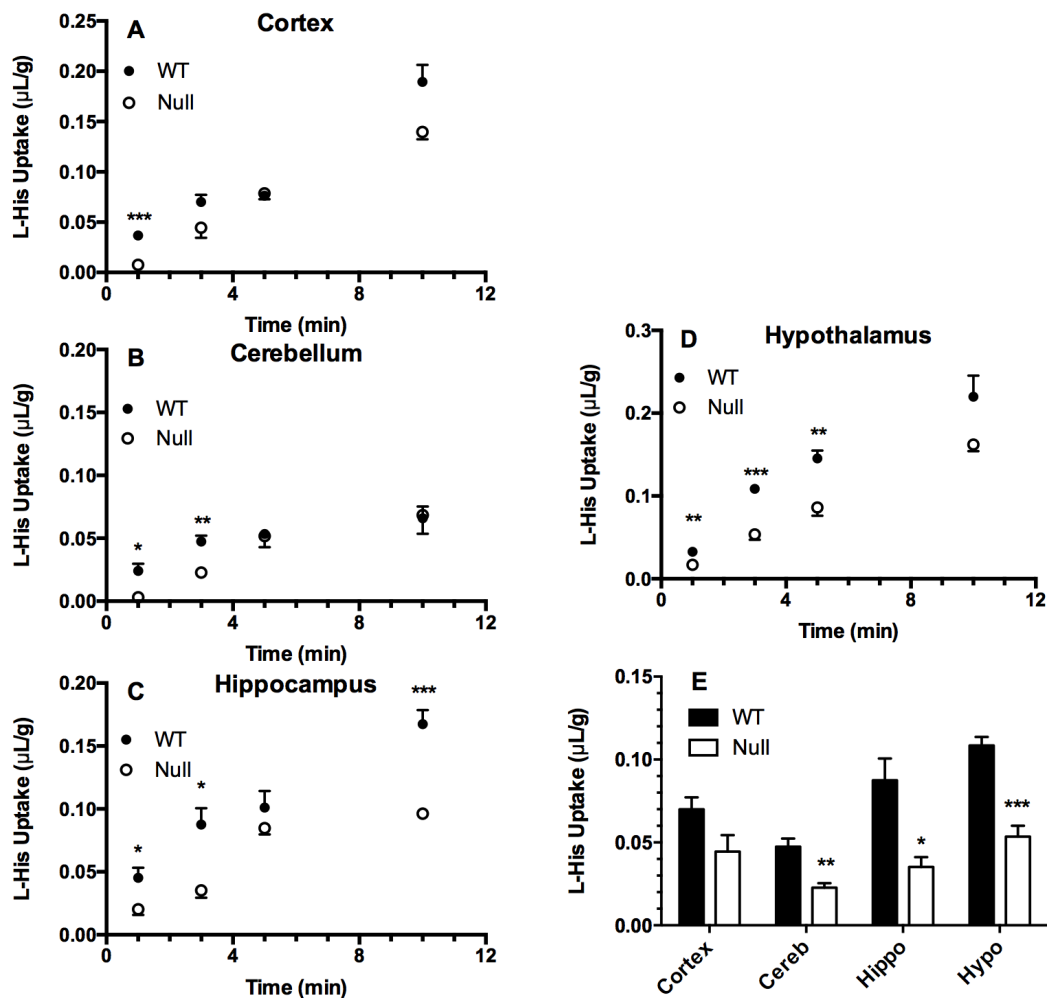
Figure 3-4 Uptake of 2 μM L-[^{3}H]histidine in brain slices of adult wildtype (WT) and *Pht1* null (Null) mice as a function of time (A) and under initial-rate conditions (i.e., 3-min incubation) (B). Values are mean ± SE (n = 4). *p ≤ 0.05, **p ≤ 0.01 and ***p ≤ 0.001, as compared to WT mice, using a Student's t-test.
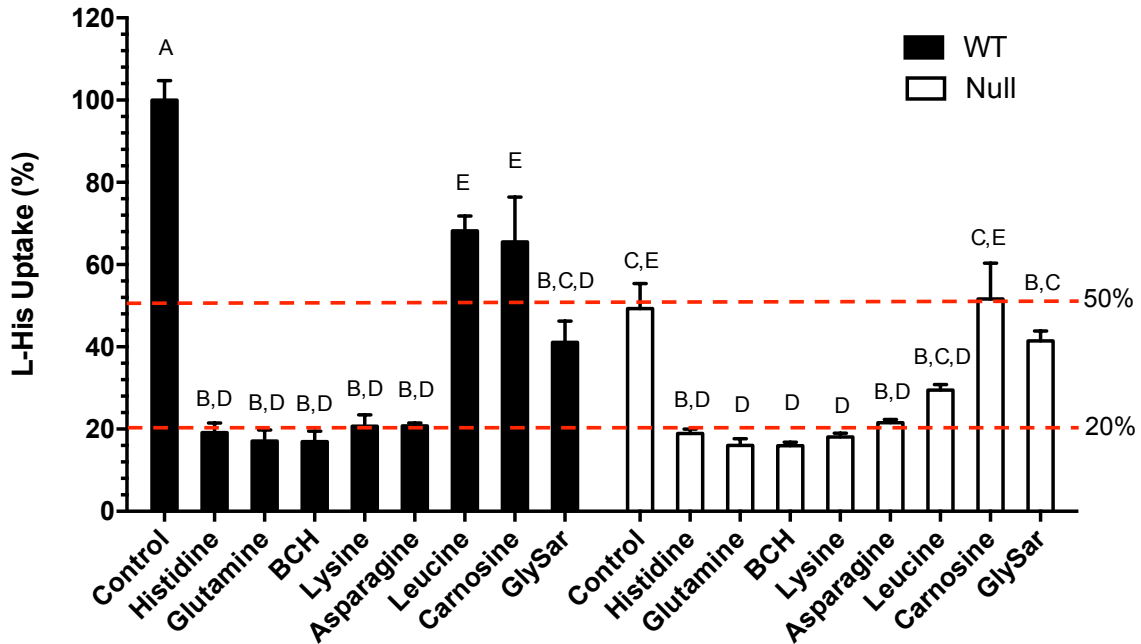
Figure 3-5 Uptake of 2 μM L-[³H]histidine at 3 min in hypothalamus slices of adult wildtype (WT) and *Pht1* null (Null) mice in the absence (control) or presence of potential inhibitors (5 mM). Values are mean ± SE (n=4). All treatment groups were compared, regardless of genotype, and those treatments with the same capital letter (i.e., A, B, C, D, or E) were not significantly different from one another. BCH, 2-aminobicyclo [2.2.1]heptane-2-carboxylic acid; GlySar, glycylsarcosine.
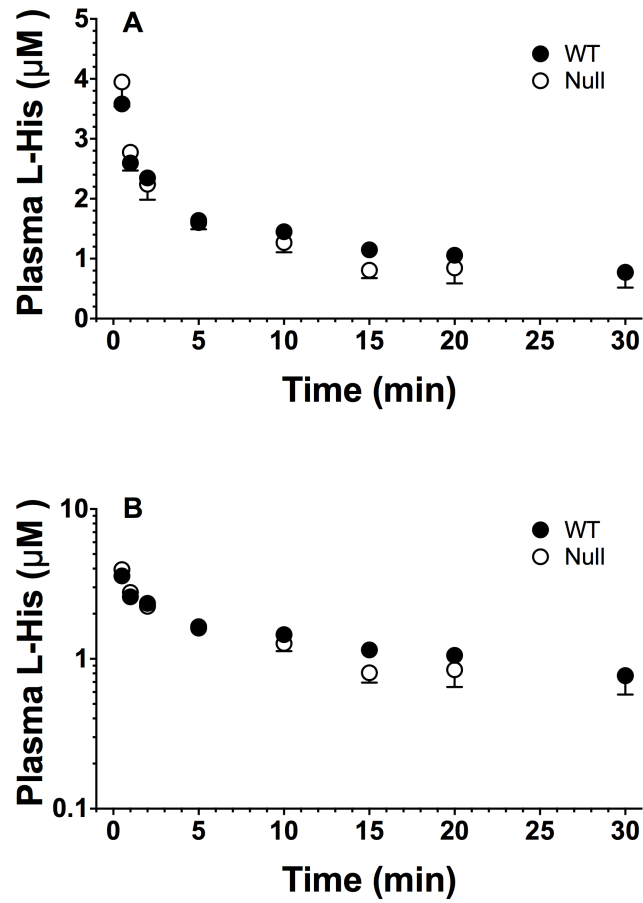
Figure 3-6 Plasma concentration-time profiles of L-[¹⁴C]histidine in wildtype (WT) and *Pht1* null (Null) mice after 1 nmol/g intravenous bolus dose. Data are expressed as mean ± SE (n=11 for WT and 12 for Null) in which the y-axis is displayed on a linear scale (A) and on a logarithmic scale (B).
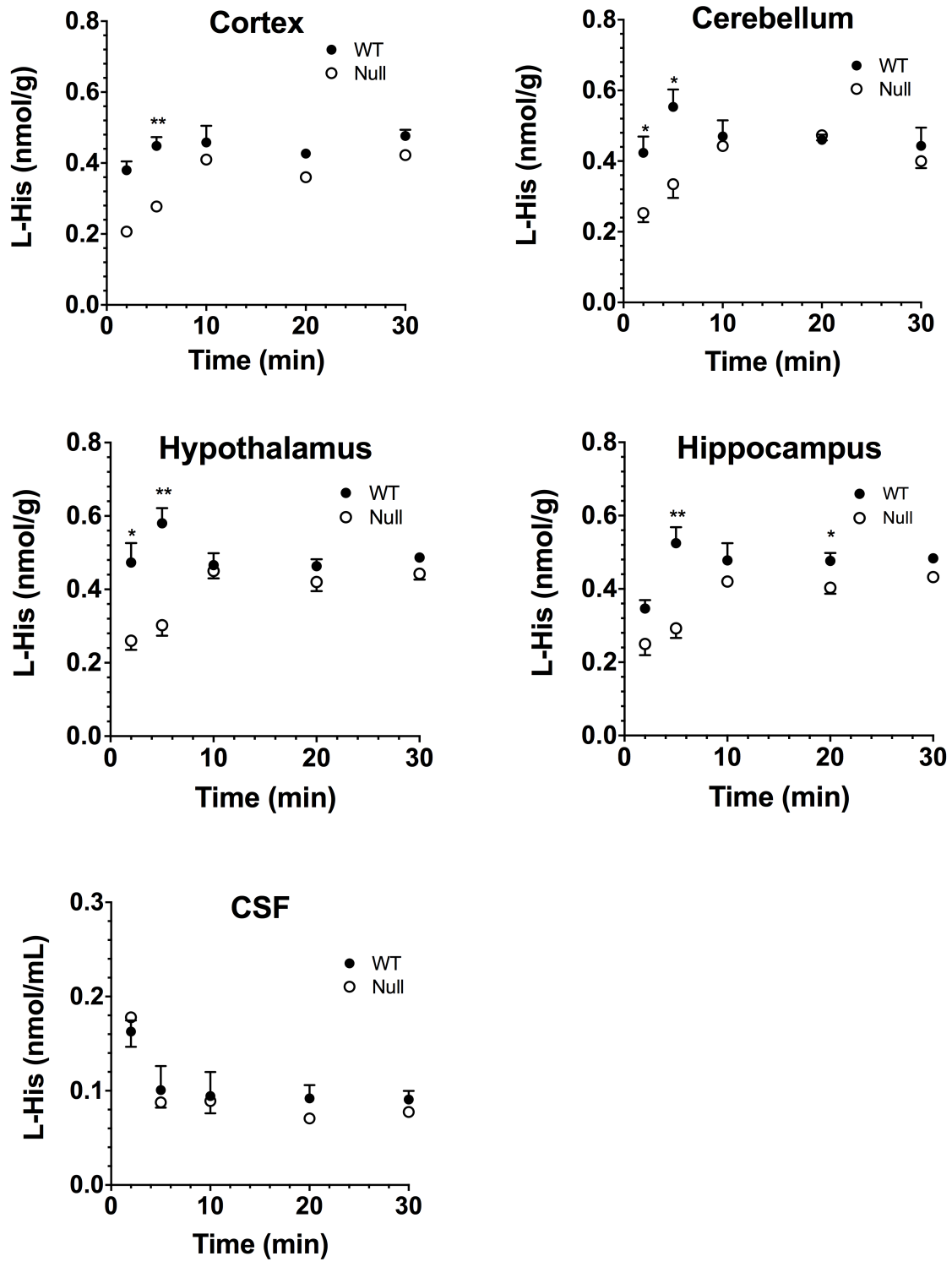
Figure 3-7 Tissue and cerebrospinal fluid (CSF) concentrations of L-[¹⁴C]histidine

in brain regions of wildtype (WT) and *Pht1* null (Null) mice after 1

nmol/g intravenous bolus dose. Data are expressed as mean ± SE (n =

3-6). *p < 0.05 and **p < 0.01, as compared to WT mice, using a

Student's t-test.

REFERENCES

1. Smith, D.E., B. Clemencon, and M.A. Hediger, *Proton-coupled oligopeptide transporter family SLC15: physiological, pharmacological and pathological implications.* Mol Aspects Med, 2013. **34**(2-3): p. 323-36.

2. Yamashita, T., et al., *Cloning and functional expression of a brain peptide/histidine transporter.* J Biol Chem, 1997. **272**(15): p. 10205-11.

3. Sakata, K., et al., *Cloning of a lymphatic peptide/histidine transporter.* Biochem J, 2001. **356**(Pt 1): p. 53-60.

4. Martres, M.P., M. Baudry, and J.C. Schwartz, *Histamine synthesis in the developing rat brain: evidence for a multiple compartmentation.* Brain Res, 1975. **83**(2): p. 261-75.

5. Reiner, P.B., et al., *Ontogeny of histidine-decarboxylase-immunoreactive neurons in the tuberomammillary nucleus of the rat hypothalamus: time of origin and development of transmitter phenotype.* J Comp Neurol, 1988. **276**(2): p. 304-11.

6. Subramanian, N., et al., *Ontogeny of histaminergic neurotransmission in the rat brain: concomitant development of neuronal histamine, H-1 receptors, and H-1 receptor-mediated stimulation of phospholipid turnover.* J Neurochem, 1981. **36**(3): p. 1137-41.

7. Tran, V.T., et al., *Ontogenetic development of histamine H1-receptor binding in rat brain.* J Neurochem, 1980. **34**(6): p. 1609-13.

8. Toledo, A., et al., *Properties and ontogenic development of membrane-bound histidine decarboxylase from rat brain.* J Neurochem, 1988. **51**(5): p. 1400-6.

9. Hu, Y., et al., *Divergent Developmental Expression and Function of the Proton-Coupled Oligopeptide Transporters PepT2 and PhT1 in Regional Brain Slices of Mouse and Rat.* J Neurochem, 2014. **129**(6): p. 955-965.

10. Romano, A., et al., *Functional expression of SLC15 peptide transporters in rat thyroid follicular cells.* Mol Cell Endocrinol, 2010. **315**(1-2): p. 174-81.

11. Everaert, I., et al., *Gene expression of carnosine-related enzymes and transporters in skeletal muscle.* Eur J Appl Physiol, 2013. **113**(5): p. 1169-79.

12. Kopple, J.D. and M.E. Swendseid, *Evidence that histidine is an essential amino acid in normal and chronically uremic man.* J Clin Invest, 1975. **55**(5): p. 881-91.

13. Stifel, F.B. and R.H. Herman, *Histidine metabolism.* Am J Clin Nutr, 1971. **24**(2): p. 207-17.

14. Schioth, H.B., et al., *Evolutionary origin of amino acid transporter families SLC32, SLC36 and SLC38 and physiological, pathological and therapeutic aspects.* Mol Aspects Med, 2013. **34**(2-3): p. 571-85.

15. Hagglund, M.G., et al., *Identification of SLC38A7 (SNAT7) protein as a glutamine transporter expressed in neurons.* J Biol Chem, 2011. **286**(23): p. 20500-11.

16. Usui, T., et al., *Beta-alanine and l-histidine transport across the inner blood-retinal barrier: potential involvement in L-carnosine supply.* Exp Eye Res, 2013. **113**: p. 135-42.

17. Broer, A., et al., *The heterodimeric amino acid transporter 4F2hc/y+LAT2 mediates arginine efflux in exchange with glutamine.* Biochem J, 2000. **349 Pt 3**: p. 787-95.

18. Fredriksson, R., et al., *The solute carrier (SLC) complement of the human genome: phylogenetic classification reveals four major families.* FEBS Lett, 2008. **582**(27): p. 3811-6.

19. Hagglund, M.G., et al., *Characterization of the transporterB0AT3 (Slc6a17) in the rodent central nervous system.* BMC Neurosci, 2013. **14**: p. 54.

20. Hagglund, M.G., et al., *B(0)AT2 (SLC6A15) is localized to neurons and astrocytes, and is involved in mediating the effect of leucine in the brain.* PLoS One, 2013. **8**(3): p. e58651.

21. Bhardwaj, R.K., et al., *The functional evaluation of human peptide/histidine transporter 1 (hPHT1) in transiently transfected COS-7 cells.* Eur J Pharm Sci, 2006. **27**(5): p. 533-42.

22. Schwartz, J.C., et al., *Histaminergic transmission in the mammalian brain.* Physiol Rev, 1991. **71**(1): p. 1-51.

23. Yoshimatsu, H., et al., *Histidine suppresses food intake through its conversion into neuronal histamine.* Exp Biol Med (Maywood), 2002. **227**(1): p. 63-8.

24. Vaziri, P., K. Dang, and G.H. Anderson, *Evidence for histamine involvement in the effect of histidine loads on food and water intake in rats.* J Nutr, 1997. **127**(8): p. 1519-26.

25. Haas, H.L., O.A. Sergeeva, and O. Selbach, *Histamine in the nervous system.* Physiol Rev, 2008. **88**(3): p. 1183-241.

26. Sasawatari, S., et al., *The solute carrier family 15A4 regulates TLR9 and NOD1 functions in the innate immune system and promotes colitis in mice.* Gastroenterology, 2011. **140**(5): p. 1513-25.

27. Hu, Y., et al., *Targeted disruption of peptide transporter Pept1 gene in mice significantly reduces dipeptide absorption in intestine.* Mol Pharm, 2008. **5**(6): p. 1122-30.

28.   Hu, Y., et al., *Development and Characterization of a Novel Mouse Line Humanized for the Intestinal Peptide Transporter PEPT1.* Mol Pharm, 2014.

29.   Shen, H., et al., *Immunolocalization of the proton-coupled oligopeptide transporter PEPT2 in developing rat brain.* Mol Pharm, 2004. **1**(4): p. 248-56.

30.   Shen, H., et al., *Localization of PEPT1 and PEPT2 proton-coupled oligopeptide transporter mRNA and protein in rat kidney.* Am J Physiol, 1999. **276**(5 Pt 2): p. F658-65.

31.   Teuscher, N.S., et al., *Functional evidence for presence of PEPT2 in rat choroid plexus: studies with glycylsarcosine.* J Pharmacol Exp Ther, 2000. **294**(2): p. 494-9.

32.   Kobayashi, T., et al., *The histidine transporter SLC15A4 coordinates mTOR-dependent inflammatory responses and pathogenic antibody production.* Immunity, 2014. **41**(3): p. 375-88.

33.   O'Kane, R.L. and R.A. Hawkins, *Na+-dependent transport of large neutral amino acids occurs at the abluminal membrane of the blood-brain barrier.* Am J Physiol Endocrinol Metab, 2003. **285**(6): p. E1167-73.

34.   He, L., K. Vasiliou, and D.W. Nebert, *Analysis and update of the human solute carrier (SLC) gene superfamily.* Hum Genomics, 2009. **3**(2): p. 195-206.

35.   Reimer, R.J., et al., *Amino acid transport system A resembles system N in sequence but differs in mechanism.* Proc Natl Acad Sci U S A, 2000. **97**(14): p. 7715-20.

36.   Conti, F. and M. Melone, *The glutamine commute: lost in the tube?* Neurochem Int, 2006. **48**(6-7): p. 459-64.

37.   Nakanishi, T., et al., *Structure, function, and tissue expression pattern of human SN2, a subtype of the amino acid transport system N.* Biochem Biophys Res Commun, 2001. **281**(5): p. 1343-8.

38.   Fei, Y.J., et al., *Primary structure, genomic organization, and functional and electrogenic characteristics of human system N 1, a Na+- and H+-coupled glutamine transporter.* J Biol Chem, 2000. **275**(31): p. 23707-17.

39.   Hatanaka, T., et al., *Evidence for the transport of neutral as well as cationic amino acids by ATA3, a novel and liver-specific subtype of amino acid transport system A.* Biochim Biophys Acta, 2001. **1510**(1-2): p. 10-7.

40.   Zaia, K.A. and R.J. Reimer, *Synaptic Vesicle Protein NTT4/XT1 (SLC6A17) Catalyzes Na+-coupled Neutral Amino Acid Transport.* J Biol Chem, 2009. **284**(13): p. 8439-48.

41.   Marcaggi, P. and D. Attwell, *Role of glial amino acid transporters in synaptic transmission and brain energetics.* Glia, 2004. **47**(3): p. 217-25.

CHAPTER 4

SEMI-MECHANISTIC POPULATION PHARMACOKINETIC MODELING OF L-HISTIDINE DISPOSITION AND BRAIN UPTAKE IN WILDTYPE AND PHT1 NULL MICE

4.1 Abstract

Purpose: To develop a semi-mechanistic population pharmacokinetic model to quantitate the disposition kinetics of L-histidine, a peptide-histidine transporter 1 substrate, in plasma, cerebrospinal fluid and brain parenchyma of wildtype and *Pht1* knockout mice.

Methods: L-[^{14}C]Hisidine (L-His) was administrated to wildtype (WT) and *Pht1* knockout (KO) mice via tail vein injection. Serial samples from plasma, cerebrospinal fluid (CSF) and brain parenchyma were collected. A pharmacokinetic (PK) model was developed using non-linear mixed effects modeling (NONMEM). The disposition of L-His between the plasma, brain, and CSF was described by a combination of PHT1-mediated uptake, passive diffusion, CSF bulk flow and first-order microrate constants.

Results: The profiles of L-His in plasma, CSF and brain parenchyma were best described by a four-compartment model. A more rapid uptake of L-His in brain parenchyma was observed in WT mice due to PHT1-mediated uptake, a process

characterized by a Michaelis-Menten component (V_{max} = 0.14 nmoL/min and K_m = 39.88 µM), accounting for 24% of the total.

Conclusions: A semi-mechanistic population pharmacokinetic model was successfully developed, for the first time, to quantitatively characterize the disposition kinetics of L-His in brain under *in vivo* conditions. The model should provide useful in predicting the uptake of L-His, and possibly other PHT1 peptide/mimetic substrates, for drug delivery to the brain.

4.2 Introduction

Proton-coupled oligopeptide transporters (POTs) are responsible for translocating various di/tripeptides and peptidomimetics across biological membranes [1, 2]. They have a significant influence on the pharmacokinetics (PK) and pharmacodynamics (PD) of their substrates [3-5]. To date, four mammalian members of the POT superfamily have been identified, including peptide transporter 1 (PEPT1) and 2 (PEPT2), and peptide/histidine transporter 1 (PHT1) and 2 (PHT2). Unlike PEPT1 and PEPT2, which have been well studied through experiments and modeling approaches [3-5], there is limited information available for PHT1, especially regarding its *in vivo* PK properties.

PHT1 was first been cloned from rat brain in 1997 [6]. It was highly expressed in the brain and retina of rat, and showed high affinity to L-histidine (L-His) in *Pht1*-transfected Xenopus laevis oocytes [6, 7]. Our preliminary studies in rat and mice showed that PHT1 had a dominant function in brain uptake of the dipeptide substrate glycylsarcosine [8], as well as in regulating the brain distribution of L-His [9]. PHT1 has also been found in human and rat intestinal

tissue segments [10, 11], however, its relevance in substrate absorption is unclear. Moreover, PHT1 expressed in dendritic cells is intimately involved in immunologic diseases related to TLR9 stimulation, such as lupus, colitis and persistent viral infection [12-14]. Recent genome-wide association studies on systemic lupus erythematosus identified PHT1 variants as an Asian-specific locus for this disease [15-17].

L-histidine (L-His) was chosen as the model substrate of PHT1 used in this study. It is one of the essential amino acids, which can be degraded to many important metabolic products [18]. One of the most important metabolites of L-His in the brain is histamine, a neurotransmitter. It is known that histamine has difficulty passing through the barrier systems of the brain [19, 20]. The production of histamine in the central nerves system (CNS) is not only dependent upon the activity of histidine decarboxylase (HDC) [19], but also on the availability of its precursor, L-His. Therefore, the entry of L-His in brain is correlated with histamine homeostasis [21, 22]. Brain histamine is produced in histaminergic neuronal and mast cells. There are several transporters responsible for translocating L-His into the brain cells, including L-amino acid transporters (e.g., SNATs, LATs and CATs) and PHT1 [8, 11, 23-26]. However, it appears that PHT1 accounts for 50% of the uptake of L-His, as determined in mouse brain slices, while L-amino acid transporters account for 30% and other unidentified non-saturable processes for 20% of the uptake [8, 9].

Previous studies suggest that PHT1 may play an important role in histidine/histamine homeostasis in brain, as well as in neuropeptide regulation.

75

Thus, understanding the uptake kinetics of PHT1 substrates could facilitate the development of drug delivery strategies for the treatment of neurological diseases related to brain histamine levels. A semi-mechanistic model could provide a useful tool in predicting the brain entry of PHT1 substrates. In order to construct the model, a nonlinear mixed effects modeling (NONMEM) approach was performed. NONMEM is widely used in analyzing population PK data by virtue of addressing variability with different sources. In this study, a population PK model of L-His was developed in wildtype and *Pht1*-deficient mice. By analyzing and comparing the data collected from the two genotypes, we were able to characterize the PK properties and relative significance of PHT1 on the disposition of L-His in brain.

4.3 Materials and methods

4.3.1 Animals

Gender- and age-matched *Pht1*-competent (wildtype or WT) and *Pht1*-deficient (knockout or KO) mice (8 to 10 weeks) were used in this study. The genotype, gender, age and body weight were recorded before the experiments. *Pht1* KO mice were a generous gift of Dr. Noriko Toyama-Sorimachi [14]. All animals were bred on a C57BL/6 background (≥99%). The mice were housed in a temperature-controlled environment with 12 h light and dark cycles, and received a standard diet and water ad libitum (Unit of Laboratory Animal Medicine, University of Michigan, Ann Arbor, MI). All animal studies were performed in accordance with the Guide for the Care and Use of Laboratory Animals as adopted and promulgated by the U.S. National Institutes of Health.

4.3.2 *In vivo* PK and tissue distribution of L-His

The *in vivo* PK and tissue distribution data were generated previously in our laboratory [27]. In brief, a 100-µl volume of L-[^{14}C]His solution (1 nmol/g, 0.4 µCi/mouse) was administrated to WT and *Pht1* KO mice via tail vein injection. Serial blood samples (15-20 µl), via tail nicks, were then collected at 0.5, 1, 2, 5, 10, 20, and 30 min after dosing. Heparinized blood samples were centrifuged immediately at 3000 g for 3 min at ambient temperature. Radioactivity of the plasma samples was measured using a dual-channel liquid scintillation counter. CSF samples (5 µl) were obtained from the cisterna magna of mice along with brain parenchyma at specified times (e.g., 2, 5, 10, 20 or 30 min after dosing). The samples were weighed and dissolved in 330 µl of 1 M hyamine hydroxide and incubated overnight at 37°C. An intravenous bolus injection of [^{3}H]dextran-MW 70,000 (0.25 µCi/mouse) was administered just prior to harvesting the tissue samples to correct for vascular space.

4.3.3 Population PK modeling of L-His in plasma, CSF and brain parenchyma

The concentration-time profiles of these biological fluids and tissue were analyzed using non-linear mixed effects modeling with NONMEM v7.3 (ICON Development Solutions, MD, USA). A subroutine ADVAN6 TRANS1 and the first-order conditional estimation with interaction were used to build the compartment models throughout the modeling procedure. Model development was guided by the likelihood ratio test using objective function values, graphical goodness-of-fit, and non-parametric bootstrap analysis. A stepwise compartmental model building approach was performed in model development to characterize the disposition

kinetics of L-His in the plasma, CSF and brain parenchyma. First, a PK model was developed for the plasma concentration-time data, and one-, two-, and three-compartment models were compared. Once the model for the plasma concentration-time data was established, it was expanded to include the CSF and brain parenchymal compartments as shown in Figure 4-1. The schematic structure model in brain was adopted and modified based on another model [28].

Mass-balance equations for each compartment were shown in the following equations:

For the plasma central and peripheral compartments

$$\frac{dA_1}{dt} = -K_{12} \times A_1 + K_{21} \times A_2 - K_{13} \times A_1 + K_{31} \times A_3 - \frac{V_{max,PHT1} \times A_1}{K_{m,PHT1} \cdot V_1 + A_1} \times Genotype$$
$$-K_{14} \times A_1 + K_{41} \times A_4 + K_{bulk} \times A_4 - K_{10} \times A_1$$

$$\frac{dA_2}{dt} = K_{12} \times A_1 - K_{21} \times A_2$$

For the brain parenchyma

$$\frac{dA_3}{dt} = K_{13} \times A_1 - K_{31} \times A_3 + \frac{V_{max,PHT1} \times A_1}{K_{m,PHT1} \cdot V_1 + A_1} \times Genotype + K_{43} \times A_4 - K_{34} \times A_3$$

For the CSF

$$\frac{dA_4}{dt} = K_{14} \times A_1 - K_{41} \times A_4 - K_{bulk} \times A_4 - K_{43} \times A_4 + K_{34} \times A_3$$

where A_1, A_2, A_3 and A_4 were the amount of L-His in plasma central, plasma peripheral, brain parenchyma and CSF compartments, respectively. V_1 was the volume of distribution of the plasma central compartment. K_{10}, K_{12}, K_{21}, K_{13}, K_{31}, K_{14}, K_{41}, K_{bulk}, K_{34} and K_{43} were the first-order microrate constants between the respective compartments. *Genotype* was the indicator for the mouse genotype

(*Genotype* = 1 for WT, *Genotype* = 0 for KO). In WT mice, L-His entered the brain via active transport by PHT1 as described by a Michaelis-Menten term ($V_{max,PHT1}$ and $K_{m,PHT1}$), and by other pathways which were simplified as one first-order process (K_{13}). There was no PHT1 function in the KO mice. There was passive diffusion of L-His describing its exchange between the brain parenchyma and CSF compartments. The intercomparment clearance (Q_2), which was assumed to be inversely proportional to the one-half power of molecular weight (*MW*), was shown in the following equation [28]:

$$Q_2 = \frac{0.379}{\sqrt{MW}}$$

The distribution of L-His between plasma and CSF was also assumed to be first-order processes. In addition, L-His was drained from CSF to plasma central compartment through bulk flow (Q_{bulk} = 0.0016 mL/min [29]). Volumes of distribution of the brain and CSF compartments were set to physiological values (V_3 = 0.36 mL, V_4 = 0.09 mL) [29]. The relationships between microrate constants (e.g., K_{34}, K_{43} and K_{bulk}) and flows (e.g., Q_2 and Q_{bulk}) were shown in the following equations:

$$Q_2 = K_{34} \times V_3 = K_{43} \times V_4$$

$$Q_{bulk} = K_{bulk} \times V_4$$

Inter-animal variability (IIV) of the PK parameters was assumed to follow a log-normal distribution and described by an exponential error model. Additive, proportional and mixed error models were evaluated for the residual unexplained variability. The impact of genotype, gender, age and body weight of animal on PK

parameters was evaluated. IIVs, residual errors and covariates were included in the model only if they were associated with a decrease in OFV by at least 3.84 (χ^2 p value ≤ 0.05).

The final PK model was evaluated by nonparametric bootstrap analysis and visual predictive checks using Perl-speaks-NONMEM (PsN 4.2.0). Two hundred bootstrap samples were generated from the original data set and then fitted to the final population PK model to obtain parameter estimates. The median and 90% bootstrap confidence interval calculated from the successful bootstrap runs were compared with final model estimates. For visual predictive checks, 1000 hypothetical patient datasets were simulated using the parameter estimates of the final model. The 90% prediction intervals were calculated and checked by visual inspection to see how the intervals overlapped with the observed data.

4.4 Results

4.4.1 Differential brain biodistribution of L-[^{14}C]His in WT and *Pht1* KO mice

As shown in Figure 4-2, brain L-[^{14}C]His concentrations were significantly lower in *Pht1* KO mice compared to WT animals at early time points (before 10 min) but less so in later ones, suggesting a difference on the distribution rate of L-[^{14}C]His from the plasma to brain. The plasma and CSF concentration-time profiles of L-[^{14}C]His were comparable in the two genotypes. Based on these findings, genotype differences would be considered a covariate for the uptake rate constant of L-His in brain.

4.4.2 Population PK Modeling of L-His in plasma, CSF and brain parenchyma

A stepwise compartmental model building approach was performed to characterize the disposition kinetics of L-[14C]His in the plasma, CSF and brain parenchyma. The disposition kinetics of L-[14C]His in plasma was best described by a two-compartment model. The expanded four-compartment model, including brain parenchyma and CSF, was shown in Figure 4-1. The estimated PK parameters and bootstrap results were listed in Table 4-1. Consistent with our previous noncompartmental analysis [9], the plasma PK parameters of L-[14C]His were comparable in WT and *Pht1* KO mice. The total plasma clearance (CL) of L-[14C]His was 0.31 mL/min, and its volumes of distribution in the central (V_1) and peripheral (V_2) compartments were 4.49 mL and 5.47 mL, respectively. The distribution kinetics between plasma and CSF compartments were also similar in the two genotypes. A more rapid uptake of L-His occurred in the brain parenchyma of WT mice, as compared to *Pht1* KO mice, due to its active transport by PHT1 ($V_{max,PHT1}$ = 0.14 nmoL/min, $K_{m,PHT1}$ = 39.88 μM), demonstrating that PHT1 plays an important role as an uptake transporter for L-[14C]His in the brain. In the pilot study, L-His concentrations in brain parenchyma reached a plateau at 20 min post dose, which was consistent with the literature [30]. Therefore, we only characterized the first 30 min after dosing. The first-order rate constant directing L-[14C]His from brain parenchyma to the plasma (K_{31}) was fixed as zero in the final model. The impact of mouse genotype, gender, age and body weight on the PK parameters was evaluated. Only genotype was incorporated as a covariate in the final model. Additive error model was used to describe the residual unexplained variability.

4.4.3 Final model validation

Basic goodness-of-fit plots for the final PK model were displayed in Figure 4-3. Individual predictions showed a good correlation with observed concentrations in all of the plasma, brain parenchyma and CSF compartments. Conditional weighted residuals randomly distributed along the zero ordinate line with no obvious deviations. As shown in the visual predicted check plots (Figure 4-4), observed concentrations in all of the compartments were in good agreement with the prediction intervals of 1000 simulations based on parameter estimates from the final model. According to nonparametric bootstrap analyses (Table 4-1), all of the parameter estimates were close to the median and were inside the 90% confidence intervals of the bootstrap estimates.

4.5 Discussion

There is emerging evidence showing that PHT1 plays an important role in the brain as an uptake transporter. In particular, the protein expression of PHT1 in brain increased with age in both mice and rats, and its function dominated the uptake of glycylsarcosine in brain slices [8]. Moreover, our previous findings showed that PHT1 was the major transporter in regulating the in vitro distribution of L-His in brain, where it accounted for 50% of the total uptake of L-His in hypothalamus slices. In contrast, the L-amino acid transporters accounted for 30% of the uptake and other nonsaturable pathways for the other 20% [9]. Brain

82

distribution of L-His *in vivo* was also significantly reduced in *Pht1*-deficient mice, as compared to wildtype mice.

In the present study, the PK properties of PHT1 *in vivo* were characterized for the first time and several new findings were revealed. Specifically, a four-compartment PK model was successfully developed to define the distribution kinetics of the PHT1 substrate L-[14C]His in brain. By comparing wildtype with *Pht1* KO mice, we could quantify the PHT1-mediated active transport of L-[14C]His from the plasma to brain *in vivo* with a single Michaelis-Menten term ($V_{max,PHT1}$ = 0.14 nmoL/min, $K_{m,PHT1}$ = 39.88 µM). Moreover, the similar disposition kinetics of L-[14C]His in plasma and CSF between the two genotypes suggested the absence of PHT1 at the blood-CSF and the brain parenchyma-CSF interfaces.

Based on the final model, the *in vivo* $K_{m,PHT1}$ of L-[14C]His (39.88 µM) was similar to the *in vitro* measurement of L-His (K_m = 17 µM) in rat *Pht1*-expressing Xenopus oocytes [6], suggesting the plausibility of the current model regarding the PHT1-mediated plasma-to-brain uptake of L-His. This result also indicated that mouse PHT1 was a high affinity transporter, as shown for the rat isoform [6].

Under linear-conditions (i.e., plasma concentrations << $K_{m,PHT1}$), the PHT1-mediated uptake of L-[14C]His, calculated as $V_{max}/(V_1*K_m)$, was $7.8*10^{-4}$ 1/min. The rate constant representing the uptake mediated by other pathways (K_{13}) was equal to $2.5*10^{-3}$ 1/min (Table 4-1). Using these numbers, the total first-order plasma-to-brain uptake of L-[14C]His was $3.28*10^{-3}$ 1/min in wildtype mice, which was close to the literature values of $0.5*10^{-3}$ to $13.4*10^{-3}$ 1/min in rat [21, 31]. Thus, the PHT1-mediated uptake of L-[14C]His was calculated as 23.8% *in vivo*, which was smaller

than the 50% value determined previously *in vitro* in mouse brain slices [9]. Although speculative, this difference may reflect the fact that in vitro brain slice results are obtained from a stagnant system whereas in vivo brain results are dynamic with temporal aspects of blood flow and other factors.

A semi-mechanistic model would be more valuable if we were able to extrapolate these findings in mice to humans. Thus, it would be important to determine the protein expression levels of PHT1 and related transporters in human so that brain distribution of L-His or future PHT1-substrate drugs could be simulated. Moreover, considering the number of PHT1 variants and their association with lupus systemic erythematosus [15-17], further investigation of PHT1 localization, structure-function and regulation in the brain is warranted.

In conclusion, a semi-mechanistic population pharmacokinetic model was developed in mice that successfully characterized the disposition of L-His, a model PHT1 substrate, in blood, CSF and brain parenchyma. By modeling the data collected from *Pht1*-competent and *Pht1*-deficient mice simultaneously, we were able to quantitatively describe for the first time the plasma-to-brain uptake of L-His under *in vivo* conditions. This model may provide a tool in predicting the brain distribution of L-His in humans, and PHT1 as a possible target in brain for the delivery of peptide/mimetic therapeutics.

TABLES AND FIGURES

Table 4-1 Population pharmacokinetics and bootstrap results of L-[^{14}C]histidine as estimated in wildtype and *Pht1* knockout mice

Parameters	Estimates (% RSE)	Bootstrap estimates	
		Median	90% CI
CL (mL/min)	0.31 (10)	0.32	0.29, 0.36
V_1 (mL)	4.49 (10)	4.25	3.82, 5.35
V_2 (mL)	5.47 (16)	5.12	4.29, 6.75
Q_1 (mL/min)	2.12 (8)	2.14	1.94, 2.65
K_{13} (1/min)	0.0025 (10)	0.0025	0.0021, 0.0029
K_{14} (1/min)	0.0033 (26)	0.0029	0.0013, 0.0048
K_{41} (1/min)	3.12 (26)	2.78	1.92, 4.31
$K_{m,PHT1}$ (μM)	39.88 (10)	39.90	39.89, 39.90
$V_{max,PHT1}$ (nmoL/min)	0.14 (36)	0.14	0.05, 0.22
IIV %CV (% RSE)			
ω (CL)	55 (28)	55	44, 69
ω (V_1)	11 (159)	13	4, 19
ω (V_2)	74 (33)	70	55, 87
Residual error			
σ_{plasma} (μM)	0.11 (6)	0.10	0.07, 0.14
σ_{brain} (nmoL/g)	0.0011 (33)	0.001	0.0005, 0.0019
σ_{CSF} (μM)	0.014 (33)	0.013	0.009, 0.017

CL, total plasma clearance; V_1 and V_2, volumes of distribution in central and peripheral compartments; Q_1, intercompartmental clearance between the central and peripheral compartments, $Q1 = K_{12} \times V_1 = K_{21} \times V_2$; K_{13}, K_{14} and K_{41}, the first-order microrate constants between the respective compartments; $V_{max,PHT1}$, the maximum rate of active transport of L-[^{14}C]histidine from plasma to brain mediated by PHT1; $K_{m,PHT1}$, Michaelis-Menten constant for the PHT1-mediated uptake of L-[^{14}C]histidine from plasma to brain; σ_{plasma}, σ_{brain} and σ_{CSF}, residual error; IIV, inter-individual

variability; CV, coefficient of variation; RSE, relative standard error; CI, confidence

interval.
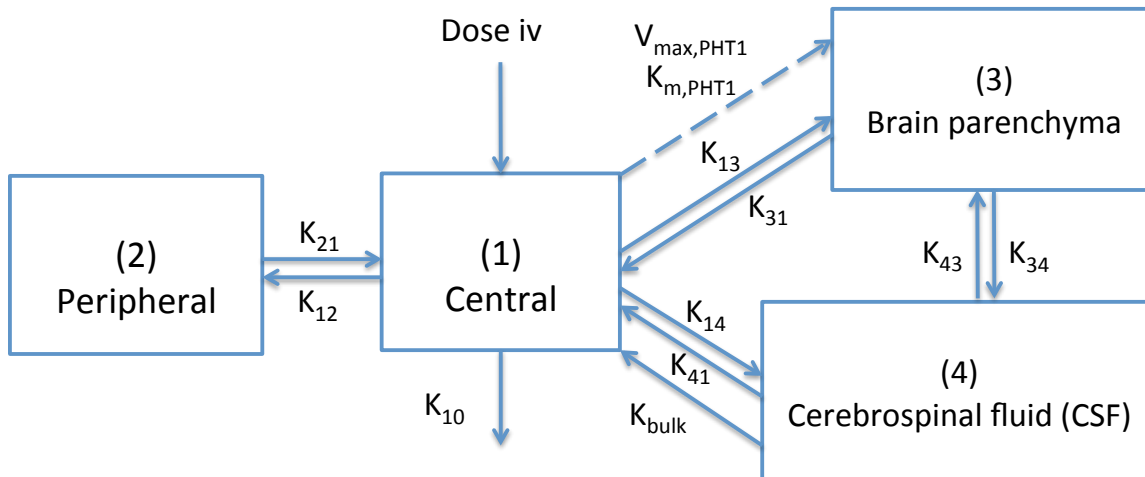
Figure 4-1 Schematic structural model of L-[^{14}C]histidine disposition in mice after an intravenous (iv) bolus dose. $V_{max,PHT1}$, and $K_{m,PHT1}$, the maximum rate and Michaelis-Menten constant of PHT1-mediated active transport of L-[^{14}C]histidine from plasma to brain; K_{10}, K_{12}, K_{21}, K_{13}, K_{31}, K_{14}, K_{41}, K_{34} and K_{43} first-order microrate constants between the respective compartments; K_{bulk}, first-order microrate constant of CSF bulk flow. The dashed line indicates a process existing only in wildtype mice.
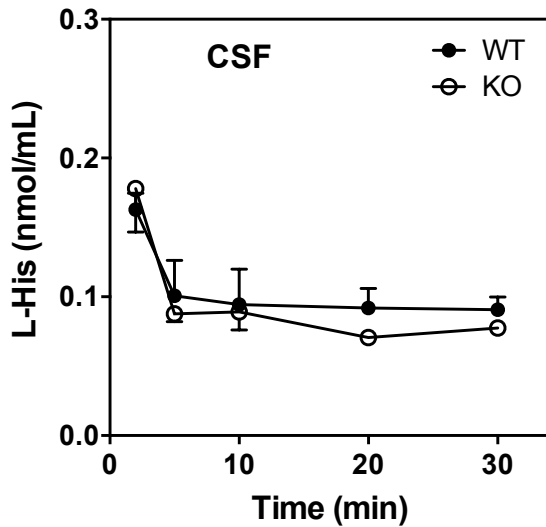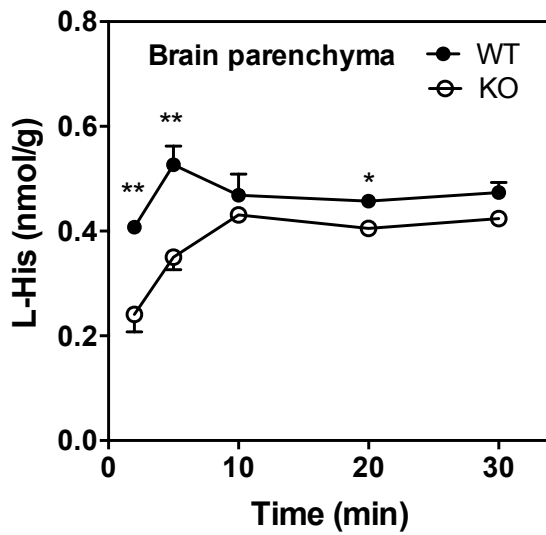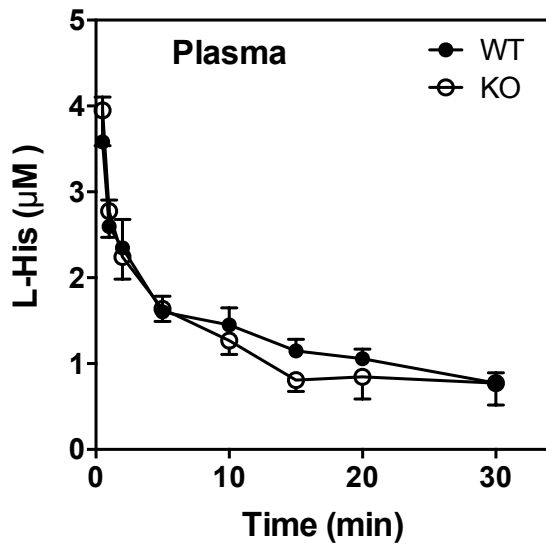
Figure 4-2 L-[^{14}C]histidine concentration versus time plots in plasma, brain parenchyma and CSF compartments of wildtype (WT) and *Pht1* knockout (KO) mice. *p ≤ 0.05 and **p ≤ 0.01. The figures were adapted from a previous paper for genotype comparisons [9].
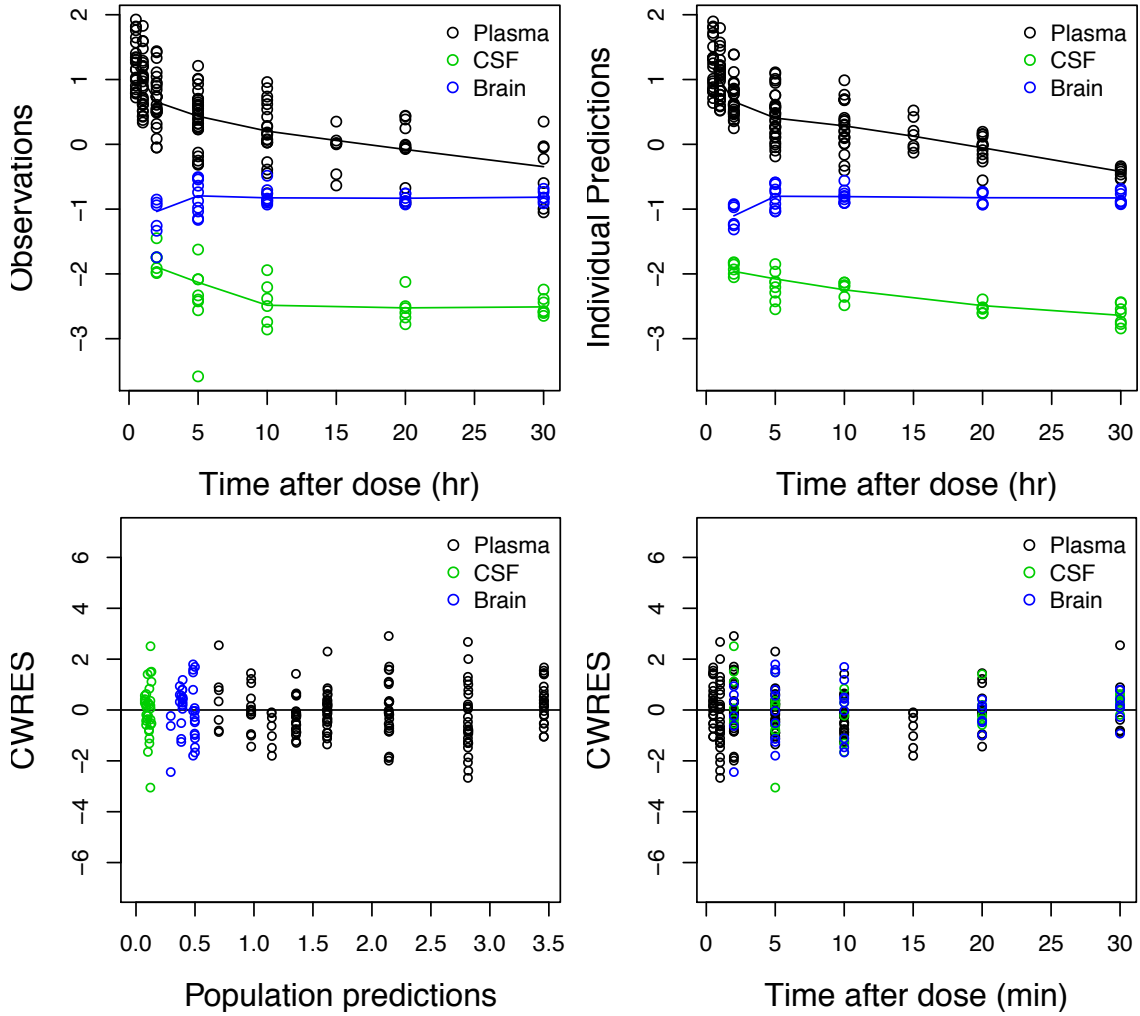
Figure 4-3 Basic goodness-of-fit plots of population pharmacokinetic parameters.

CWRES, conditional weighted residual.
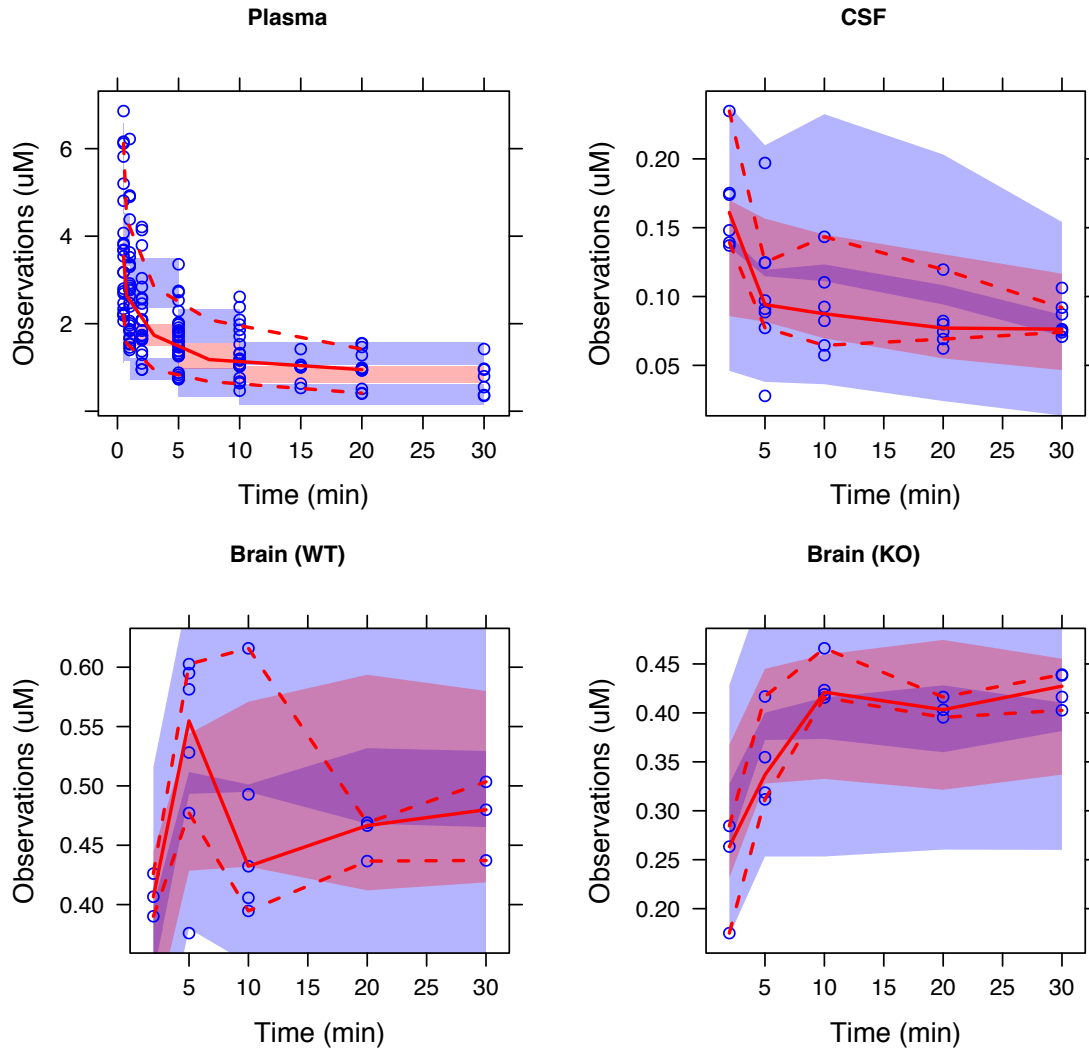
Figure 4-4 Visual predictive check of the final pharmacokinetic model of L-[14C]histidine in plasma, brain and CSF of wildtype (WT) and *Pht1* knockout (KO) mice, based on 1000 simulations. Observed data are shown as circles. Solid and dashed lines represent the median, and 10th and 90th percentiles of the observed data. The semitransparent red field represents the 95% confidence interval of the simulated median. The semitransparent blue fields represent the 95% confidence interval of the simulated percentiles.

REFERENCE

1.   Smith DE, Clemencon B, Hediger MA. Proton-coupled oligopeptide transporter family SLC15: physiological, pharmacological and pathological implications. Mol Aspects Med. 2013;34(2-3):323-36.

2.   Daniel H, Kottra G. The proton oligopeptide cotransporter family SLC15 in physiology and pharmacology. Pflugers Arch. 2004;447(5):610-8.

3.   Huh Y, Hynes SM, Smith DE, Feng MR. Importance of Peptide transporter 2 on the cerebrospinal fluid efflux kinetics of glycylsarcosine characterized by nonlinear mixed effects modeling. Pharm Res. 2013;30(5):1423-34.

4.   Xie Y, Shen H, Hu Y, Feng MR, Smith DE. Population pharmacokinetic modeling of cefadroxil renal transport in wild-type and Pept2 knockout mice. Xenobiotica. 2015;10.3109/00498254.2015.1080881:1-8.

5.   Yang B, Hu Y, Smith DE. Impact of peptide transporter 1 on the intestinal absorption and pharmacokinetics of valacyclovir after oral dose escalation in wild-type and PepT1 knockout mice. Drug Metab Dispos. 2013;41(10):1867-74.

6.   Yamashita T, Shimada S, Guo W, Sato K, Kohmura E, Hayakawa T, et al. Cloning and functional expression of a brain peptide/histidine transporter. J Biol Chem. 1997;272(15):10205-11.

7.   Sakata K, Yamashita T, Maeda M, Moriyama Y, Shimada S, Tohyama M. Cloning of a lymphatic peptide/histidine transporter. Biochem J. 2001;356(Pt 1):53-60.

8.   Hu Y, Xie Y, Keep RF, Smith DE. Divergent Developmental Expression and Function of the Proton-Coupled Oligopeptide Transporters PepT2 and PhT1 in Regional Brain Slices of Mouse and Rat. J Neurochem. 2014;129(6):955-65.

9.   Wang XX, Hu Y, Keep RF, Toyama-Sorimachi N, Smith DE. A novel role for PHT1 in the disposition of l-histidine in brain: In vitro slice and in vivo pharmacokinetic studies in wildtype and Pht1 null mice. Biochem Pharmacol. 2017;124:94-102.

10.   Herrera-Ruiz D, Wang Q, Gudmundsson OS, Cook TJ, Smith RL, Faria TN, et al. Spatial expression patterns of peptide transporters in the human and rat gastrointestinal tracts, Caco-2 in vitro cell culture model, and multiple human tissues. AAPS PharmSci. 2001;3(1):E9.

11.   Bhardwaj RK, Herrera-Ruiz D, Eltoukhy N, Saad M, Knipp GT. The functional evaluation of human peptide/histidine transporter 1 (hPHT1) in transiently transfected COS-7 cells. Eur J Pharm Sci. 2006;27(5):533-42.

12.   Baccala R, Gonzalez-Quintial R, Blasius AL, Rimann I, Ozato K, Kono DH, et al. Essential requirement for IRF8 and SLC15A4 implicates plasmacytoid dendritic cells in the pathogenesis of lupus. Proc Natl Acad Sci U S A. 2013;110(8):2940-5.

13.   Dosenovic P, Adori M, Adams WC, Pedersen GK, Soldemo M, Beutler B, et al. Slc15a4 function is required for intact class switch recombination to IgG2c in response to TLR9 stimulation. Immunol Cell Biol. 2014;10.1038/icb.2014.82.

14.   Sasawatari S, Okamura T, Kasumi E, Tanaka-Furuyama K, Yanobu-Takanashi R, Shirasawa S, et al. The solute carrier family 15A4 regulates TLR9 and NOD1 functions in the innate immune system and promotes colitis in mice. Gastroenterology. 2011;140(5):1513-25.

15.   Han JW, Zheng HF, Cui Y, Sun LD, Ye DQ, Hu Z, et al. Genome-wide association study in a Chinese Han population identifies nine new susceptibility loci for systemic lupus erythematosus. Nat Genet. 2009;41(11):1234-7.

16.   Lee HS, Kim T, Bang SY, Na YJ, Kim I, Kim K, et al. Ethnic specificity of lupus-associated loci identified in a genome-wide association study in Korean women. Ann Rheum Dis. 2014;73(6):1240-5.

17.   Wang C, Ahlford A, Jarvinen TM, Nordmark G, Eloranta ML, Gunnarsson I, et al. Genes identified in Asian SLE GWASs are also associated with SLE in Caucasian populations. Eur J Hum Genet. 2013;21(9):994-9.

18.   Stifel FB, Herman RH. Histidine metabolism. Am J Clin Nutr. 1971;24(2):207-17.

19.   Sakurai E, Sakurai E, Watanabe T, Yanai K. Uptake of L-histidine and histamine biosynthesis at the blood-brain barrier. Inflamm Res. 2009;58 Suppl 1:34-5.

20.   Schwartz JC, Arrang JM, Garbarg M, Pollard H, Ruat M. Histaminergic transmission in the mammalian brain. Physiol Rev. 1991;71(1):1-51.

21.   Hegstrand LR, Simon JR. Histidine transport into rat brain synaptosomes. J Neurochem. 1985;45(2):407-14.

22.   Neame KD. Effect of Amino Acids on Uptake of L-Histidine by Rat Brain Slices. J Neurochem. 1964;11:67-76.

23.   Schioth HB, Roshanbin S, Hagglund MG, Fredriksson R. Evolutionary origin of amino acid transporter families SLC32, SLC36 and SLC38 and physiological, pathological and therapeutic aspects. Mol Aspects Med. 2013;34(2-3):571-85.

24.   Hagglund MG, Sreedharan S, Nilsson VC, Shaik JH, Almkvist IM, Backlin S, et al. Identification of SLC38A7 (SNAT7) protein as a glutamine transporter expressed in neurons. J Biol Chem. 2011;286(23):20500-11.

25.   Usui T, Kubo Y, Akanuma S, Hosoya K. Beta-alanine and l-histidine transport across the inner blood-retinal barrier: potential involvement in L-carnosine supply. Exp Eye Res. 2013;113:135-42.

26.   Broer A, Wagner CA, Lang F, Broer S. The heterodimeric amino acid transporter 4F2hc/y+LAT2 mediates arginine efflux in exchange with glutamine. Biochem J. 2000;349 Pt 3:787-95.

27.   Wang X-X, Hu Y, Keep RF, Smith DE. A Novel Role for PHT1 in the Disposition of L-Histidine in Brain: In Vitro Slice and In Vivo Pharmacokinetic Studies in Wildtype and Pht1 Null Mice. 2016.

28.   Kodaira H, Kusuhara H, Fuse E, Ushiki J, Sugiyama Y. Quantitative investigation of the brain-to-cerebrospinal fluid unbound drug concentration ratio under steady-state conditions in rats using a pharmacokinetic model and scaling factors for active efflux transporters. Drug Metab Dispos. 2014;42(6):983-9.

29.   Badhan RK, Chenel M, Penny JI. Development of a physiologically-based pharmacokinetic model of the rat central nervous system. Pharmaceutics. 2014;6(1):97-136.

30.   Battistin L, Varotto M, Lorenzi AD. Amino acid uptake in vivo by the mouse brain and by various regions of the rabbit brain after drug-induced convulsions. Brain Res. 1975;89(2):215-24.

31.   Vahvelainen ML, Oja SS. Kinetics of influx of phenylalanine, tyrosine, tryptophan, histidine and leucine into slices of brain cortex from adult and 7-day-old rats. Brain Res. 1972;40(2):477-88.

CHAPTER 5

FUTURE DIRECTION

Compared with PEPT1 and PEPT2, little is known about the peptide/histidine transporter PHT1 regarding the expression, localization, function and pharmacological relevance. Based on previous but limited information, PHT1 protein was expressed in the brain and retina of rat, and showed high affinity for L-histidine (L-His). PHT1 protein was also expressed in the brain of adult but not neonatal rats and mice, showing a dominant role in glycylsarcosine brain uptake in adult rodents. However, the significance of PHT1 in uptake of its amino acid substrate, L-His, in brain was not evaluated in these studies. Thus, the *in vitro* brain slice and *in vivo* pharmacokinetic/biodistribution studies proposed here for L-His in brain are a good starting point from which to understand the role and significance of PHT1 in neuropeptide regulation, histamine homeostasis, and the potential for targeted drug delivery to neuronal and non-neuronal cell types. In this dissertation, the localization of PHT1 in different brain regions was confirmed. We also observed that the depletion of *Pht1* gene could cause an up-regulation of PEPT2 in both mRNA and protein levels. The transcription of several selected L-His amino acid transporters in brain were up/down-regulated between the genotypes, however, there is no consistent pattern of change in either a specific amino acid transporter or a brain region. In the future, a comprehensive evaluation of all the transporters

and enzymes related to histamine production in the brain is needed in order to better understand the impact of *Pht1* depletion on gene regulation, as well as the compensatory role of the histerminergic system.

One of the most important physiological functions of L-His in the brain is as a precursor of histamine. The dysfunction of PHT1 may contribute to the reduced levels of brain histamine under certain pathological conditions. Therefore, endogenous histamine levels may be a good indicator of PHT1 relevance in the histaminergic system in the brain. If the endogenous concentration of histamine was altered by *Pht1* ablation, further studies could be performed to test the behavioral phenotypes in *Pht1* null mice (e.g., pain sensitivity, sleep-wake cycle, food intake). In this dissertation, the significant role of PHT1 in the brain entry of L-His was demonstrated via *in vitro* brain slice and *in vivo* pharmacokinetic/biodistribution studies. Besides, uptake kinetics of PHT1 was quantified, for the first time, under *in vivo* condition via a non-linear mixed effect modeling approach. The substrate used is L-[^{3}H]His. However, by measuring the overall radioactivity of the biology samples using scintillation counter, we were not able to differentiate between L-His and its metabolites. A better separation analysis method is needed in order to quantify the products of exogenous L-His, such as HPLC coupled to a radioactivity detector. This information may provide us an insight of the correlation between *Pht1* gene polymorphism and neurological diseases.

Based on the substrate specificity study, the transport of L-His by PHT1 could be inhibited, as expected, by dipeptides (e.g., carnosine and glycylsarcosine) and excess L-His. However, an interesting finding was that several amino acids

substantially reduced the uptake of L-His via PHT1. This phenomenon has not been reported previously. Therefore, the interaction between amino acids with positive (L-His, L-lysine) or uncharged polar (L-asparagine, L-glutamine) side chains and PHT1 needs further investigation to test whether other amino acids, in addition to L-His, are substrates for PHT1. *Pht1*-transfected cell culture systems could be applied so that we could directly test the uptake of various amino acids and peptide/mimetics.

APPENDIX A

INDIVIDUAL DATA FROM CHAPTER 3

Table A-1 Uptake (µL/10g tissue) of 2 µM L-[³H]histidine in brain slices of adult

wildtype (WT) and *Pht1* null (Null) mice.

Time (min)	Cortex							
	WT				Null			
1	0.37	0.42	0.31	0.37	0.05	0.11	0.11	0.03
3	0.65	0.59	0.91	0.65	0.60	0.21	0.35	0.62
5	0.81	0.85	0.72	0.67	0.64	0.74	0.89	0.87
10	1.75	1.73	1.70	2.40	1.27	1.52	1.40	1.40
Time (min)	Cerebellum							
	WT				Null			
1	0.28	0.38	0.13	0.17	0.02	0.07	0.02	0.01
3	0.45	0.35	0.55	0.55	0.23	0.16	0.23	0.29
5	0.55	0.58	0.45	0.56	0.30	0.61	0.46	0.70
10	0.90	0.70	0.46	0.58	0.50	0.57	0.98	0.68
Time (min)	Hippocampus							
	WT				Null			
1	0.49	0.40	0.66	0.27	0.26	0.28	0.20	0.07
3	0.51	1.10	1.02	0.87	0.28	0.23	0.48	0.42
5	0.88	0.83	1.40	0.94	0.92	0.94	0.72	0.82
10	1.46	1.66	1.99	1.59	0.96	0.87	1.06	0.96
Time (min)	Hypothalamus							
	WT				Null			
1	0.27	0.38	0.37	0.29	0.16	0.20	0.13	0.17
3	1.14	0.93	1.13	1.14	0.59	0.36	0.52	0.67
5	1.68	1.54	1.27	1.31	0.58	1.02	0.99	0.85
10	1.69	1.84	2.56	2.71	1.48	1.68	1.50	1.82

Table A-2 Uptake (μL/10g tissue) of 2 μM L-[³H]histidine at 3 min in hypothalamus slices of adult wildtype (WT) and *Pht1* null (Null) mice in the absence (control) or presence of potential inhibitors (5 mM). BCH, 2-aminobicyclo [2.2.1]heptane-2-carboxylic acid; GlySar, glycylsarcosine.

	WT				Null			
Control	1.14	0.93	1.13	1.14	0.59	0.36	0.52	0.67
Histidine	0.20	0.27	0.21	0.15	0.21	0.21	0.22	0.17
Glutamine	0.17	0.15	0.27	0.15	0.21	0.14	0.19	0.15
BCH	0.14	0.19	0.26	0.15	0.17	0.15	0.20	0.18
Lysine	0.18	0.19	0.22	0.31	0.18	0.19	0.18	0.23
Asparagine	0.24	0.21	0.22	0.24	0.22	0.22	0.24	0.25
Leucine	0.79	0.66	0.69	0.82	0.36	0.29	0.33	0.30
Carnosine	0.40	0.72	0.98	0.75	0.79	0.40	0.65	0.40
GlySar	0.40	0.40	0.36	0.61	0.44	0.44	0.52	0.40

Table A-3   Plasma concentration-time profiles of L-[^{14}C]histidine (μM) in wildtype

(WT) and *Pht1* null (Null) mice after 1 nmol/g intravenous bolus dose.

Time (min)	WT										
	1	2	3	4	5	6	7	8	9	10	11
0.5	2.80	3.67	6.86	2.06	3.17	2.20	6.16	2.19	3.18	3.54	
1.0	1.84	2.47	3.33	2.01	1.40	1.55	4.90	1.96	2.82	3.36	2.92
2.0	1.65	2.56	2.84	1.74	1.09	1.29	4.21	1.71	2.59	3.79	
5.0	1.46	1.74	2.02	1.38	0.83	0.73	2.72	1.29	1.91	2.29	1.26
10.0							1.98	1.07	1.31	1.86	1.03
15.0									1.02	1.42	1.00
20.0									0.95	1.28	0.94
30.0									0.80	0.97	0.55

Time (min)	Null											
	1	2	3	4	5	6	7	8	9	10	11	12
0.5	3.80		2.47	3.84	6.12	2.69	2.74	2.24	4.81	5.82	5.20	3.69
1.0	2.64	3.52	1.67	2.87		1.67	2.06	1.84	2.39	3.63	4.93	3.30
2.0	2.09	2.46	1.37	3.04		1.67	1.84	1.65	2.09	2.07	4.14	
5.0	1.85	1.61	0.88	1.98	2.75	1.80	1.50	1.32	1.37	1.26		1.69
10.0					2.09	1.53	1.20	1.08	1.03	0.76		1.18
15.0									0.63	0.53	1.01	1.06
20.0									0.51	0.40	1.54	0.93
30.0									0.35	0.37	1.42	0.95

Table A-4 Tissue and cerebrospinal fluid (CSF) concentrations of L-[^{14}C]histidine in brain regions of wildtype (WT) and *Pht1* null (Null) mice after 1 nmol/g intravenous bolus dose.

Time (min)	Cortex (nmol/g) WT						Null			
2.0	0.33	0.41	0.40				0.08	0.25	0.29	
5.0	0.45	0.45	0.48	0.33	0.48	0.50	0.28	0.29	0.35	0.19
10.0	0.64	0.41	0.44	0.37	0.43		0.47	0.42	0.34	0.41
20.0	0.42	0.42	0.44				0.32	0.41	0.35	
30.0	0.51	0.47	0.45				0.41	0.41	0.47	0.40

Time (min)	Cerebellum (nmol/g) WT						Null			
2.0	0.34	0.50	0.43				0.21	0.30	0.25	
5.0	0.46	0.64	0.52	0.38	0.62	0.70	0.38	0.35	0.39	0.22
10.0	0.65	0.40	0.45	0.42	0.43		0.47	0.42	0.46	0.42
20.0	0.43	0.48	0.47				0.47	0.50	0.45	
30.0	0.50	0.49	0.34				0.45	0.38	0.36	0.41

Time (min)	Hypothalamus (nmol/g) WT						Null			
2.0	0.58	0.42	0.42				0.21	0.28	0.29	
5.0	0.66	0.68	0.48	0.43	0.63	0.60	0.35	0.33	0.31	0.22
10.0	0.56	0.41	0.53	0.41	0.42		0.48	0.42	0.49	0.41
20.0	0.44	0.45	0.50				0.40	0.39	0.47	
30.0	0.49	0.48	0.49				0.47	0.41	0.47	0.42

Time (min)	Hippocampus (nmol/g) WT						Null			
2.0	0.30	0.37	0.37				0.21	0.23	0.31	
5.0	0.54	0.64	0.43	0.36	0.59	0.59	0.26	0.28	0.37	0.26
10.0	0.62	0.40	0.55	0.37	0.45		0.44	0.43	0.39	0.42
20.0	0.46	0.52	0.45				0.42	0.37	0.42	
30.0	0.50	0.48	0.47				0.42	0.41	0.46	0.44

Time (min)	CSF (nmol/mL) WT						Null			
2.0	0.14	0.18	0.17				0.24	0.14	0.15	
5.0	0.03	0.04	0.09	0.12	0.12	0.20	0.08	0.10	0.09	
10.0	0.06	0.08	0.14				0.11	0.07	0.09	
20.0	0.12	0.07	0.08				0.07	0.06	0.08	
30.0	0.11	0.09	0.07				0.09	0.07	0.08	0.08

APPENDIX B

POPULATION PHARMACOKINETICS OF MYCOPHENOLIC ACID IN LUNG TRANSPLANT RECIPIENTS WITH AND WITHOUT CYSTIC FIBROSIS

ABSTRACT

Purpose The objective of this work was to characterize and compare the population pharmacokinetics (PK) mycophenolic acid (MPA) in adult lung transplant recipients with cystic fibrosis (CF) and without the disease (NCF) following repeated oral administration of the prodrug mycophenolate mofetil (MMF) as an immunosuppressant.

Methods Three separate 12-hr PK visits were conducted for lung transplant patients with or without CF following repeated MPA treatment with at least a 2-week break between the visits. A population PK model was developed using nonlinear mixed effects modeling (NONMEM) and the contribution of physiological and pathological factors and time dependence of apparent oral clearance (CL/F) were assessed.

Results For both CF and NCF patients, MPA serum concentration-time profiles were best described by a two-compartment PK model with first-order absorption. CF patients had a slower absorption rate (K_a), and elevated CL/F and volume of

distribution (Vd/F) compared with NCF patients. There is a significant contribution of body weight and CF disease to MPA CL/F, and both were included in the final model as covariates.

Conclusions The population PK model developed from our study successfully characterizes the absorption, distribution, and elimination of MPA in lung transplant recipients with or without CF disease. The decrease of MPA absorption and increase of both oral clearance (CL/F) and volume of distribution (V_2/F and V_3/F) in the CF patients would suggest the importance of MPA therapeutic monitoring for this group.

INTRODUCTION

Mycophenolate mofetil (MMF) has become a mainstay immunosuppressant in lung transplantation, in which approximately 50% of all lung transplant recipients worldwide were treated with MMF combined with tacrolimus between 1995 and 2011 [1]. MMF is a prodrug of mycophenolic acid (MPA). It is well known that the pharmacokinetics (PK) of MPA exhibit high inter-individual variability [2]. Co-morbidities that contribute to the PK parameter variability include severe renal impairment, hypoalbuminemia, and cystic fibrosis (CF) [2].

CF is the third leading cause for lung transplantation, accounting for 17% of all lung transplant indications [1]. CF is caused by mutations in the CF transmembrane conductance regulator gene (CFTR) leading to abnormal sodium chloride transport in multiple organs including the gastrointestinal tract [3]. Pancreatic ductal epithelium, intestinal epithelium, and the hepatobiliary ductal system can be affected by CFTR mutations leading to pancreatic insufficiency,

intestinal obstruction, and focal biliary cirrhosis as well as cholelithiasis and cholecystitis, all of which can affect drug absorption and metabolism [4]. In recent years, lung transplantation has been introduced as a treatment for patients with end-stage lung disease including those patients with CF. However, information concerning the population PK properties of MPA in lung transplantation is limited, especially in CF patients.

The objective of this work was to evaluate and compare the population PK and time-dependent oral clearance of MPA in adult lung transplant recipients with CF or without the disease (NCF) using nonlinear mixed effects modeling (NONMEM). Further understanding of MPA population PK in patients with CF undergoing lung transplantation could help to improve dose optimization and treatment outcomes, and reduce allograft rejection in this patient population.

METHODS

Patients

Adult lung transplant patients (5 CF and 5 NCF) were enrolled in this pilot, open-label, PK study. The NCF patients underwent transplantation owing to idiopathic pulmonary fibrosis, emphysema, or pulmonary hypertension. All patients were maintained on tacrolimus, MMF and prednisone. Only lung transplant patients on tacrolimus were included in this PK study to avoid the effect of cyclosporine on multidrug resistance protein 2 and its subsequent effect on the second peak of MPA levels. In addition, all the patients were receiving insulin due to diabetes as well as proton pump inhibitor for gastric acid suppression.

Patients were given repeated daily oral doses of MMF with dosages ranging from 500 to 1500 mg twice a day. Three separate 12-hr PK visits were conducted for each patient with at least a 2-week break between the visits (Supplementary Table S1). Patients were admitted to the clinical research unit after an overnight fast. Patients had serial blood samples (5 mL each) drawn at various times at predose and 0.5, 1, 2, 3, 4, 6, 8 and 12 hours after the MMF morning dose. Serum concentrations of MPA were determined by a validated liquid chromatography-tandem mass spectrometry method [5]. Demographic (age, weight, gender) and clinical (serum creatinine (Scr), albumin, creatinine clearance (CrCL)) data were collected and summarized in Table S1. CrCl (ml/min) was calculated with the Cockroft–Gault formula.

This study was approved by our institutional review board (#HUM00020989) and registered in clinical trials.gov (NCT00908830). Written informed consent was obtained from all patients.

Non-compartmental pharmacokinetic analysis

Serum concentration versus time curves of MPA was initially fit to a non-compartmental model, using WinNonlin version 5.0.1 (Pharsight Inc., Mountain View, CA). Total area under the concentration-time curve (AUC_{0-12h}) was calculated using the trapezoidal rule. Apparent oral clearance (CL/F), apparent volume of distribution (Vd/F), maximum plasma concentration (C_{max}) and time to reach C_{max} (T_{max}) were calculated using standard methods. Since the oral bioavailability (F) could not be determined, values for clearance and volume of distribution were expressed as apparent values.

Population Pharmacokinetics Analysis

Population PK analysis was performed for the MPA serum concentrations from CF patients and NCF patients. Generally, the population PK modeling was carried out using a nonlinear-mixed effects modeling approach by NONMEM software version 7 (ICON Development Solutions, MD, USA). The first-order conditional estimation (FOCE) method with interaction was used to build the compartment models throughout the modeling procedure to estimate PK parameters and variability. Model development was guided by the likelihood ratio test using objective function values (OFV), graphical goodness-of-fit and potential clinical plausibility. Graphical and statistical analyses of NONMEM output and simulations were performed using S-Plus 6.2 and R version 3.0.2 with Xpose package. The compartmental pharmacokinetic model was built through a stepwise approach.

First, one-, two- and three-compartment models were performed using log-transformed or non-transformed serum concentration data. The models with or without a lag time (t_{lag}) were also evaluated. First-order absorption and elimination were assumed in our analysis. Basic pharmacokinetic parameters were estimated by NONMEM using conventional equations, including absorption rate constant (K_a), apparent volume of distribution of each compartment (V_i/F, i = 1, 2, 3), apparent clearance (CL/F) and inter-compartmental clearance (Q/F) (i.e., in multi-compartmental models).

The IIV term of the PK parameters was also assumed to follow a log-normal distribution and described by an exponential error model:

$$P_i = \theta \times exp(\eta_i)$$

where P_i represents the parameter estimate for the ith individual, θ is the typical individual, and η_i is the IIV term. The values of η_i were assumed to follow a normal distribution with mean of zero and estimated variance of ω^2.

Additive, proportional and mixed error models were evaluated for the residual unexplained variability using the following equations:

$$Y = IPRED + \varepsilon$$

$$Y = IPRED \times (1 + \varepsilon)$$

$$Y = IPRED \times (1 + \varepsilon_1) + \varepsilon_2$$

where Y is the observed concentration, $IPRED$ is the individual prediction and ε represents the residual variability. The values of ε follow a normal distribution with mean of zero and variance of σ^2.

The impact of patient demographic and clinical covariates on pharmacokinetic parameters was investigated. Covariates, η and ε terms were maintained in the model only if they can decrease OFV at least by 3.84 (χ^2 p-value $\leq$ 0.05).

Visual Predictive Check

The final PK model was evaluated by visual predictive checks. One thousand hypothetical patient data sets were simulated using the parameter estimates of the final model. The 95% prediction intervals for the simulated median, 5th and 95th percentiles were calculated and compared with the observed data points.

RESULTS

Demographic and clinical data of CF and NCF in lung transplantation patients were summarized in Supplementary Table S1. CF patients recruited in this study were significantly younger than NCF patients and had lower serum albumin levels. MPA PK parameters were estimated by both non-compartmental analysis and non-linear mixed effects modeling (NONMEM), and the results were summarized in Table B-1 and B-2. The MPA AUCs in lung transplantation patients with CF (133 μM×hr) and without CF (175 μM×hr) were comparable to those reported previously in the literature [5]. Based on the results of non-compartmental analysis, it appears that the CF group had a lower MPA C_{max} and a longer T_{max}, suggesting a slower absorption in those patients (Table B-1). In addition, both MPA CL/F and Vd/F in the CF group appear higher than the corresponding values in the NCF group (Table B-1). When MPA PK parameters from visits 1, 2 and 3 were compared, an increase of MPA CL/F with time was observed in the CF patients, while no obvious time dependency of other parameters were observed. The contribution of time to MPA CL/F in CF patients was further evaluated during population PK model development using NONMEM.

During the population PK analysis, MPA serum concentration-time profiles for both CF and NCF patients were best described by a two-compartment model with first-order absorption. A proportional error model was selected in the final model for the residual unexplained variability. The contribution of CF disease, demographic and clinical covariates (e.g., age, gender, body weight, CrCL) was

evaluated during model development. There is a significant contribution ($p \leq 0.05$) of body weight (WT) and CF disease to CL/F and both were included as covariates in the final model (Table B-2). As mentioned above, the time-dependency of CL/F was also evaluated during model development. The final model incorporating time as a covariate for CL/F in the CF patients significantly improved model prediction ($p \leq 0.05$), and increase of CL/F with time in each CF patient was shown in Fig. B-1. The basic goodness-of-fit plots for the final model was presented in Fig. B-2. One thousand hypothetical patient data sets were simulated using the parameter estimates from the final model and the plot was presented in Fig. B-3. The 95% prediction intervals of the median, 5th and 95th percentiles of simulated results could cover the observed data percentiles.

DISCUSSION

MMF is widely used in combination with calcineurin inhibitors to prevent acute allograft rejection in solid organ transplantation. Its PK characteristics are well investigated in renal and hepatic transplant recipients with therapeutic MPA AUC ranging from 30 - 60 mg×hr/L as reported in the literature [5-7]. In recent years, lung transplantation has been introduced as a treatment for patients with end-stage lung disease including those patients with CF. However, information on MPA population PK in lung transplantation is limited, especially in CF patients. Meanwhile, highly variable and unpredictable PK of MPA in solid organ transplant recipients with various diseases often challenges the optimization of MPA dosage regimens [7-10]. In this study, MPA PK properties were evaluated and compared in lung transplant patients with and without CF disease. In the population PK analysis,

MPA PK profiles were best described by a 2-compartment model in both NCF and CF patients. In general, the disposition of many drugs is altered in CF patients, and changes in PK can include decreased absorption, increased volume of distribution, decreased plasma concentration, and enhanced renal and sometimes non-renal elimination of drugs. In our study, alterations in MPA absorption, and possibly distribution and elimination were also observed in the CF patients. Patients with CF disease had a slower absorption rate (mean K_a = 1.05 hr^{-1}), along with enhanced oral clearance (mean CL/F = 17.83 L/hr) and volume of distribution (mean V_2/F = 83.68 L, V_3/F = 151.6 L) (The mean value of MPA PK parameters in the CF group were calculated based on the individual PK parameters of all visits estimated from the final population PK model). Even after correction for body weight, the CL/F (0.25 L/hr/kg in CF vs. 0.14 L/hr/kg in NCF) (Fig. B-4), V_2/F (1.2 L/kg in CF vs. 0.36 L/kg in NCF), and V_3/F (2.41 L/kg in CF vs. 1.49 L/kg in NCF) were still higher in the CF group. According to the NCA, CL/F for CF patients was 12.68 L/hr, which was 71% of the value obtained from the compartmental model. The discrepancy may due to different calculation algorithms being used by NONMEM and WinNonlin. For WinNonlin, CL/F was mainly based on the fit of terminal phase, while for NONMEM, CL/F was determined according to the overall drug concentration profile. The reduced K_a of MPA in CF patients is possibly due to gastrointestinal malabsorption, intestinal obstruction, focal biliary cirrhosis, and pancreatic insufficiency associated with CF disease [11-14]. MPA is primarily eliminated by hepatic oxidative metabolism followed by conjugation and biliary excretion, and increased hepatic metabolism has been reported previously in the literature for several other drugs

(e.g., theophylline, lorazepam, ibuprofen, tobramycin, doxycycline) in patients with CF [15-19]. The altered CL/F of MPA in CF patients may be explained by several reasons. First, the CF group had a significantly lower serum albumin level than the NCF group (Supplementary Table S1). In the blood, approximately 97% of MPA is bound to serum albumin and other plasma proteins, and albumin concentration is positively correlated with MPA plasma protein binding [20]. The hepatic metabolism of MPA is directly affect by its protein binding ratio [21]; in other words, a lower albumin concentration observed in CF patients may explain the enhancement of CL/F for MPA if the free fraction of MPA in serum is increased [22, 23]. Second, if the intrinsic hepatic clearance increased in CF patients, an elevated CL/F might also be observed. Third, MPA is a substrate of p-glycoprotein, and elevated p-glycoprotein level in the CF patients was reported previously, which may help to explain the decrease in oral availability, and increase in CL/F and Vd/F of MPA [24, 25]. Finally, the higher CL/F value may be explained by the reduced bioavailability due to complications of CF as mentioned previously, which can be confirmed by studying the kinetics after intravenous dosing. Similarly, the higher Vd/F of MPA in CF patients may also be explained by relatively lower plasma albumin level and lower oral bioavailability compared with the NCF patients. In addition, a lower free fraction of MPA in the tissues of CF patients may increase Vd/F, as more drug molecules are bound to peripheral tissues.

A significant contribution of time, associated with MPA CL/F in the CF group, was observed during population PK model development (Fig. B-1). The time-dependent changes in the PK of patients with CF were also reported in the literature

for tobramycin, ceftazidime, and other drugs [15, 26, 27]. In our study, the final PK model incorporating a time-dependent term for the CL/F in CF patients significantly improved model prediction. However, incorporating time for CL/F in the NCF patients did not change model prediction. The time dependency for K_a, V_2/F and V_3/F in both CF and NCF groups was also assessed in model development and no significant contributions were identified. For lung transplant recipients, a high risk of allograft failure exists due to acute rejection, which may be caused by insufficient immunosuppression. The apparent increase of CL/F with time in the CF group, and the differences of MPA PK parameters in the CF and NCF patients suggest that therapeutic drug monitoring of MPA may be needed after lung transplantation, especially for the CF patients, to help reduce the risk of treatment failure and acute post-transplant rejection [1, 28, 29].

In conclusion, the population PK model developed from our study successfully characterizes the absorption, distribution, and elimination of MPA in lung transplant recipients with or without CF disease. The decrease of MPA absorption and increase of both apparent oral clearance (CL/F) and volume of distribution (V_2/F and V_3/F) in the CF patients would suggest the importance of MPA therapeutic monitoring for this group.

FIGURES AND TABLES
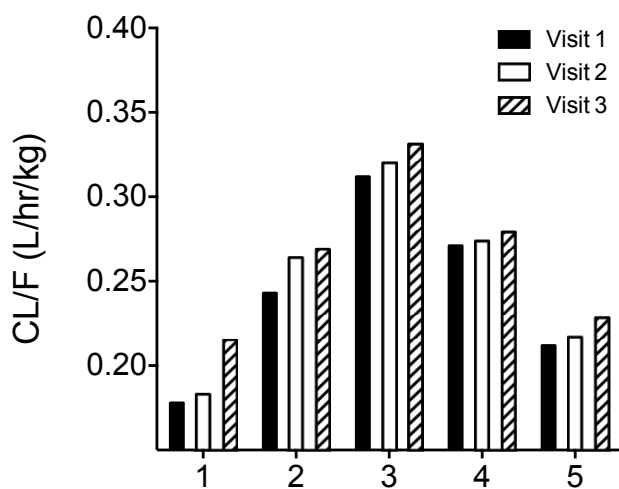
Fig. B-1 Changes of apparent oral clearance corrected by body weight (CL/F) in each cystic fibrosis patient with time based on population pharmacokinetic model.
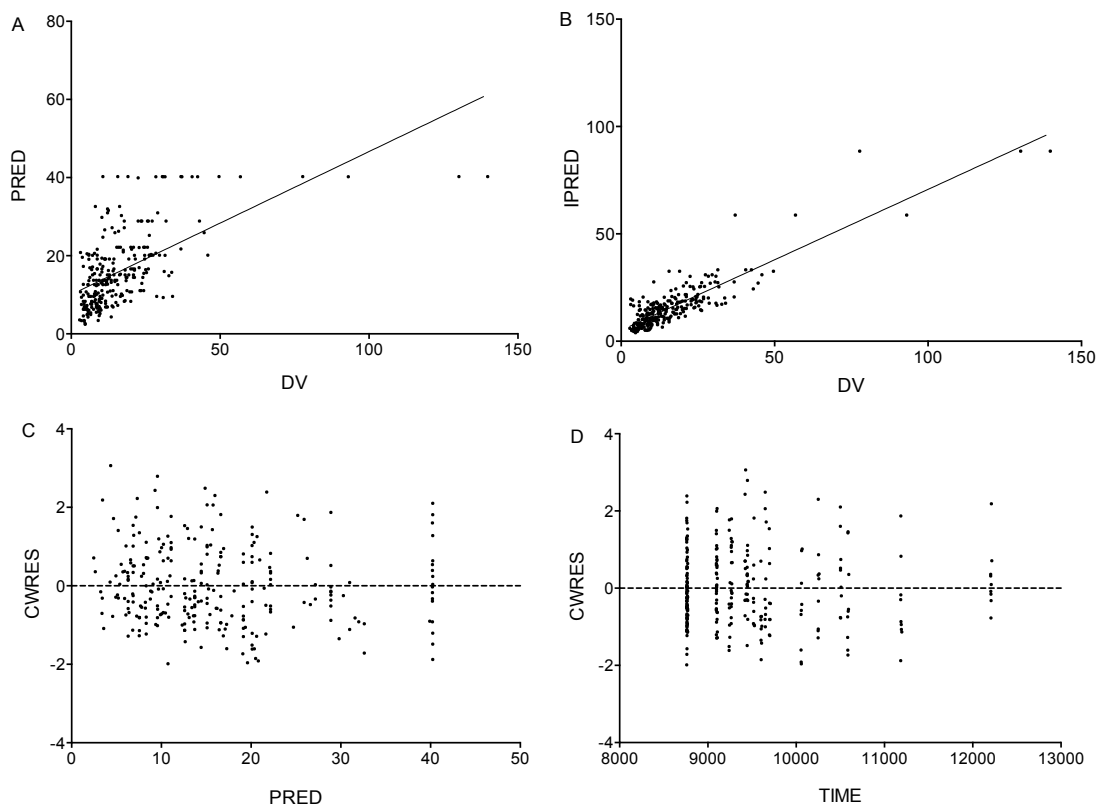
Fig. B-2 Basic goodness-of-fit plots of population pharmacokinetic parameters in two groups of patients. PRED population predicted mycophenolic acid (MPA) concentration (μM), DV observed MPA concentration (μM), IPRED individually predicted MPA concentration (μM), CWRES conditional weighted residual

113
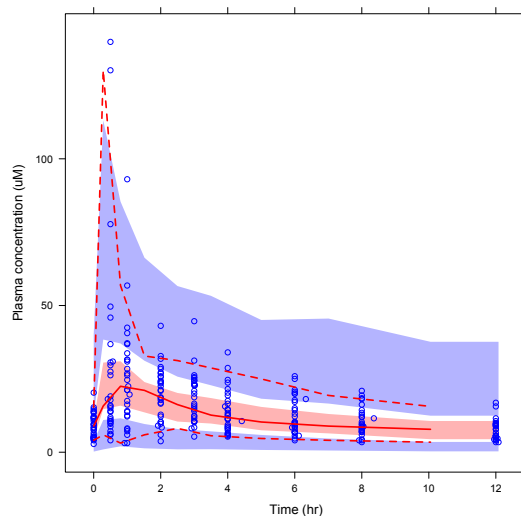
Fig. B-3 Visual predictive check of the final pharmacokinetic model of mycophenolic acid (MPA) in patients based on 1000 simulations. Observed data are shown as dots. Solid and dashed lines represent the median, 5th and 95th percentiles of observed data. Semitransparent red field represents the 95% confidence interval for the simulated median. Semitransparent blue fields represent the 95% confidence interval for the simulated percentiles.
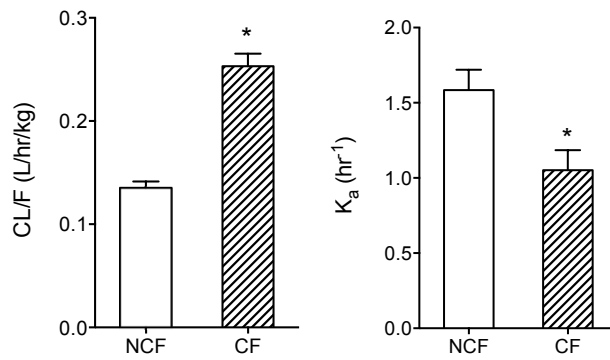
Fig. B-4 Comparison of population pharmacokinetic parameters between patients with cystic fibrosis (CF) or without the disease (NCF). Values are mean ± SE (n=5). *p≤0.05 as compared to NCF patients

Table B-1 Non-compartmental pharmacokinetic parameters in patients with cystic

fibrosis (CF) or without the disease (NCF)

Parameter	NCF		CF	
	Mean	%CV	Mean	%CV
Dose range (µmol)	577-2307		1153-3460	
T_{max} (hr)	1.14	82	2.07*	73
C_{max} (µM)	44.9	81	25.0*	37
C_{max} /(Dose/100)	2.63	NA	1.24*	NA
AUC_{0-12h} (µM×hr)	175	54	133*	35
AUC_{0-12h} /(Dose/100)	15.9	NA	11.6*	NA
Vd/F (L)	78.0	58	120*	69
CL/F (L/hr)	7.32	38	12.7*	52
$t_{1/2}$ (hr)	8.50	87	7.17	61

%CV coefficient of variation for variability, NA not applicable

*p≤0.05 as compared to NCF patients

The parameters were calculated using all of the data from three visits

Table B-2 Population pharmacokinetic parameter estimates for mycophenolic acid with time-dependent apparent oral clearance (CL/F) for cystic fibroses (CF) patients

Parameter	Estimates (%RSE)	IIV %CV (%RSE)
$CL/F = (\theta_1 + (\theta_2 + TIME{\times}\theta_3){\times}FLAG_i){\times}(WT_i/71)^{\theta_4}$		
CL/F (L/hr)		18.7 (34)
θ_1	9.30 (12)	
θ_2	8.53 (21)	
θ_3	$2.51{\times}10^{-2}$ (22)	
θ_4	1.59 (29)	
V_2/F (L)	42.3 (28)	99.5 (49)
Q/F (L/hr)	31.4 (20)	57.3 (56)
V_3/F (L)	125 (60)	62.6 (120)
K_a (hr^{-1})	1.19 (44)	76.4 (66)
Residual variability	0.139 (13)	

θ_1 is the CL/F for a 71-kg weighing NCF patient, θ_2 is the difference on CL/F between CF and NCF patient at the first visit, θ_3 is the rate at which CL/F increase with time in CF patients, θ_4 is the estimated effect of body weight on CL/F. *FLAG*$_i$ is 1 when *i*th individual has the CF disease and 0 otherwise, WT body weight (kg), TIME time after the first visit (day), IIV inter-individual variability, CV coefficient of variation, RSE relative standard error

Table B-3 Clinical information [median (range)] of patients with cystic fibrosis (CF)

or without the disease (NCF)

	Age (years)	Weight (kg)	Gender		Time intervals between each visit (days)	Scr (mg/dl)	CrCL (ml/min)	Albumin (g/dl)
			male	female				
CF	27 (25-38)	62.4 (51-92.9)	2	3	21 (14-116)	1.03 (0.87-1.8)	96.1 (33.5-128.3)	3.8 (3.7-4)
NCF	59 (46-69)*	71.4 (65.8-84.2)	2	3	17 (14-87)	1.17 (0.93-1.37)	60 (52.1-88)	4.1 (3.9-4.3)*

Scr serum creatinine, CrCL creatinine clearance

*p≤0.05 as compared to NCF patients

REFERENCES

1.   Christie JD, Edwards LB, Kucheryavaya AY, Benden C, Dipchand AI, Dobbels F, et al. The Registry of the International Society for Heart and Lung Transplantation: 29th adult lung and heart-lung transplant report-2012. J Heart Lung Transplant. 2012;31(10):1073-86.

2.   Staatz CE, Tett SE. Clinical pharmacokinetics and pharmacodynamics of mycophenolate in solid organ transplant recipients. Clin Pharmacokinet. 2007;46(1):13-58.

3.   Kasper DL, Harrison TR. Harrison's principles of internal medicine. New York: McGraw-Hill, Medical Pub. Division; 2005. 2 v. (various pagings) p.

4.   Rey E, Treluyer JM, Pons G. Drug disposition in cystic fibrosis. Clin Pharmacokinet. 1998;35(4):313-29.

5.   Stuckey L, Clark Ojo T, Park JM, Annesley T, Bartos C, Cibrik DM. Mycophenolic acid pharmacokinetics in lung transplant recipients with cystic fibrosis. Ther Drug Monit. 2014;36(2):148-51.

6.   Karlsson MO, Sheiner LB. The importance of modeling interoccasion variability in population pharmacokinetic analyses. J Pharmacokinet Biopharm. 1993;21(6):735-50.

7.   Shaw LM, Figurski M, Milone MC, Trofe J, Bloom RD. Therapeutic drug monitoring of mycophenolic acid. Clin J Am Soc Nephrol. 2007;2(5):1062-72.

8.   Ting LS, Partovi N, Levy RD, Riggs KW, Ensom MH. Pharmacokinetics of mycophenolic acid and its glucuronidated metabolites in stable lung transplant recipients. Ann Pharmacother. 2006;40(9):1509-16.

9.   van Hest RM, Mathot RA, Pescovitz MD, Gordon R, Mamelok RD, van Gelder T. Explaining variability in mycophenolic acid exposure to optimize mycophenolate mofetil dosing: a population pharmacokinetic meta-analysis of mycophenolic acid in renal transplant recipients. J Am Soc Nephrol. 2006;17(3):871-80.

10.   Jiao Z, Zhong JY, Zhang M, Shi XJ, Yu YQ, Lu WY. Total and free mycophenolic acid and its 7-O-glucuronide metabolite in Chinese adult renal transplant patients: pharmacokinetics and application of limited sampling strategies. Eur J Clin Pharmacol. 2007;63(1):27-37.

11.   de Winter BC, Monchaud C, Premaud A, Pison C, Kessler R, Reynaud-Gaubert M, et al. Bayesian estimation of mycophenolate mofetil in lung transplantation, using

a population pharmacokinetic model developed in kidney and lung transplant recipients. Clin Pharmacokinet. 2012;51(1):29-39.

12.   Gerbase MW, Fathi M, Spiliopoulos A, Rochat T, Nicod LP. Pharmacokinetics of mycophenolic acid associated with calcineurin inhibitors: long-term monitoring in stable lung recipients with and without cystic fibrosis. J Heart Lung Transplant. 2003;22(5):587-90.

13.   Pittman FE, Denning CR, Barker HG. Albumin Metabolism in Cystic Fibrosis. Am J Dis Child. 1964;108:360-5.

14.   Strober W, Peter G, Schwartz RH. Albumin metabolism in cystic fibrosis. Pediatrics. 1969;43(3):416-26.

15.   Horner GW, Stempel DA. Tobramycin elimination rate change from first to later doses in older cystic fibrosis patients. Drug Intell Clin Pharm. 1987;21(3):276-8.

16.   Kearns GL, Mallory GB, Jr., Crom WR, Evans WE. Enhanced hepatic drug clearance in patients with cystic fibrosis. J Pediatr. 1990;117(6):972-9.

17.   James LP, Stowe CD, Farrar HC, Menendez AA, Argao EA. The pharmacokinetics of oral ranitidine in children and adolescents with cystic fibrosis. J Clin Pharmacol. 1999;39(12):1242-7.

18.   Beringer PM, Owens H, Nguyen A, Benitez D, Rao A, D'Argenio DZ. Pharmacokinetics of doxycycline in adults with cystic fibrosis. Antimicrob Agents Chemother. 2012;56(1):70-4.

19.   Konstan MW, Hoppel CL, Chai BL, Davis PB. Ibuprofen in children with cystic fibrosis: pharmacokinetics and adverse effects. J Pediatr. 1991;118(6):956-64.

20.   Bullingham RE, Nicholls AJ, Kamm BR. Clinical pharmacokinetics of mycophenolate mofetil. Clin Pharmacokinet. 1998;34(6):429-55.

21.   Bowalgaha K, Miners JO. The glucuronidation of mycophenolic acid by human liver, kidney and jejunum microsomes. Br J Clin Pharmacol. 2001;52(5):605-9.

22.   de Winter BC, van Gelder T, Sombogaard F, Shaw LM, van Hest RM, Mathot RA. Pharmacokinetic role of protein binding of mycophenolic acid and its glucuronide metabolite in renal transplant recipients. J Pharmacokinet Pharmacodyn. 2009;36(6):541-64.

23.   van Hest RM, van Gelder T, Vulto AG, Mathot RA. Population pharmacokinetics of mycophenolic acid in renal transplant recipients. Clin Pharmacokinet. 2005;44(10):1083-96.

24.   Sawamoto T, Van Gelder T, Christians U, Okamura N, Jacobsen W, Benet L. Membrane transport of mycophenolate mofetil and its active metabolite, mycophenolic acid in MDCK and MDR1-MDCK cell monolayers. J Heart Lung Transplant. 2001;20(2):234-5.

25.   Susanto M, Benet LZ. Can the enhanced renal clearance of antibiotics in cystic fibrosis patients be explained by P-glycoprotein transport? Pharm Res. 2002;19(4):457-62.

26.   Padoan R, Brienza A, Crossignani RM, Lodi G, Giunta A, Assael BM, et al. Ceftazidime in treatment of acute pulmonary exacerbations in patients with cystic fibrosis. J Pediatr. 1983;103(2):320-4.

27.   Billaud EM, Guillemain R, Berge M, Amrein C, Lefeuvre S, Louet AL, et al. Pharmacological considerations for azole antifungal drug management in cystic fibrosis lung transplant patients. Med Mycol. 2010;48 Suppl 1:S52-9.

28.   Arns W, Cibrik DM, Walker RG, Mourad G, Budde K, Mueller EA, et al. Therapeutic drug monitoring of mycophenolic acid in solid organ transplant patients treated with mycophenolate mofetil: review of the literature. Transplantation. 2006;82(8):1004-12.

29.   Rousseau A, Laroche ML, Venisse N, Loichot-Roselmac C, Turcant A, Hoizey G, et al. Cost-effectiveness analysis of individualized mycophenolate mofetil dosing in kidney transplant patients in the APOMYGRE trial. Transplantation. 2010;89(10):1255-62.

APPENDIX C

POPULATION PHARMACOKINETICS OF MYCOPHENOLIC ACID AND ITS GLUCURONIDE METABOLITE IN LUNG TRANSPLANT RECIPIENTS WITH AND WITHOUT CYSTIC FIBROSIS

ABSTRACT

Cystic fibrosis (CF) is a disease affecting multiple organs that may reduce the systemic exposure of some drugs. The objective of this work was to characterize and compare the population pharmacokinetics (PK) of the immunosuppressant mycophenolic acid (MPA), and its glucuronide metabolite (MPAG) in adult lung transplant recipients with and without CF (NCF) following repeated oral administration of the prodrug mycophenolate mofetil (MMF).

A population PK model was developed, with simultaneously modeling of MPA and MPAG, using nonlinear mixed effects modeling. MPA and MPAG serum concentration-time data were adequately described by a compartmental model including enterohepatic recirculation (EHR). Both MPA and MPAG apparent clearance values were significantly elevated (> 65%) in CF patients (24.1 and 1.95 L/hr, respectively) compared to the values in the NCF patients (14.5 and 1.12 L/hr, respectively), suggesting a notable influence of CF on MPA absorption and disposition.

The population PK model developed from our study successfully characterized the absorption, distribution, elimination and EHR of MPA and the metabolite MPAG in lung transplant recipients with or without CF. This model may help to further understand the impact of CF to the overall clinical effects of MPA therapy including immunosuppression and gastrointestinal side effects.

INTRODUCTION

Mycophenolate mofetil (MMF) is an immunosuppressant prodrug of mycophenolic acid (MPA). It has been used widely for the prophylaxis of acute allograft rejection in solid organ transplantation. For adult lung transplant recipients, MMF combined with tacrolimus accounts for approximately 50% of maintenance immunosuppressant therapy [1-3].

After oral administration, MMF was rapidly and nearly completely hydrolyzed to the active metabolite MPA resulting in undetectable MMF level in plasma [4]. The MPA was then primarily (~90%) converted to a stable metabolite, MPA-7-O-glucuronide (MPAG) in the body [3, 5]. MPAG is a pharmacologically inactive metabolite that may undergo enterohepatic recirculation (EHR), and converted back to MPA, contributing approximately 40% of MPA area under the concentration-time curve (AUC) [5, 6]. EHR of MPAG may prolong the exposure of MPA in intestinal epithelium [7], which is closely linked to significant gastrointestinal side effects such as leukopenia and diarrhea [8, 9]. Therefore, a better understanding of the pharmacokinetics (PK) of MPAG EHR is needed considering its contributions to the systemic exposure and gastrointestinal toxicity of MPA.

Cystic fibrosis (CF) is one of the top three leading causes for lung transplantation, which is caused by a defect in CF transmembrane conductance regulator (CFTR) in epithelial cells [10]. Lung transplantation may eventually be required due to progressive respiratory insufficiency, in order to improve survival and quality of life in patients with end-stage CF [10]. Altered pathophysiology in epithelial cells of multiple organs, including gastrointestinal tract, heart, liver and kidney, may affect the disposition and increase inter-individual variability (IIV) of PK parameters of drugs administered to CF patients through various complications, including gastric acid hypersecretion, bile acid malabsorption, proximal small intestinal mucosal injury, hypoalbuminaemia, hepatobiliary dysfunction and renal dysfunction [2, 11]. In addition, CF disease may also influence the EHR of several substrates. For example, a preclinical study showed that CFTR deficient mice had disrupted EHR of bile acids, owing to defects in gallbladder emptying [12]. Oral vitamin D supplementation also showed less effectiveness in CF patients which was caused by interruption of the EHR [13]. However, PK studies on MPA and the EHR of its metabolite, MPAG, in lung transplant recipients are limited, especially in CF patients [3].

According to our preliminary results [14], patients with lung transplantation owing to CF show significantly slower absorption and higher apparent clearance for MPA than NCF patients. However, in this study, the enterohepatic recirculation of MPAG was not considered. Given the critical association of this process, the back conversion of MPAG to MPA in the intestine, and the significant contribution to MPA systemic exposure and gastrointestinal toxicity, our original PK model was refined

to better integrate this complexity. Therefore, the objective of this work was to characterize and compared the EHR process in this specific disease population with other disease populations, and potentially provide useful information for MPA pharmacotherapy and gastrointestinal toxicity. In this study, a population PK model was developed, with simultaneously modeling of MPA and MPAG using nonlinear mixed effects modeling (NONMEM) and the contribution of physiological and pathological factors on PK parameters was evaluated.

METHODS

Patients

This study was approved by our institutional review board (#HUM00020989) and registered in clinical trials.gov (NCT00908830). Written informed consent was obtained from all patients.

Data came from adult lung transplant patients in a pilot, open-label, PK study as described previously [14, 15]. This study was performed at the University of Michigan Medical Clinical Research Unit. Briefly, inclusion criteria were: 1) 18-70 years of age; 2) >1 year post-transplant; 3) no evidence of acute rejection at 1 year post-transplant biopsy or within three months of study entry; 4) stable mycophenolate mofetil dose; and 5) stable renal function. Exclusion criteria were: 1) >2 mg/dL serum creatinine level; 2) received pulse steroids within 3 months of the study entry; 3) chronic diarrhea; or 4) concurrently on interacting medications (e.g., cholestyramine). A total of 270 MPA and 270 MPAG serum concentration-time data points from 10 patients were available for PK analysis. Five of these patients underwent transplantation owing to cystic fibrosis and the other five owing to

idiopathic pulmonary fibrosis, emphysema, or pulmonary hypertension. All patients were maintained on MMF, tacrolimus and prednisone, and received insulin due to diabetes as well as a proton pump inhibitor for gastric acid suppression.

Patients were given repeated daily oral doses of MMF (500 mg, 750 mg, 1000 mg or 1500 mg) with 12-hour dosing interval. MMF dose was determined based on the individual patient's immunological risk and clinical response by their transplant team. The dose was not altered for this study and patients were maintained on same doses throughout the study. After at least one-year post-transplant, three separate 12-hr PK visits were conducted for each patient with at least a 2-week break between the visits. There was no significant difference on sampling occasions since the start of the treatment or since the first PK visit between CF and NCF groups. Serial blood samples were drawn at predose and 0.5, 1, 2, 3, 4, 6, 8 and 12 hours after the MMF morning dose. No concomitant medication alterations were made during the PK visits. Time points for blood sampling were determined in order to characterize the absorption phase, second peak of MPA, and the disposition phase based on previous knowledge [5]. Serum concentrations of MPA and MPAG were determined by a validated liquid chromatography-tandem mass spectrometry method as previously described [15]. The method was validated as stated in the literature [16]. The inter and intra-day precision were < 11%, and the bias was < 16%. Demographic (age, weight, gender) and clinical (serum creatinine (Scr), albumin, creatinine clearance (CLcr)) data were collected and summarized in a previous paper [14].Non-compartmental analysis (NCA) of pharmacokinetics

Serum concentration versus time curves of MPA and MPAG were initially analyzed by a non-compartmental approach using Phoenix/WinNonlin version 6.4 (Pharsight Inc., Mountain View, CA). Steady-state area under the serum concentration-time curve ($AUC_{(0-12h)}$) was calculated over the 12-hr dosing interval by trapezoidal rule and normalized by dose. Dose normalized trough concentration (C_{trough}), maximum serum concentration (C_{max}) and time to reach C_{max} (T_{max}) were estimated by visual inspection.

Population pharmacokinetics modeling

The population PK model with simultaneous modeling of MPA and MPAG was developed with nonlinear mixed effects modeling by NONMEM software version 7 (ICON Development Solutions, MD, USA). Model structure selection was guided by the likelihood ratio test using objective function values (OFV), diagnostic plots, and potential clinical plausibility. Graphical and statistical analyses of NONMEM output and simulations were performed using R version 3.2.2 with Xpose version 4.5.3.

MPA and MPAG serum concentration-time data, after MMF oral administration, were adequately described by a model including first-order absorption of MPA from the gastrointestinal tract (GIT), central and peripheral compartments for MPA disposition, and a compartment for MPAG formation and enterohepatic recirculation (EHR) (Figure C-1). Several assumptions were made in model development: (1) the conversion from MMF to MPA was rapid and complete prior to reaching the systemic circulation; (2) the fraction of MPA metabolized to MPAG was fixed (90%) based on literature information [5]; and (3) all distribution

and elimination processes of drug and metabolite were first-order. Furthermore, MMF doses and MPA and MPAG serum concentrations were transformed into molar equivalents during the PK modeling procedure.

Inter-individual variability (IIV) of the PK parameters was assumed to follow a log-normal distribution and described by an exponential error model. Additive, proportional and mixed error models were evaluated for the residual unexplained variability using the following equations:

$$Y = F + \varepsilon$$
$$Y = F \times (1 + \varepsilon)$$
$$Y = F \times (1 + \varepsilon_1) + \varepsilon_2$$

where Y is the observed concentration, F is the individual prediction and ε is the residual variability. The impact of patient demographic and clinical covariates on PK parameters was evaluated. IIVs, residual errors and covariates were included in the model only if they were associated with a decrease in OFV by at least 3.84 (χ^2 p-value ≤ 0.05).

The impact of patient demographic and clinical covariates on Due to the limited number of patients included in this study (n=10), we had difficulty in estimation of the IIV for several PK parameters. Serial values for IIV were tested (0-100%) during the model development. 10% IIV produced the best fit among successful runs according to OFV and other model diagnostics. Therefore, those IIV values were fixed at 10%.

The final PK model was evaluated by non-parametric bootstrap analysis and visual predictive checks using Perl-speaks-NONMEM (PsN 4.2.0). The original dataset was resampled with 100 replicate datasets and the medians and 90%

confidence intervals of the parameter estimates from bootstrap samples were compared with final model estimates. For visual predictive checks, 500 hypothetical patient datasets were simulated using the parameter estimates of the final model. The 95% prediction intervals for the simulated median, 5th and 95th percentiles were calculated and compared with the observed data points of MPA or MPAG, respectively.

RESULTS

Dose normalized C_{max} and AUC_{ss} values of MPA and MPAG, and the corresponding T_{max} calculated by NCA, for each clinical visit are presented in Figure C-2. The Bland-Altman plot of the difference on dose normalized area under the serum concentration-time curve (AUC) between CF and NCF patients was shown in Figure C-3. It appears that the C_{max} and AUC_{ss} of both MPA and MPAG in the NCF patients were consistently higher than the corresponding values in the CF patients in all three visits. Dose normalized C_{trough} and $AUC_{(0-12h)}$ of MPAG and MPA in CF and NCF patients were listed and compared in Table C-1. $AUC_{(0-12h)}$ values of both MPAG and MPA were significantly lower in CF patients compared with patients without the disease. C_{trough} values were also lower in CF patients, but only showed statistical significance for MPAG.

Serum MPA and MPAG concentration-time profiles, after MMF oral administration, were adequately described by the compartmental model shown in Figure C-1. A mixed error model with both additive and proportional components was selected as the final model for the residual unexplained variability. The estimated rate constant describing biliary excretion and EHR of MPAG (K_{41}) is

129

comparable to literature values [17]. CF disease was included as a covariate for CL_{MPA}/F in the final model based on its statistically significant contribution (Table C-2).

For model diagnosis, goodness-of-fit plots (Figure C-3) did not show systematic bias for the PK model predictions. As shown in the visual predicted check plots (Figure C-4), observed MPA and MPAG concentration data were in good agreement with the 95% prediction intervals of 500 simulations of patient data sets based on parameter estimates from the final model. All model parameter estimates were within the 90% confidence intervals obtained by the bootstrap analysis (Table C-2).

DISCUSSION

MPAG is a major metabolite of MPA in human. Although MPAG may not directly contribute to the immunosuppression effect, it competes with MPA at plasma protein binding sites and may cause an increase of the free and pharmacologically active MPA concentration [5, 6]. Therefore, MPAG may indirectly contribute to the overall immunosuppression activity of MPA. MPAG is excreted into the bile where it may be deconjugated back to MPA and reabsorbed in the colon. It has been estimated that, on average, enterohepatic recycling contributes approximately 40% (range 10–60%) to MPA exposure [5]. Due to the presence of EHR, the exposure of MPA intestinal epithelium was prolonged and this effect is closely linked with side effects such as leukopenia and diarrhea [7-9]. Therefore, a better understanding of the PK associated with MPAG EHR is needed considering the gastrointestinal toxicity of MPA as well as its significant contribution to MPA

systemic exposure. Although several studies on the population PK modeling of MPA and MPAG have been published in patients with renal or hepatic transplantation [6, 7, 17, 18], limited information is available in lung transplant recipients, especially in patients with CF disease [3]. In the present study, a population PK model was developed that successfully characterized the absorption, distribution, elimination and EHR of both MPA and MPAG in lung transplant recipients with or without CF (Figure C-1). CF was identified as a covariate for CL_{MPA}/F in our current work. A significant decrease of MPA absorption and increase of both MPA and MPAG apparent clearance was identified in the CF patients, indicating the urgency of personalized medicine in MPA immune-suppression therapy especially for those patients with CF disease.

The model estimated population means of the absorption rate constant K_a (2.36 h^{-1}), apparent clearance CL_{MPA}/F (14.5 L/hr), and volumes of distribution ($V_{C,MPA}/F$ = 42.1 L, $V_{P,MPA}/F$ = 402 L) in the NCF group are close to the values reported in the literature (K_a: 2.27 - 4.10 h^{-1}, CL/F: 11.9 - 33.0 L/hr, V/F: 10.3 – 631.8 L) [19, 20]. Similarly, the population means of MPAG CL_{MPAG}/F (1.12 L/hr) and V_{MPAG}/F (8.9 L) from our model estimation were also consistent with literature values as reported previously (CL/F = 1.12 – 4.75 L/hr, V/F = 3.92 - 8.91 L) [6, 17-22]. Shrinkage values of CL_{MPA}/F, V_c/F, V_p/F, Q/F, K_a, CL_{MPAG}/F, V_{MPAG}/F, K_{41} and residual errors were 3.9%, 3.8%, 61.6%, 76.2%, 14.6%, 2.6%, 2.6%, 55%, 2.7% and 2.7%, respectively. Among these numbers, the shrinkage values of V_p/F, Q/F and K_{41} were higher than 30%, which could be an issue when data become sparse and uninformative, and affect model diagnostics (IWRES) [23]. However, in this study,

each dosing interval had at least 8 data points, and each patient's data came from 3 PK visits. In addition, the %RSE values (an index of the accuracy for the estimation of each parameter) for V_p/F, Q/F and K_{41} were $\leq 20\%$. As cited above, the population means of MPA and MPAG PK parameters estimated from our model were consistent with literature values reported previously. The model estimated rate constant describing EHR of MPAG (K_{41} = 0.09 hr^{-1}) was also comparable to literature values [17]. Therefore, shrinkage on these three parameters should not be a concern in this kind of circumstances [24].

CF is a genetic, autosomal recessive disorder, which leads to reduced mucociliary clearance and an increased risk of infections in the lungs. As the disease progresses, bilateral lung transplantation becomes a viable treatment option. Besides the lungs, CF affects the gut resulting in gastrointestinal (GI) malabsorption and pancreatic insufficiency and, therefore, may alter the disposition of both MPA and MPAG in lung transplant recipients with CF disease following the treatment of the immunosuppressant MMF. CF can affect the disposition of drugs in various aspects including decreased absorption, increased volume of distribution, decreased plasma concentration, and enhanced elimination [25-28]. In the present study, we have found a >44% decrease of MPA C_{max}, AUC, and the absorption rate constant K_a, and a 66% increase of MPA CL_{MPA}/F in CF patients (Figure C-2, Table C-2). The disposition of the metabolite, MPAG, was also affected by CF disease with a >39% lower C_{max} and AUC_{ss} values, and a 74% higher CL_{MPAG}/F. CF is caused by a defect in the cystic fibrosis transmembrane conductance regulator (CFTR) in epithelial cells. The differences observed in the PK parameters in the CF patients are not

unexpected. The CFTR protein functions as a cyclic AMP-regulated chloride channel and genetic mutations in this protein lead to abnormal chloride channel activity in multiple tissues including the GI tract. Pancreatic ductal epithelium, intestinal epithelium, and the hepatobiliary ductal system can be affected by CFTR mutations leading to pancreatic insufficiency, intestinal obstruction, focal biliary cirrhosis, and alterations in drug absorption and disposition [29]. MPAG is mainly excreted in the urine via glomerular filtration and/or tubular secretion [2, 5], therefore, renal function may influence the pharmacokinetics of MPAG to some extent [5]. Changes in the renal clearance of drugs in CF patients have been widely studied with conflicting results reported in the literature [11]. In our current study, a linear correlation between the MPAG apparent clearance and the creatinine clearance (CLcr) was observed as shown in Figure C-5 ($r^2=0.65$). The CLcr values appear higher in majority of the CF patients [15], suggesting the increase of MPAG apparent clearance may be associated with the enhanced glomerular filtration and/or tubular secretion in the CF group.

CONCLUSIONS

In conclusion, the population PK model developed from our study successfully characterized the absorption, distribution, elimination and EHR of MPA and the metabolite MPAG in lung transplant recipients with or without CF. This model may help to further understand the contribution of both MPA and MPAG to the overall clinical effects of MPA therapy including immunosuppression and gastrointestinal side effects, and could potentially be used to project the appropriate dose of MMF to achieve the targeted MPA efficacious exposure and the

immunosuppression effect in lung transplantation patients with or without the CF disease.
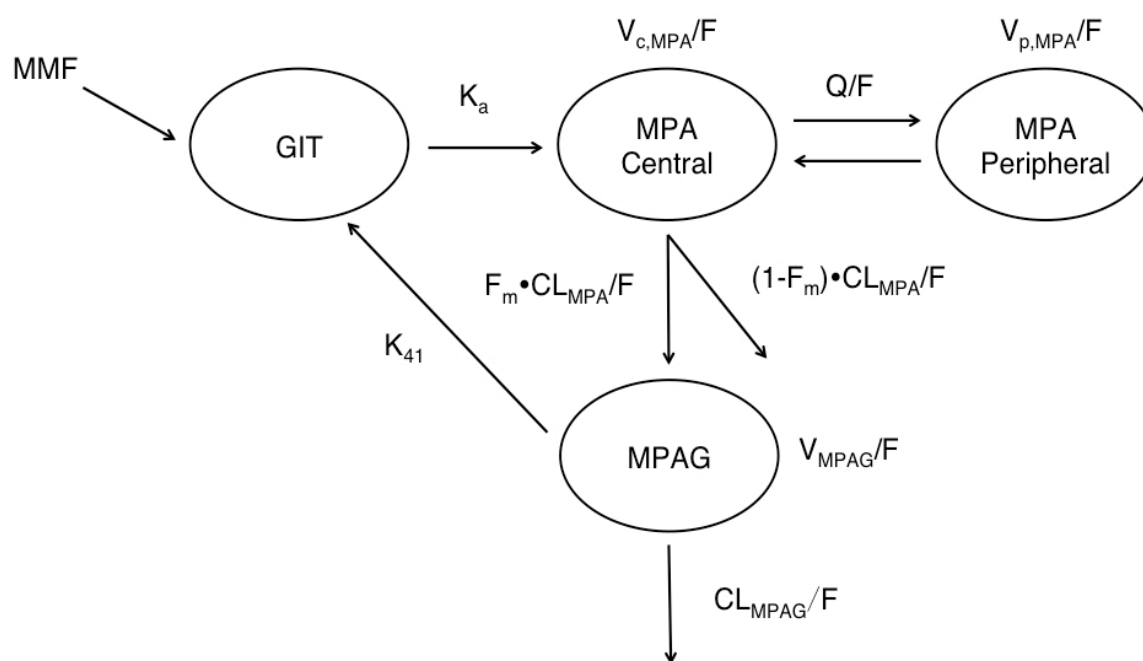
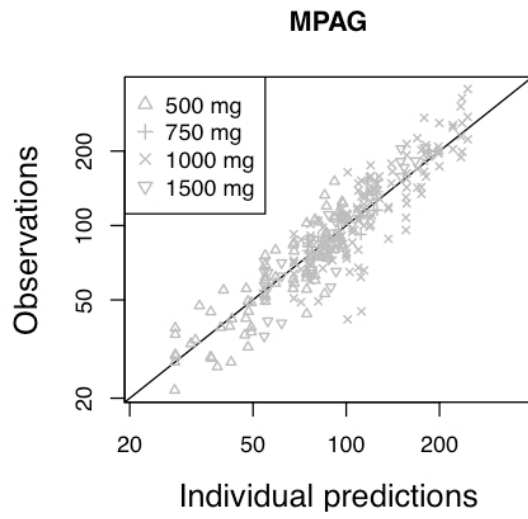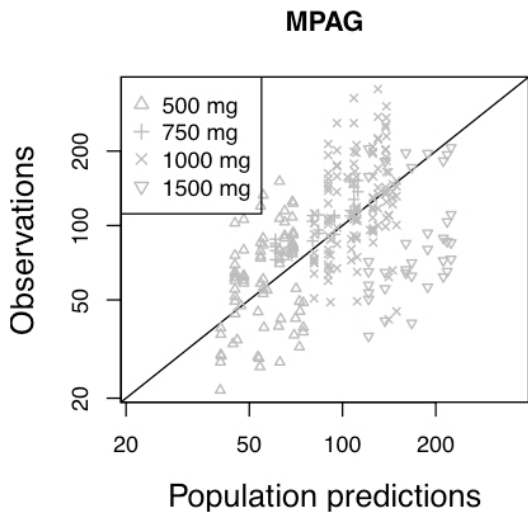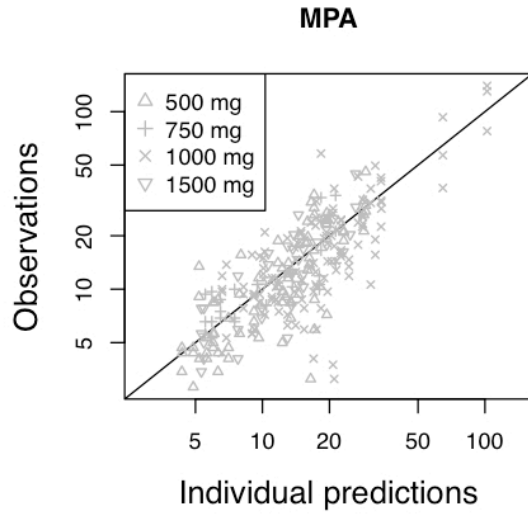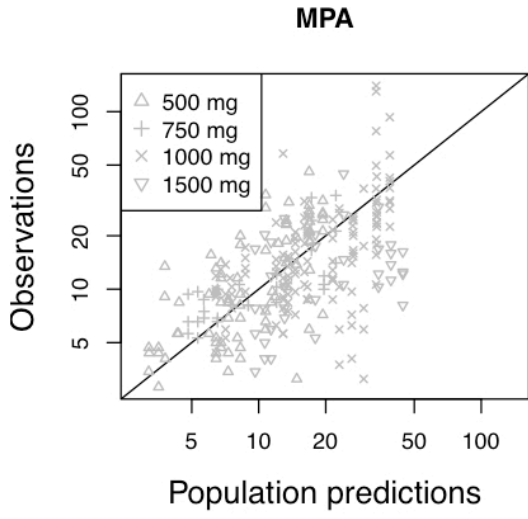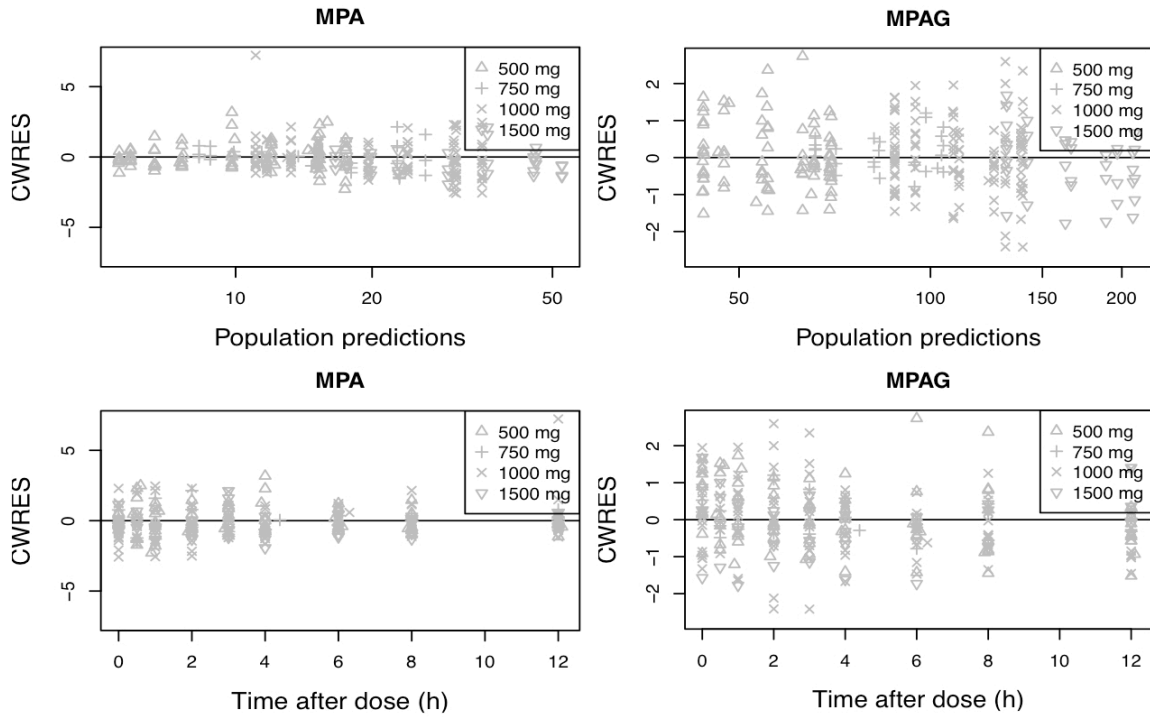**Figure C-1.** Population pharmacokinetic model of mycophenolic acid (MPA) and the mycophenolic glucuronide (MPAG). CL_{MPA}/F and CL_{MPAG}/F, apparent clearance of MPA and MPAG; $V_{c,MPA}/F$ and $V_{p,MPA}/F$, apparent volume of distribution of MPA in central and peripheral compartments; V_{MPAG}/F, apparent volume of distribution of MPAG; Q/F, apparent compartmental clearance between the MPA central and peripheral compartments; K_a, absorption rate constant of MPA; F_m, fraction of MPA metabolized to MPAG; K_{41}, rate constant for biliary excretion and enterohepatic recycling of MPA.
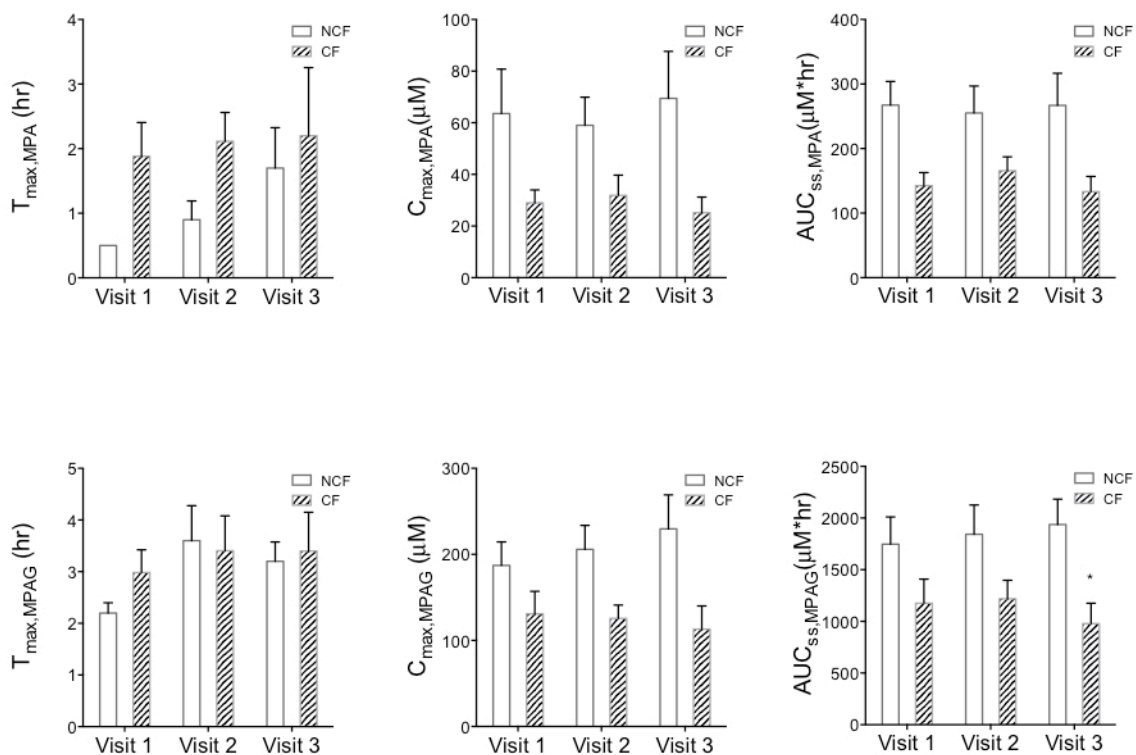
Figure C-2. Comparison of pharmacokinetic parameters between patients with cystic fibrosis (CF) or without the disease (NCF) by visit, as determined by non-compartmental analysis. AUC_{ss}, steady-state area under the serum concentration-time curve, normalized by 1000 mg dose; C_{max}, maximum serum concentration, normalized by 1000 mg dose; T_{max}, time to reach C_{max}. Values are mean $\pm$ SE (n=5). *$p \leq 0.05$ as compared to NCF patients.

MPA

MPA

MPAG

MPAG

Figure C-3. Basic goodness-of-fit plots of population pharmacokinetic parameters in pooled data from patients with cystic fibrosis (CF) or without the disease (NCF). MPA, mycophenolic acid; MPAG, MPA-7-O-glucuronide; CWRES, conditional weighted residual.
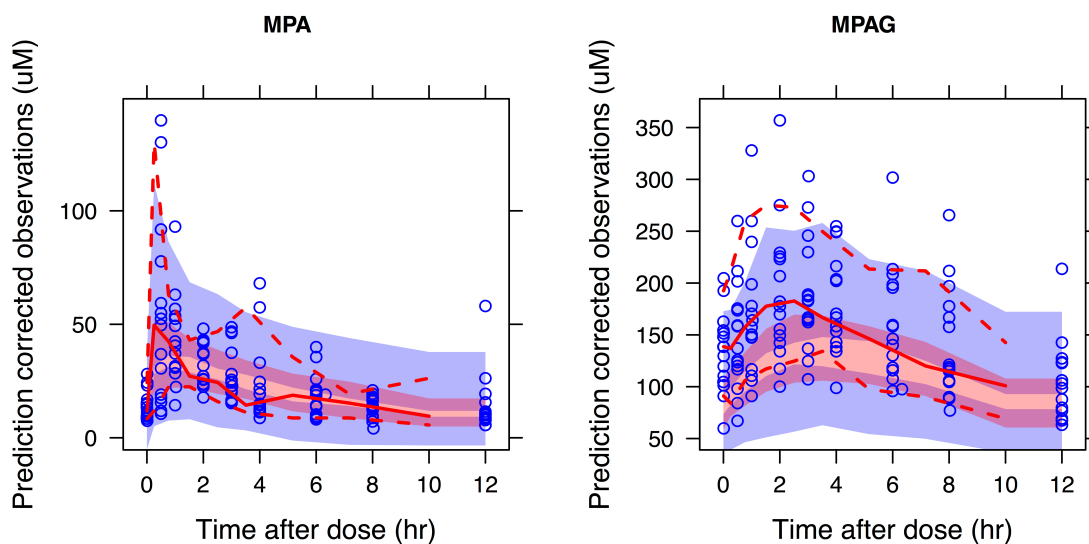
Figure C-4. Visual predictive check of the final pharmacokinetic model of mycophenolic acid (MPA) and metabolite (MPAG) in patients with cystic fibrosis (CF) or without the disease (NCF) based on 500 simulations. Observed data are shown as dots. Solid and dashed lines represent the median, 5th and 95th percentiles of observed data. Semitransparent red field represents the 95% confidence interval for the simulated median. Semitransparent blue fields represent the 95% confidence interval for the simulated percentiles.
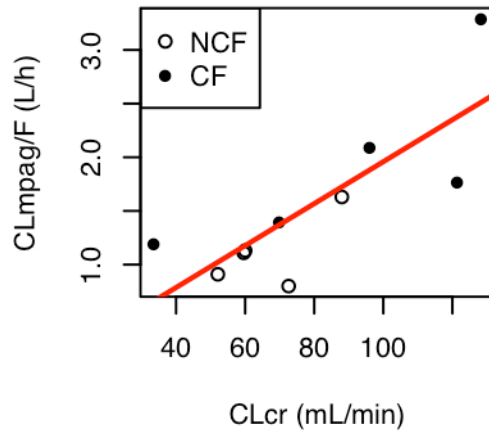
Figure C-5. Linear correlation between the mycophenolic glucuronide (MPAG) apparent clearance (CL_{MAPG}/F) and the creatinine clearance (CLcr) in patients with cystic fibrosis (CF) or without the disease (NCF).
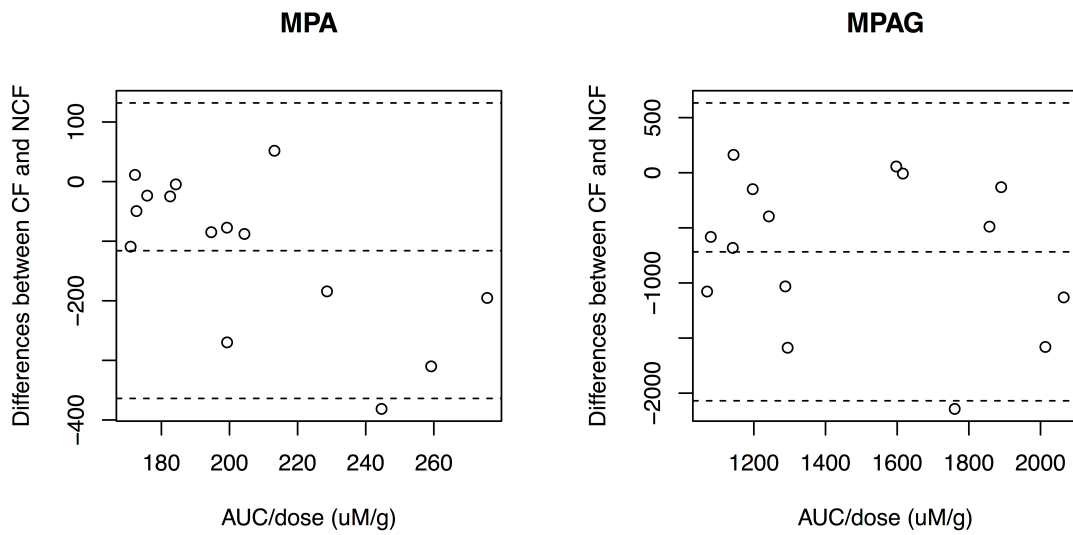
Figure C-6. Bland-Altman plot of the difference on dose corrected area under the

serum concentration-time curve (AUC) between CF and NCF patients.

Table C-1. Dose normalized C_{trough} ($\pm$SE) and $AUC_{(0-12h)}$ ($\pm$SE) of MPAG and MPA in

patients with cystic fibrosis (CF) or without the disease (NCF)

	All	NCF	CF
MPA			
C_{trough}**/dose (μM/mmol)**	4.83 (4.33)	6.23 (5.74)	3.43 (1.25)
$AUC_{(0-12h)}$**/dose (μM*hr/mmol)**	138 (51.4)	159 (50.7)	116* (38.1)
MPAG			
C_{trough}**/dose (μM/mmol)**	38.7 (16.1)	46.4 (16.73)	31.1* (11.6)
$AUC_{(0-12h)}$**/dose (μM*hr/mmol)**	1476 (1240)	1817 (1657)	1135* (436)

MPA, mycophenolic acid; MPAG, MPA glucuronide metabolite; C_{trough}, trough

concentration; $AUC_{(0-12h)}$, steady-state area under the serum concentration-time

curve; Values are mean ($\pm$ SE) (n=5); *$p \leq 0.05$ as compared to NCF patients.

Table C-2. Population pharmacokinetic parameter estimates for mycophenolic acid (MPA) and its glucuronide metabolite (MPAG) in patients with cystic fibrosis (CF) and without the disease (NCF)

Parameters	Estimates (%RSE)	Bootstrap estimates	
		Median	90% CI
CL_{MPA}/F NCF	14.5 (16)	12.5	9.7, 21.7
(L/hr) CF	24.1 (19)	20.0	11.2, 51.7
$V_{c,MPA}/F$ (L)	46.2 (33)	51.8	20.9, 102.2
$V_{p,MPA}/F$ (L)	401.0 (16)	403.4	354.7, 452.5
Q/F (L/hr)	13.3 (15)	14.8	4.3, 40.4
K_a (hr^{-1})	1.4 (44)	1.5	0.5, 3.5
CL_{MPAG}/F (L/hr)	1.4 (6)	1.4	1.1, 1.8
V_{MPAG}/F (L)	9.7 (16)	7.7	6.3, 15.0
K_{41} (hr^{-1})	0.09 (20)	0.07	0.04, 0.21
IIV %CV (%RSE)			
ω (CL_{MPA}/F)	28 (43)	25	16, 36
ω ($V_{c,MPA}/F$)	73 (71)	74	66, 123
ω (K_a)	107 (139)	89	32, 155
Residual error			
σ_1 (additive) (μM)	17 (29)	17	2, 33
σ_2 (proportional) %CV	24% (15)	0.06	0.04, 0.08

CL_{MPA}/F and CL_{MPAG}/F, apparent clearance of MPA and MPAG; $V_{c,MPA}/F$ and $V_{p,MPA}/F$, apparent volume of distribution of MPA in central and peripheral compartments; V_{MPAG}/F, apparent volume of distribution of MPAG; Q/F, apparent compartmental clearance between the MPA central and peripheral compartments; K_a, absorption rate constant of MPA; K_{41}, rate constant for biliary excretion and enterohepatic recycling of MPAG; σ_1 and σ_2, residual error; IIV, inter-individual variability; CV, coefficient of variation; RSE, relative standard error; CI, confidence interval. The IIV (ω) for Q/F, $V_{p,MPA}/F$, CL_{MPAG}/F, $V_{c,MPAG}/F$, and K_{41} were fixed based on results from the pilot runs.

REFERENCES

1.   Christie JD, Edwards LB, Kucheryavaya AY, Benden C, Dobbels F, Kirk R, et al. The Registry of the International Society for Heart and Lung Transplantation: Twenty-eighth Adult Lung and Heart-Lung Transplant Report--2011. J Heart Lung Transplant. 2011;30(10):1104-22.

2.   Staatz CE, Tett SE. Clinical pharmacokinetics and pharmacodynamics of mycophenolate in solid organ transplant recipients. Clin Pharmacokinet. 2007;46(1):13-58.

3.   Ting LS, Partovi N, Levy RD, Riggs KW, Ensom MH. Pharmacokinetics of mycophenolic acid and its glucuronidated metabolites in stable lung transplant recipients. Ann Pharmacother. 2006;40(9):1509-16.

4.   Fujiyama N, Miura M, Kato S, Sone T, Isobe M, Satoh S. Involvement of carboxylesterase 1 and 2 in the hydrolysis of mycophenolate mofetil. Drug Metab Dispos. 2010;38(12):2210-7.

5.   Bullingham RE, Nicholls AJ, Kamm BR. Clinical pharmacokinetics of mycophenolate mofetil. Clin Pharmacokinet. 1998;34(6):429-55.

6.   Colom H, Lloberas N, Andreu F, Caldes A, Torras J, Oppenheimer F, et al. Pharmacokinetic modeling of enterohepatic circulation of mycophenolic acid in renal transplant recipients. Kidney Int. 2014;85(6):1434-43.

7.   Sam WJ, Akhlaghi F, Rosenbaum SE. Population pharmacokinetics of mycophenolic acid and its 2 glucuronidated metabolites in kidney transplant recipients. J Clin Pharmacol. 2009;49(2):185-95.

8.   Woillard JB, Rerolle JP, Picard N, Rousseau A, Drouet M, Munteanu E, et al. Risk of diarrhoea in a long-term cohort of renal transplant patients given mycophenolate mofetil: the significant role of the UGT1A8 2 variant allele. Br J Clin Pharmacol. 2010;69(6):675-83.

9.   Sugioka N, Sasaki T, Kokuhu T, Ito Y, Shibata N, Okamoto M, et al. Clinical pharmacokinetics of mycophenolate mofetil in Japanese renal transplant recipients: A retrospective cohort study in a single center. Biol Pharm Bull. 2006;29(10):2099-105.

10.   Quattrucci S, Rolla M, Cimino G, Bertasi S, Cingolani S, Scalercio F, et al. Lung transplantation for cystic fibrosis: 6-year follow-up. J Cyst Fibros. 2005;4(2):107-14.

11.   Rey E, Treluyer JM, Pons G. Drug disposition in cystic fibrosis. Clin Pharmacokinet. 1998;35(4):313-29.

12.   Debray D, Rainteau D, Barbu V, Rouahi M, El Mourabit H, Lerondel S, et al. Defects in gallbladder emptying and bile Acid homeostasis in mice with cystic fibrosis transmembrane conductance regulator deficiencies. Gastroenterology. 2012;142(7):1581-91 e6.

13.   Stead RJ, Houlder S, Agnew J, Thomas M, Hodson ME, Batten JC, et al. Vitamin D and parathyroid hormone and bone mineralisation in adults with cystic fibrosis. Thorax. 1988;43(3):190-4.

14.   Wang XX, Feng MR, Nguyen H, Smith DE, Cibrik DM, Park JM. Population pharmacokinetics of mycophenolic acid in lung transplant recipients with and without cystic fibrosis. Eur J Clin Pharmacol. 2015;71(6):673-9.

15.   Stuckey L, Clark Ojo T, Park JM, Annesley T, Bartos C, Cibrik DM. Mycophenolic acid pharmacokinetics in lung transplant recipients with cystic fibrosis. Ther Drug Monit. 2014;36(2):148-51.

16.   Benoit-Biancamano MO, Caron P, Levesque E, Delage R, Couture F, Guillemette C. Sensitive high-performance liquid chromatography-tandem mass spectrometry method for quantitative analysis of mycophenolic acid and its glucuronide metabolites in human plasma and urine. J Chromatogr B Analyt Technol Biomed Life Sci. 2007;858(1-2):159-67.

17.   Cremers S, Schoemaker R, Scholten E, den Hartigh J, Konig-Quartel J, van Kan E, et al. Characterizing the role of enterohepatic recycling in the interactions between mycophenolate mofetil and calcineurin inhibitors in renal transplant patients by pharmacokinetic modelling. Br J Clin Pharmacol. 2005;60(3):249-56.

18.   Ling J, Shi J, Jiang Q, Jiao Z. Population pharmacokinetics of mycophenolic acid and its main glucuronide metabolite: a comparison between healthy Chinese and Caucasian subjects receiving mycophenolate mofetil. Eur J Clin Pharmacol. 2014;10.1007/s00228-014-1771-1.

19.   Shum B, Duffull SB, Taylor PJ, Tett SE. Population pharmacokinetic analysis of mycophenolic acid in renal transplant recipients following oral administration of mycophenolate mofetil. Br J Clin Pharmacol. 2003;56(2):188-97.

20.   van Hest RM, van Gelder T, Vulto AG, Mathot RA. Population pharmacokinetics of mycophenolic acid in renal transplant recipients. Clin Pharmacokinet. 2005;44(10):1083-96.

21.   Johnson HJ, Swan SK, Heim-Duthoy KL, Nicholls AJ, Tsina I, Tarnowski T. The pharmacokinetics of a single oral dose of mycophenolate mofetil in patients with varying degrees of renal function. Clin Pharmacol Ther. 1998;63(5):512-8.

22.   van Hest RM, Mathot RA, Pescovitz MD, Gordon R, Mamelok RD, van Gelder T. Explaining variability in mycophenolic acid exposure to optimize mycophenolate mofetil dosing: a population pharmacokinetic meta-analysis of mycophenolic acid in renal transplant recipients. J Am Soc Nephrol. 2006;17(3):871-80.

23.   Savic RM, Karlsson MO. Importance of shrinkage in empirical bayes estimates for diagnostics: problems and solutions. AAPS J. 2009;11(3):558-69.

24.   Wang X, Kay A, Anak O, Angevin E, Escudier B, Zhou W, et al. Population pharmacokinetic/pharmacodynamic modeling to assist dosing schedule selection for dovitinib. J Clin Pharmacol. 2013;53(1):14-20.

25.   de Winter BC, Monchaud C, Premaud A, Pison C, Kessler R, Reynaud-Gaubert M, et al. Bayesian estimation of mycophenolate mofetil in lung transplantation, using a population pharmacokinetic model developed in kidney and lung transplant recipients. Clin Pharmacokinet. 2012;51(1):29-39.

26.   Gerbase MW, Fathi M, Spiliopoulos A, Rochat T, Nicod LP. Pharmacokinetics of mycophenolic acid associated with calcineurin inhibitors: long-term monitoring in stable lung recipients with and without cystic fibrosis. J Heart Lung Transplant. 2003;22(5):587-90.

27.   Pittman FE, Denning CR, Barker HG. Albumin Metabolism in Cystic Fibrosis. Am J Dis Child. 1964;108:360-5.

28.   Strober W, Peter G, Schwartz RH. Albumin metabolism in cystic fibrosis. Pediatrics. 1969;43(3):416-26.

29.   R B. Cystic Fibrosis. In: Isselbacher KJ BE, eds, editor. Harrison's Principles of Internal Medicine. New York, NY: McGraw-Hill Inc; 1994. p. 1194-7.